178
16

The Effects Of Thermal Cycling On Residual Stresses In Thick-Walled Stainless Steel Pipe

by

Nancy Abigail Morgan

Thesis submitted to the Faculty of the
Virginia Polytechnic Institute and State University
in partial fulfillment of the requirements for the degree of

MASTER OF SCIENCE

in

Materials Engineering

Approved:

R. W. Hendricks
Dr. Robert W. Hendricks, chairman

Stan David
Dr. Stan David

George Swift
Dr. George Swift

V. A. Dowling
Dr. Norman Dowling

Jack L. Lytton
Dr. Jack Lytton

Febuary 1, 1990

Blacksburg, Virginia

c.2

The Effects Of Thermal Cycling On

Residual Stresses In Thick-Walled Stainless Steel Pipe

by

Nancy A. Morgan

Committee Chairman: Robert W. Hendricks
Materials Engineering

(ABSTRACT)

The effects of thermal cycling on residual stresses are studied in thick-walled 316L stainless steel pipe. A relatively small ΔT of 280° F is considered. The residual stresses are measured by an x-ray diffraction technique. The initial stress state of the pipe wall shows periodic and random variability in stress from -30 to 20 ksi. The pipe was thermal cycled between a furnace and a quenchant bath. The macro residual stresses became 10 ksi more compressive after the first thermal cycle. Thereafter no significant changes are measured in the macro residual stresses, however, the micro residual stresses continue to increase linearly with the number of cycles.

Acknowledgements

I would very much like to thank my advisor, Dr. Robert W. Hendricks, for adopting me at the beginning of my graduate career, for his input and guidance, and friendship. Special thanks to Dr. Stan David and L. C. Manely of Oak Ridge National Laboratory for their kind and generous help and involvement with my project. I would like to acknowledge the input and efforts of Dr. George Swift; his work was an asset to this project. I thank Dr. Jack Lytton and Dr. Norman Dowling for taking on the unrewarded job of being a theses committee member. To Dr. Mac Louthan, thanks for influencing me to go to graduate school and then fleeing to industry. I couldn't resist this opportunity to acknowledge, but tease him.

I would also like to thank my many cohorts for their help and friendship. They are Venki Iyer, Jinmyun Jo, Ken Imrich, Michael Laurant, Kathy Rohr, Noel Shultz, and Bill Halley. Thanks to Darcy Hays and Dr. Robert Foutz of their statistical expertise and help.

Many times I felt this research project would never be completed, and I'm sure I would not have been able to persevere much less finish mentally intact without the encouragement of my sister Anne, my good friend Robin, and especially my roommates: Lucy, Nancy, and Jenny. Thanks to Larry and Greg for the Burger King graduate seminars. Your concurring misery and endurance gave me hope and laughter. Thanks, Mom and Dad, for giving me the environment to desire education. But most of all I thank my Lord and Savior, Jesus Christ, for faithfully loving me and using this experience to show me how dependant on Him I am.

I would like to express my gratitude to those who provided funds for this project. This research was funded by Philip Morris USA, the Institute for Materials Science and Engineering of the Center for Innovative Technology, and a Materials Science Summer Study Program sponsored by Oak Ridge National Laboratory, the Southeastern Universities Research Association, and Oak Ridge Associated Universities.

Table Of Contents

List Of Figures

List Of Tables

1.0 Introduction

Residual stresses are "self-equilibrating internal stresses existing in a free body which has no external forces or constraints acting on its boundary."(1) Residual stresses are ubiquitous with the solid phase. It is not a question of the existence of residual stresses, but a question of their magnitude. Residual stresses range in magnitude from the large forces needed to equilibrate weld warpage to the small forces balancing atom misalignment.

Residual stresses are one of the more insidious and critical materials factors. Young says "the accumulation of residual stresses induced intentionally by design and manufacture or experience in service determine a part's life."(2) The same alloy or externally identical component can have very different stress states depending on its specific history. Designers can overlook these inherent stresses too easily, resulting in unexpected and possibly catastrophic results. Residual stress is not necessarily detrimental and sometimes is deliberately induced for its performance enhancing effects as in the case of shot peening. Unfortunately in many instances residuary stresses, especially in tension, are deleterious to a part's life. Two very serious phenomena augmented by tensile residual stress are stress corrosion cracking (SCC) and fatigue. Residuary stresses must be understood and accounted for to assure safety and reliability.

The quantity of the stress state can be as high as the material's yield strength or higher. Parts have been known to explode into sections while lying completely

unloaded. Imagine placing this component into an engineering design and expecting top performance.

Induced by plastic flow of a nonuniform nature, residual stresses are caused by a multitude of processes. Three natural classifications of different phenomena which can induce stress are mechanical, chemical, and thermal. Mechanically incarnated stresses involve such procedures as shot peening, polishing, grinding, forming, drawing, rolling, machining, and assembling. Modes of chemical residual stress are via oxidation, corrosion, and electroplating. Welding, casting, and heat treating are some examples of thermal procedures which can create residuary stresses.

Thermally induced residual stress is the main interest of this research project. The problem examined concerns the thermal gradients in a welded structure found in a food processing plant. During production the piping in which the product flows is rapidly thermally cycled through a relatively small temperature change. Will these thermal fluctuations be sufficient to cause stresses above yielding, thus plastically deforming the material, and permanently changing the pipe's state of stress? These stresses are further complicated by interaction with an initial stress field from a girth weld in the seamless pipe.

Large temperature gradients have been extensively studied and characterized while the effects of small ΔT's have been almost ignored. By measuring the change in residual stress, this project explored the effect of thermal stresses created by small ΔT thermal cycling in a thick-walled 316L stainless steel pipe. The method of residual stress quantification was multiple angle x-ray diffraction.

2.0 Literature Review

The ensuing literature survey reviews some history of thermal stress analysis, the conditions necessary for thermal stresses, and a few closed form solutions pertaining to the geometry of interest, a cylinder. Section 2.4 discusses material resonances to thermal stresses including thermal shock, thermal fatigue, and thermomechanical fatigue (TMF). This is followed in Section 2.5 and 2.6 by a more detailed examination of two processes which induce large thermal stresses-- quenching and welding. Final discussion in Section 2.7 addresses thermal stress due to small temperature changes.

2.1 History of Thermal Stress Analysis

Even though many engineering components fail because of thermal stresses, most thermal stress analysis and high temperature technology has only evolved in the last forty years. Earlier there was no driving force to develop thermal stress theory because failure by thermal stresses was mainly a nondisastrous event. The genesis of thermal cracks are usually on a surface region.(3) They ruin the surface finish and create stress raisers but inspection and replacement were a satisfactory solution. So what instigated a change, and why is sophisticated analysis needed now? The answer is the nuclear industry. In the nuclear field the consequences of failure are unacceptable. Also nuclear systems have to work well and work over a period of time because in-service inspection or shutdown is exorbitant in cost.

2.1.1 The Nuclear Industry

Stress analysis of a reactor and its auxiliary components includes many complicated

phenomena. For maximum power efficiency a reactor should operate at the highest possible temperature so high temperature and creep resistance are factors. Change in coolant flow, start up, shut down, pump failure, power changes, and nonuniform gamma heating produce thermal gradients and thermal transients. Exotic materials and radiation damage create additional complexity. These conditions coupled with "constant" mechanical loads can be disastrous unless their effects are given careful consideration. One reactor component which has been extensively examined is the piping or tubing, and it is known that tube life is significantly reduced, both by fatigue and by long term deformation growth, in thermal gradients. (4) To minimize damage, thermal cycles must be kept to as few as possible.(5)

2.1.2 Non-Nuclear Industries

The merit of experimental and theoretical research on thermal stresses is justified in non-nuclear fields also. Conventional power plants face many similar thermal power problems -- diurnal power needs, transient temperatures, creep, etc. inherent in the nuclear industry.

Central solar receiving plants with a thirty year plant life expectancy are designed for 10,000 thermomechanical cycles. These plants can try to minimize thermal cycling from within but have no control over frequent cycling which will occur by cloud passage.(6)

Power production is not the only field concerned with failures caused by thermal fluctuations. Others include the petroleum and chemical industries and many forms of aircraft parts from turbine blades to shuttle tiles.

2.2 Conditions For Thermal Stress

Two conditions must exist to create thermal stress. They are temperature and constraint. By definition thermal stress implies temperature. No stress is manifested in an unconstrained homogeneous material if the temperature changes at equilibrium conditions. However, equilibrium transition is not realistic in most engineering applications. Knowing the temperature profile and thermal properties is a prerequisite to the calculation of thermal stresses, and there are well developed finite element methods (FEM) to determine these temperature distributions in many engineering structures.(7)

2.2.1 Internal Constraints

Constraints can be internal or external in form. In a material with no external constraints rapid or differential heating and cooling causes stress generation. The internal constraint is the material's inability to expand or contract with the rate of temperature change. Another internal constraint may be inhomogeneity in the microstructure. Different crystallographic phases which have different linear expansion coefficients will have differing volume changes which create strains.

One of the most dramatic cases of thermal stresses from internal constraint occurs in alpha uranium. Chiswick studied thermal cycling between 50 and 500° C in one-inch uranium bars with no external constraints. He found that the bars grew approximately 30% in length during 500 cycles.(8)

2.2.2 External Constraints

External constraints such as rigid mountings or hydrostatic pressure will always induce stress regardless of the rate of temperature change. Suppose a bar with fixed ends is uniformly heated. As the temperature increases the bar wishes to expand. (This discounts unique materials with a negative or zero linear expansion coefficient.) Since the ends are constrained the bar cannot extend lengthwise and is under a state of compression. For this situation the uniaxial stress, from fundamental principles of deformable bodies, is calculated by the following equation.(9)

$$\sigma = - E\alpha\Delta T \qquad \text{Eq. 2-1}$$

where

σ = stress,
E = modulus of elasticity,
α = linear expansion coefficient,
ΔT = $T_f - T_i$,
T_f = final temperature, and
T_i = initial temperature.

This relationship assumes that the stress remains in the elastic region. Change from the initial residual stress state hinges on surpassing the elastic limit or yield stress thus resulting in plastic deformation.

2.3 Stress Analyses

Besides the above fixed end bar, thermal analyses are performed on a variety of structural elements -- beams, rings, frames, trusses, plates, and shells. The principles for thermal stress development are described in many texts.(10)(11)(12)(13)(14) Theoretical calculations of thermal stresses are achieved by closed form, infinite series, numerical integration, stress functions, or minimization of strain energy methods.

2.3.1 Closed Form Solutions

In reality very few exact solutions exist for thermal loading problems. For the simplified form of a long hollow cylinder, the geometry of interest, closed form solutions have been developed which can yield accurate values depending on the assumptions incorporated. For the case of radial temperature variation and plain strain ($\epsilon_z = 0$), the elastic stresses are defined.(10)

$$\sigma_z = -\frac{\alpha E T}{1-\nu} + \frac{2\nu E C_1}{(1+\nu)\ (1-2\nu)}, \qquad \text{Eq. 2-2}$$

$$\sigma_\theta = \frac{\alpha E}{1-\nu}\frac{1}{r^2}\int_a^r Tr\ dr - \frac{\alpha E T}{1-\nu},$$

$$+ \frac{E}{1+\nu}\left[\frac{C_1}{1-2\nu} + \frac{C_2}{r^2}\right], \text{ and} \qquad \text{Eq. 2-3}$$

$$\sigma_r = -\frac{\alpha E}{1-\nu}\frac{1}{r^2}\int_a^r Tr\ dr + \frac{E}{1+\nu}\left[\frac{C_1}{1-2\nu} + \frac{C_2}{r^2}\right] \qquad \text{Eq. 2-4}$$

where

$\sigma_z, \sigma_\theta, \sigma_r$ = longitudinal, hoop, and radial stress,
C_1, C_2 = constants to be determined by the boundary conditions,
ν = Poisson's ratio,
T = temperature distribution as a function of r,
r = variable radius, and
a = inside radius.

Again, the stresses predicted by Equations 2-2 through 2-4 are elastic and present during the thermal gradient. The conditions necessary to affect the residual stress state are stresses above elastic limit and in the plastic range.

A further assumption of steady state heat transfer yields the closed form solution which predicts that the greatest magnitude of stress generated occurs on the inside and outside surfaces of the hollow cylinder.(5) Let

$$\xi = \ln\left[\frac{b}{a}\right]$$

where

b = outside radius of the cylinder. Then

$$\sigma_z = \frac{E\alpha\Delta T}{2(1-\nu)\xi}\left[1 - 2\left[\ln\frac{b}{r}\right] - \frac{2a^2}{b^2-a^2}\xi\right], \qquad \text{Eq. 2-5}$$

$$\sigma_\theta = \frac{E\alpha\Delta T}{2(1-\nu)\xi}\left[1 - \ln\frac{b}{r} - \frac{a^2}{b^2-a^2}\left[1 + \frac{b^2}{r^2}\right]\xi\right], \qquad \text{Eq. 2-6}$$

$$\sigma_r = \frac{E\alpha\Delta T}{2(1-\nu)\xi}\left[-\ln\frac{b}{r} - \frac{a^2}{b^2-a^2}\left[1 - \frac{b^2}{r^2}\right]\xi\right]. \qquad \text{Eq. 2-7}$$

The inside surface stresses are compressive while on the outside they are tensile.

Burgreen derives a similar closed form equation for thick-walled cylinders with unrestrained expansion ($\epsilon_z = \alpha\underline{T}$) given below.(13)

$$\sigma_{\theta s} = \sigma_{zs} = \frac{E\alpha}{1-\nu}\left[\underline{T} - T_s\right] \qquad \text{Eq. 2-8}$$

where

$\sigma_{\theta s}, \sigma_{zs}$ = inside or outside hoop and longitudinal stress,
T_s = temperature on the inside or outside wall, and
$\underline{T}$ = mean temperature of the cylinder.

2.3.2 Finite Element Methods

Finite element methods (FEM) or finite difference methods (FDM) are powerful computational tools for theoretical analysis of thermal stresses. FEM is a logical outgrowth of computer development, performing many calculations in small increments of time and distance. FEM are based on constitutive stress-strain temperature relationships and are only as good as the current understanding of the

true physical relationships. Even the most elegant three dimensional thermal stress analyses include simplifications or idealizations of geometry and material properties. Concepts such as elasticity, isotropy, homogeneity, etc. are mathematical notions and not inherent properties of materials. Nevertheless, FEM and FDM are tools of great worth and extensively used in thermal analysis and other fields. Many of the experimental results to be cited in this chapter were performed using one of these methods.

2.3.3 Experimental Techniques

Thermal stresses can be examined experimentally through the use of strain gages, by the observation of crack initiation and deformation growth, and by measuring changes in residual stress. Of these methods strain gages can be used to monitor strain/stress during the actual thermal stress. The other methods also investigate parameters directly affected by the thermal stress but generally can not be monitoring during the thermal load application. For example, if change in residual stress is being studied by x-ray diffraction techniques, it would be difficult to assemble the cycling apparatus under the x-ray analysis machine in a manner which would not interfere with the measuring process.

2.4 Materials' Response To Thermal Stress

The same temperature distribution will have vastly different affects on different substances. For instance, previously, glass dishes could not be placed in the oven without fear of fracture upon removal. By manipulating the compositions to modify the properties, glasses, such as Pyrex, have been devised that can withstand the change between room temperature and $\approx$ 400° F.* (* See bottom of page 10)

2.4.1 Thermal Shock

Thermal shock is defined as thermal stresses developed by a sudden change in temperature. Steep thermal gradients through the thickness and along the length of a component give rise to highly triaxial stresses. A triaxial state of stress reduces the material's freedom to deform. Therefore, embrittlement can occur even though the material's uniaxial ductility increases with higher temperature. Designated "brittle" materials, generally ceramics, are more susceptible to thermal shock than "ductile" substances. Two properties which contribute to the tolerance of thermal shock or the lack thereof are α, the linear expansion coefficient, and k, the thermal conductivity. The smaller α is, and larger k is the better the material's resistance. The Metals Handbook classifies a failure as a thermal shock failure if the failure transpires in one cycle or less.(15)

2.4.2 Thermal Fatigue

When many repetitive or cyclic generations of thermal stress are needed to evoke failure it is referred to as thermal fatigue. Thermal fatigue is defined as "fracture resulting from the presence of temperature gradients that vary with time in such a manner as to produce cyclic stresses in a structure."(16) Without pursuing the ocean of information and factors involved in the study of fatigue, a few of the concepts especially important to thermal fatigue will be addressed.

---

* Note to the reader: Following the ambivalence in the United States, mixed conventions of English and International units will be use for temperature, length, and force.

Thermal fatigue commonly occurs in heat exchangers, internal combustion engines, and turbine components. The identifying features of low cycle thermal fatigue are the following:(15)

- multiple crack initiation sites which join to form cracks,
- crack initiation along surfaces with inward growth,
- corrosion or oxidation in the cracks, and
- mostly transgranular fracture.

2.4.2.1 Cycle Variables

Fatigue is generally categorized as either high or low cycle fatigue. Manson defines the division between high and low cycle thermal fatigue at 10^5 cycles. High cycle fatigue involves microscopic strains which are elastic or have very small amounts of plasticity. Large plastic strains exist in low cycle fatigue.(17)

Disregarding material properties, the number of cycles that can be withstood before failure depends primarily on the factors involving the generation of temperature and strain.(18) A material has greater endurance for cooling cycles than for heating or alternating heating and cooling cycles.(19) The reasons for this are not entirely understood, but Tilly reports the same, that the temperature at which the peak tensile strains develop is an important factor of the life along with the shape of the temperature cycle.(20) For example, hold time and rest periods in the cycle history play a positive or negative role. In addition, the type of constraint, full or partial, contributes to the establishment of strain and, therefore, the fatigue behavior.

2.4.2.2 Material Properties

Thermal fatigue can not be retarded by inhibitors, galvanic coupling, coatings, or a change of environment, only by eliminating excessive strain. A designer can include thermal fatigue resistance in the criteria for materials selection. Desirable properties for good thermal fatigue performance include those of thermal shock resistance, low α, high k, and ductility. Also important is the material's behavior as a function of time in a high temperature environment. Aspects such as corrosion aegis and metallurgical stability are strategic at elevated temperatures. In austenitic stainless steels thermal cycling between 773-1173° K results in considerable grain growth ($51\mu m \rightarrow 185\text{-}200\mu m$).(21) This is undesirable as larger grains are more amenable to fatigue. Another example, also in connection with stainless steel, is the worry of sensitization around 600° C. If thermal cycling involves temperatures in this range, a stainless may loose its good corrosion properties.

Creep is a phenomena normally occurring at high temperature. It is time-dependant strain occurring under stress. Creep is generally assumed not to be a problem at temperatures less than or equal to $^1/_3\ T_m$ where T_m is the melting point in kelvin.(22)

How a material responds to cyclic strain is key to its fatigue resistance. Many substances work or strain harden under a cyclic load. Strain hardening is "an increase in hardness and strength caused by plastic deformation at temperatures below the recrystallization range."(16) Materials that work harden have the ability to relieve an area of high strain concentration. This helps abate fatigue. Depending on the range of temperatures, deformation and work hardening can occur by different

modes. At high temperatures thermally activated processes of climb and slip dominate while at low temperatures a variety of athermal modes are active.(23)

2.4.2.3 Thermal Fatigue Testing

Thermal cycling fatigue testing can be performed various ways. Two mechanisms of cycling are moving a specimen between two areas of differently maintained temperatures or a stationary sample with both heating and cooling apparatus around the specimen such as induction coils and air jets. Thermal fatigue testing is somewhat cumbersome, and the majority of thermal fatigue data available at present has been obtained from constant temperature uniaxial strain cycling. The difference between these two tests is thermal fatigue results from temperature cycling as opposed to fatigue at high temperatures caused by strain cycling.

Manson compares thermal fatigue for cycling between 200-500° C and isothermal mechanical fatigue at 350, 500, and 600° C in 347 stainless steel. Even though the average temperature of the thermal cycling is only 350° C, the thermally fatigued samples always fail at about half the number of cycles as the failure of the mechanically fatigued specimens. The most significant reason for this discrepancy is believed to be strain localization in the thermally cycled samples. Correlation between these two types of test vary from metal to metal.(18)

2.4.3 Thermomechanical Fatigue

In most situations a component is not subjected to purely thermal cycling but is additionally abused by constant or fluctuating mechanical loads. Hence, testing is performed by combining mechanical and thermal cycles. Thermomechanical fatigue

(TMF) is most often carried out in a closed loop, servohydraulic fatigue testing machine with programmable temperature and strain. Numerical models are often used to inspect TMF conditions. Comparing isothermal mechanical fatigue and TMF in 316 stainless steel reveals that the combined affect of load and temperature vicissitudes shorten life ≈40%.(6)

2.4.3.1 The Bree Diagram

Because of the complex synergistic nature of TMF, an accurate quick device to assess the likelihood of fatigue damage is desirable and judicious. Bree developed such a diagram for thin tubes found in nuclear reactors. The simplified Bree diagram shown in Figure 2-1 defines the boundaries of a material's response to thermal and mechanical loads.(24) In this figure σ_t is the thermal induced stress, σ_p is the stress due to load, and σ_y is the yield strength. Both axes represent a stress parameter. The abscissa is σ_p/σ_y, the primary stress parameter, while the ordinate is σ_t/σ_y, the thermal stress parameter. Disregarding fracture on the first cycle, a material behaves in one of the manners designated by the following areas:

E - the elastic zone where the combination of σ_t and σ_p remain elastic,

S - the shakedown region where plastic flow takes place on the first cycle only and the stresses remain elastic thereafter,

P - the plastic cycling zone where plastic flow occurs every cycle but there is no net growth, and

R - the ratcheting zone where plastic flow occurs on each cycle with net growth.

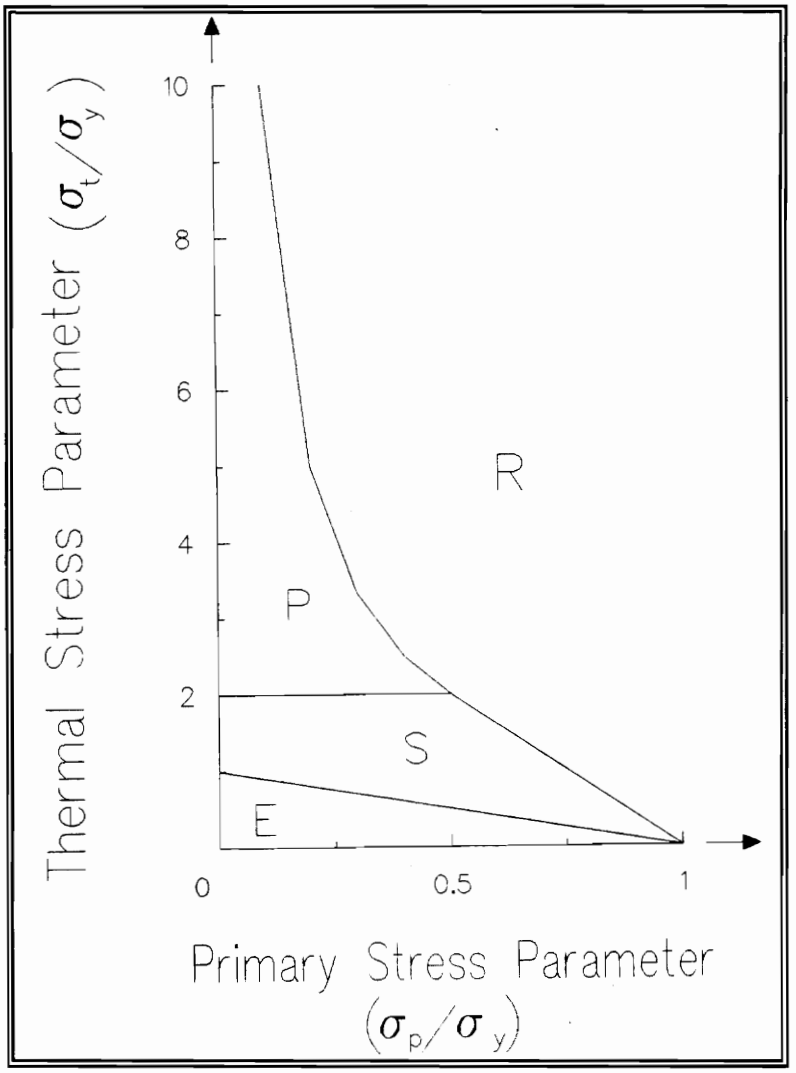

Figure 2-1 Simplified Bree Diagram

Any suitable design must avoid ratcheting altogether. In the region of plastic cycling design is possible if plastic behavior occurs only in the outer region while an interior volume maintains elastic behavior. In this case fatigue is an expected result but may not limit the part's life to an unacceptable interval.

Bree's Diagram defines a very specific problem with qualifying assumptions. It is designed for a thin circular cylindrical vessel with constant uniaxial internal pressure and temperature varying through the thickness. The material is assumed to be elastic-perfectly plastic with properties independent of temperature. Altered geometry, loading, boundary conditions, or material assumptions shift the limits in the Bree Diagram. This has prompted other investigations and interaction diagrams.

2.4.3.2 Variations of the Bree Diagram

Experimenters have made changes in the Bree diagram. Different assumptions were made which shift regions of the diagram. Some variances from Bree's work include changes in the material properties, the thermal cycling, the sample geometry, and the effects of creep.

Bree considered an elastic-perfectly plastic material. In a material which work hardens the area of "shakedown" occurs over more than one cycle as opposed to the elastic-perfectly plastic material where shakedown is a one cycle event.(25) Shakedown is, however, usually achieved in relatively few cycles compared to life. Ponter and Karadeniz examined more extreme thermal loads than did Bree and feel the classical Bree Diagram is not the most satisfactory approach. If the thermal loading exceeds $2\sigma_y$ in a critical volume of material, the structure is weakened to the

extent that the shakedown regime is bypassed and plastic collapse (ratcheting) occurs even with small or no mechanical load.(25)(26) They predict failure when

$$\sigma_t > \frac{E\alpha\Delta T}{2}. \qquad \text{Eq. 2-9}$$

In Bree's model ratcheting is not possible without a mechanical load.

The effect of creep has been added to the Bree Analysis.(27)(28)(29) Different geometries have been considered.(30) Hyde, Sahari, and Webster took into account nonuniform tube thickness which can result from corrosion or manufacturing errors. This difference increases the ratcheting range predicted by the classical diagram.(31) Constraint of the tubes shifts the Bree regimes, decreasing life with increasing restraint.(32) This shift is shown qualitatively with arrows in Figure 2-2. Zarka and Casier analyzed the presence of residual strain in both elastic-perfectly plastic and kinematically hardening materials. In neither case does initial stress change the ratcheting zones. However, it effects the number of cycles to shakedown for both models.(33)

All of the above modeling superimposes thermal and mechanical loads. This is not always permissible. Coupled solution modeling must be used in these complicated instances.(34)

2.5 Thermal Stresses of Interest

Two of the most common practices of materials processing are quenching and welding. Materials joining is necessary in almost all engineering designs, and quenching is a treatment often administered to procure desired metallurgical

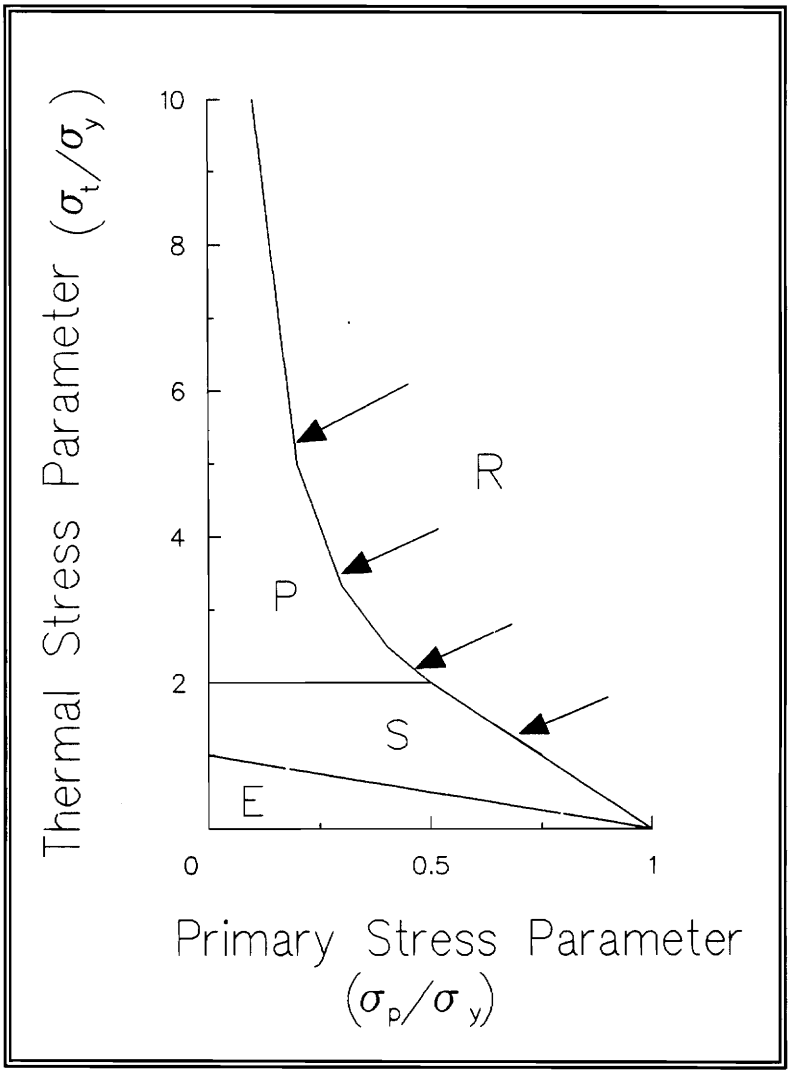

Figure 2-2 Shifted Bree Diagram With Increased Ratcheting Due To Nonuniform Tube Thickness

properties or can be encountered incidentally in service. These customary operations infuse large thermal gradients and thus have potential of producing large thermal stresses and residual stresses.

2.5.1 Thermal Stresses From Quenching

Many investigations predicting and measuring thermal stresses generated during quenching have been documented. Potentially, quenching stresses are high enough to cause cracking and certainly plastic flow. Modeling quenching stresses is extremely complex and must incorporate thermal conductivity, surface heat transfer, linear expansion, density, specific heat, elastic modulus, yield strength, etc., all of which are material and temperature dependant. Additionally, phase transformations, frequent in steels, compound modeling difficulty. Most predictions are based on simple geometries such as flat plates and long cylinders. Often modelers use an experimental method to verify the accuracy of their predictions.(35)(36)(37)

Schroder's work shows the generation of stress as a function of time in a steel cylinder and is represented in Figure 2-3.(38) The cylinder is quenched on all surfaces and, as expected during the initial stages of quenching, a tensile stress is developed on the surfaces. Figure 2-3a shows the modeled portion of the cylinder. Figure 2-3 b, c, and d are the axial, tangential, and radial stresses, respectively, after 1.7 seconds. The tensile stress develops on the surface by the following manner. When the cylinder's surface comes in contact with quenching medium, it cools and wants to contract. Because the interior material is still hot and not decreasing in volume, the exterior material is kept from doing so, thus, developing tensile stresses. If these stresses are large enough the material will yield in tension. After a period

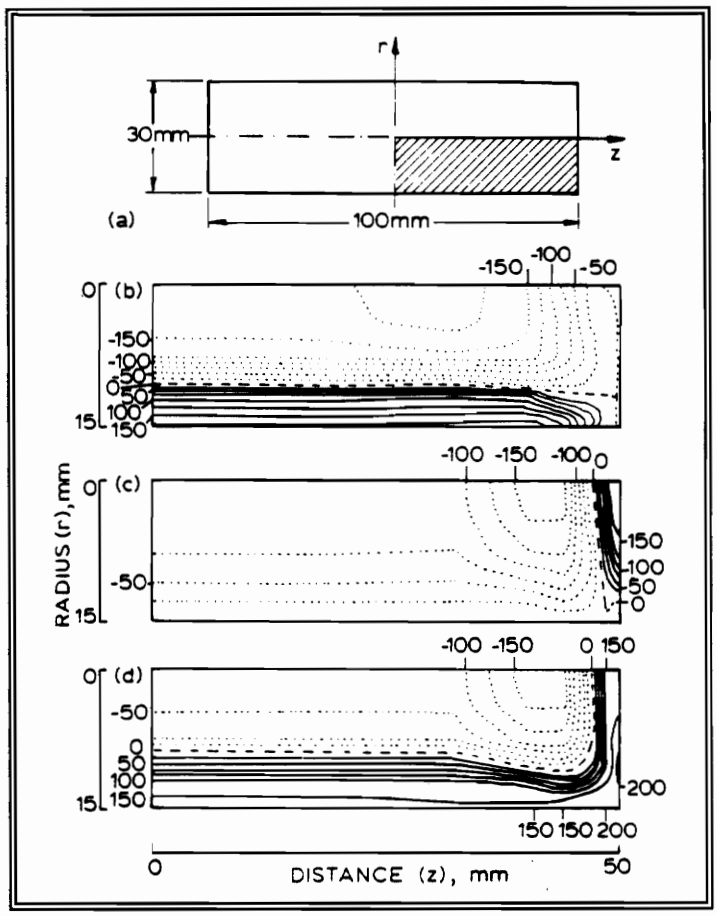

Figure 2-3 Quenching Stresses Modeled In Pipe After 1.7 Seconds (a) Pipe Sector Modeled, (b) Axial, σ_z, (c) Radial, σ_r, (d) Tangential, σ_t

the inner material will cool and accordingly contract placing the already cold exterior surface under compression.(39) Phase transformations cause additional volume changes which, in the case of the martensite transformation in steel, offset compressive stresses in the surface and often result in tension.

Comparison between FEM and x-ray determined residual stresses has been examined by Burnett and is displayed in Figure 2-4.(40) The analysis considers a temperature drop between 980 and 0° C in a carbon steel cylinder and takes into consideration the phase transformation from austenite to martensite. The agreement between theory and experiment is excellent. Todaro, et al. compare two residual stress measuring techniques for examining quenching stresses through the thickness of a cylinder of low carbon steel.(41) After sectioning, the flat faces of the cylinder were tested by x-ray and ultrasonic methods. The results parallel those of Figure 2-4 but with more scatter in the x-ray data. This can be expected because "the large scatter in the data is likely due to the broadness of the diffraction peaks, a direct result of quenching."(41)

For cylinders there is an obvious dependance of the development of thermal and residual stresses on the diameter's dimension.(42)(38) This is illustrated in Figure 2-5 with the variation in σ_t and σ_z as function of diameter. No phase transformation was considered. The magnitudes change but the profiles are similar. In small tubes this effect is estimated to disappear if the thickness is small compared to the mean radius.(4) In thick-walled cylinders curvature is a significant factor in thermal stress generation and analysis.

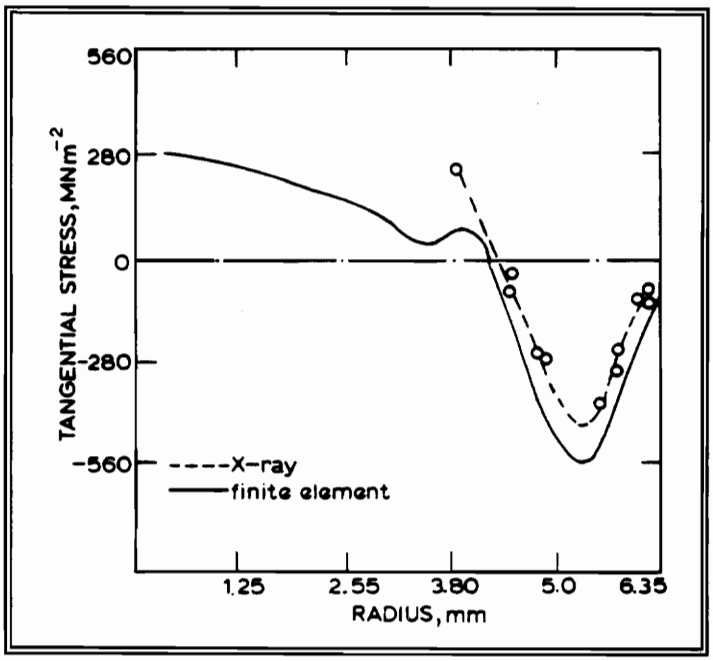

Figure 2-4 Comparison Between Residual Stresses In A Low Carbon Cylinder Determined By FEM And X-ray Diffraction

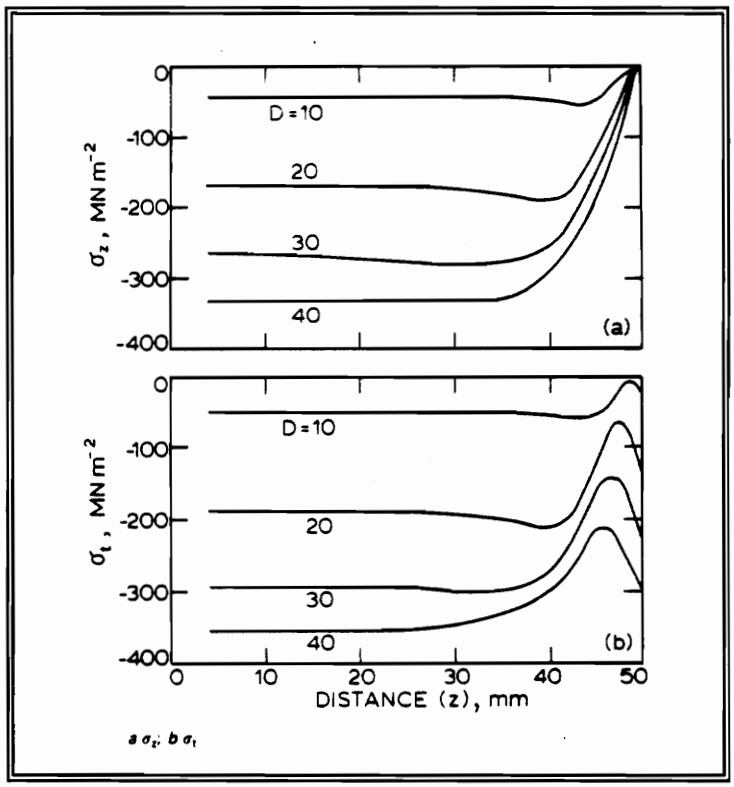

Figure 2-5 Quenching Residual Stresses In A Cylinder As A Function Of Diameter

Numerous other works on modeling investigate specialized features ranging from quenching stresses in a thick walled cylinder with an embedded, inner edge, or outer edge crack to quenching stresses in the area of a butt welded pipe.(43)(44) Also, stresses developed above and below critical shear temperatures, or stress fields in an individual metallurgical phase can be calculated.(45)(46)(47)(48)(49) Fletcher and Soomro studied the effect of the initial stress state on steel's viscoelastic response to quenching.(50) They found that residual stresses did affect the relaxation of quenching stresses. Also, the final residual stress state is influenced by the initial stress state.

2.5.2 Thermal Stresses From Welding

It is well known that welds can contain high residual stresses.(51)(52)(53)(54)(55)(56) Any materials joining process which injects steep thermal gradients as in welding is a prime candidate for damaging thermal stresses. Figure 2-6 from Analysis of Welded Structures gives an example of the differential heating in a material during welding.(51) The residual stresses and distortions produced are complex and customarily harmful to the structural integrity of the ship, bridge, pressure vessel, etc. which has been welded. High tensile stresses in weldments commonly augment brittle fracture, fatigue, and SCC. Compressive stresses or distortions reduce buckling strength. Figure 2-7 illustrates the labyrinthine stress state which can be developed in welded structures. Restraint during welding and cooling is consequential to the specific stress distribution developed.(53) Automatic welding procedures contain the drawback of fixed parts leading to higher constraints and larger residual stresses. Manual welding without fixtures can lead to misalignments. The two most important welding parameters which affect the

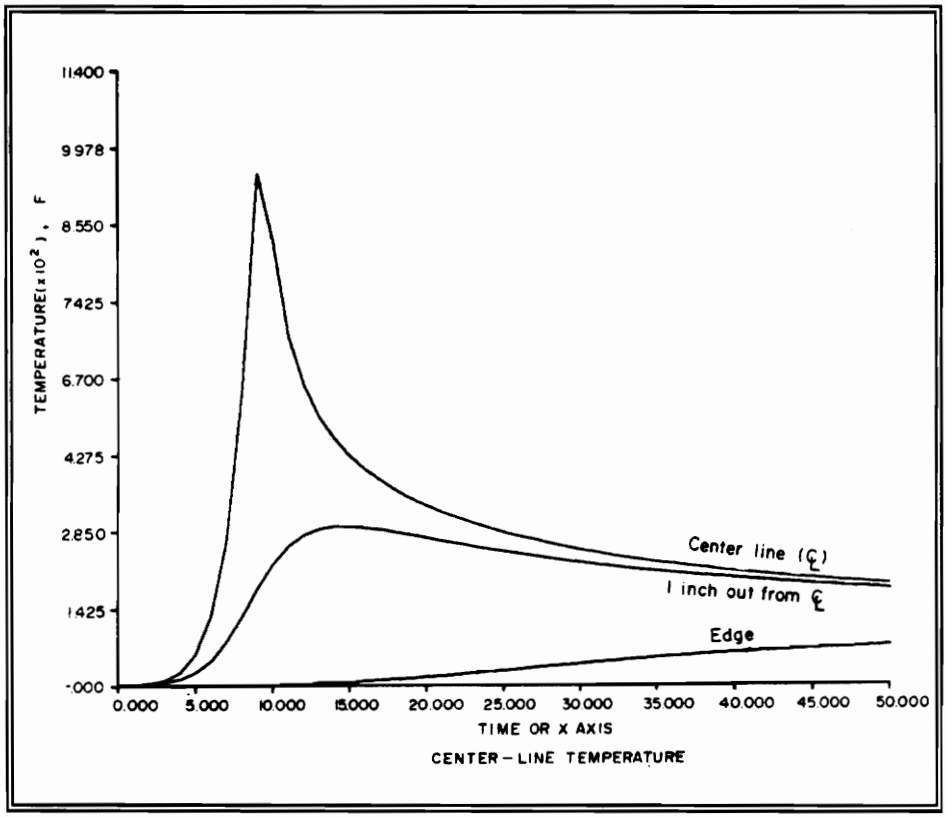

Figure 2-6 Sample Temperature Gradients In A Material During Welding

Figure 2-7 Residual Stress Contours In Welded Shape 15H290 Welds Are In The Inside Corners Of The I Shape

generation of thermal gradients and therefore, residual stresses are the energy input and the welding speed.

Modeling of welding thermal and residual stresses has the additional complications caused by quenching stresses:

- molten to solid phase transformation,
- differences in the base and filler material properties,
- inhomogeneous transient temperature fields, and
- variations in welding parameters.

Generally FEM, being able to account for nonlinearities, predicts more detailed and accurate conclusions than the classical theory of thin shells.

2.6 Circumferential Welding in Pipe

Butt welding is a common method for joining pipes. Butt welds are frequently found in power and process plants. Depending on the thickness of the pipe, the joining process may be comprised of single or multiple welding passes. After welding, the solidified filler metal and the heat affected zone (HAZ) often have stresses near the yield stress. Welding stresses are also found outside the welding zone.(57)

2.6.1 Single Pass Butt Welds

Numerous results on single pass butt welds are available.(53)(57)(58)(59)(60) A comparison of analytically calculated and experimentally measured axial (longitudinal) and hoop (tangential) stresses in a thin pipe is shown in Figure 2-8.(53) The tensile hoop stresses near the weld fusion line are balanced by compressive stresses further out from the weld center line. Jonsson and Josefson

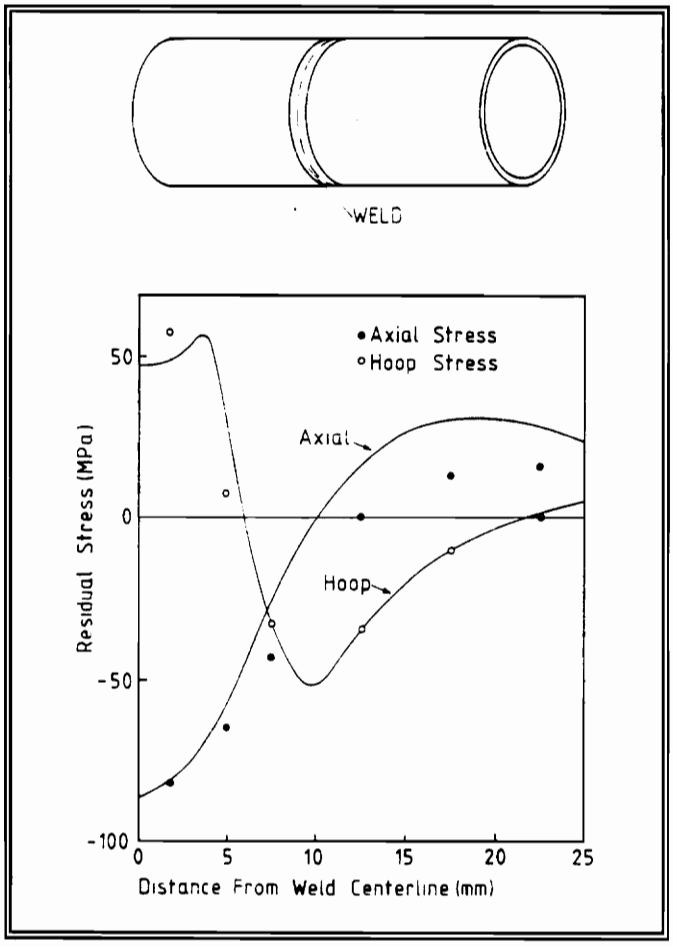

Figure 2-8 Welding Stresses From A Single Pass Butt Weld
The Theoretical Calculated Line Assumed Azimuthal Symmetry
The Circles Were Measured By X-ray Diffraction

compared welding stress conditions obtained by hole-drilling with two theoretical predictions. Their findings showed similar profiles to those of Figure 2-8, and there was good correlation among the methods even though the calculations did not include phase transformations.(59)

A simplifying assumption these calculations embrace is that of rotational symmetry. This significantly eases the calculative burden on the computer system and may be apropos. However, it is not a valid assumption. The unsymmetrical nature of these circumferential stresses will be shown later in this chapter and also in the results of of this experiment.

R. Karlsson canvassed the thermal and residual stresses of a single pass butt weld without azimuthal symmetry.(57) His experiments were performed on carbon manganese steel pipe of the ensuing dimensions; diameter = 114.3mm, length = 400mm, and thickness = 8mm. Figures 2-9 through 2-12 display the magnitudes of the thermal stresses at assorted times along with the residual stress state.(57) Figure 2-13 divulges the non-symmetric nature of the residuary stresses.(57) The calculated stresses display an azimuthal vicissitude of 250MPa.

2.6.2 Multi-Pass Butt Welds

Multi-pass butt welds are frequently needed for thicker piping, making modeling more complicated. An idealistic representation of a butt weld is shown in Figure 2-14.(53) In multi-pass welds stresses parallel with the weld extend several times the thickness of the welded specimen. In the transverse direction stress extention depends greately on the type of constraint used during welding.(61)

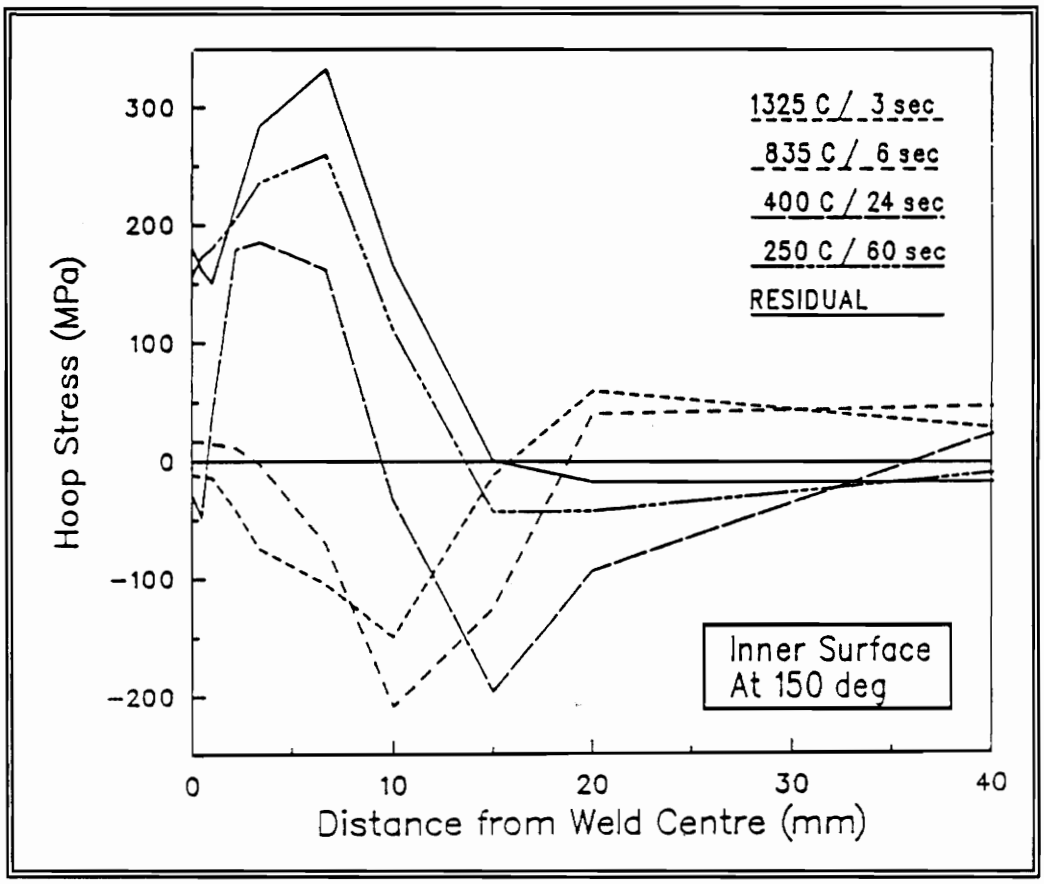

Figure 2-9 Hoop Welding Stresses On The Inner Surface Of A Cylinder With A Single Pass Butt Weld (By FEM)

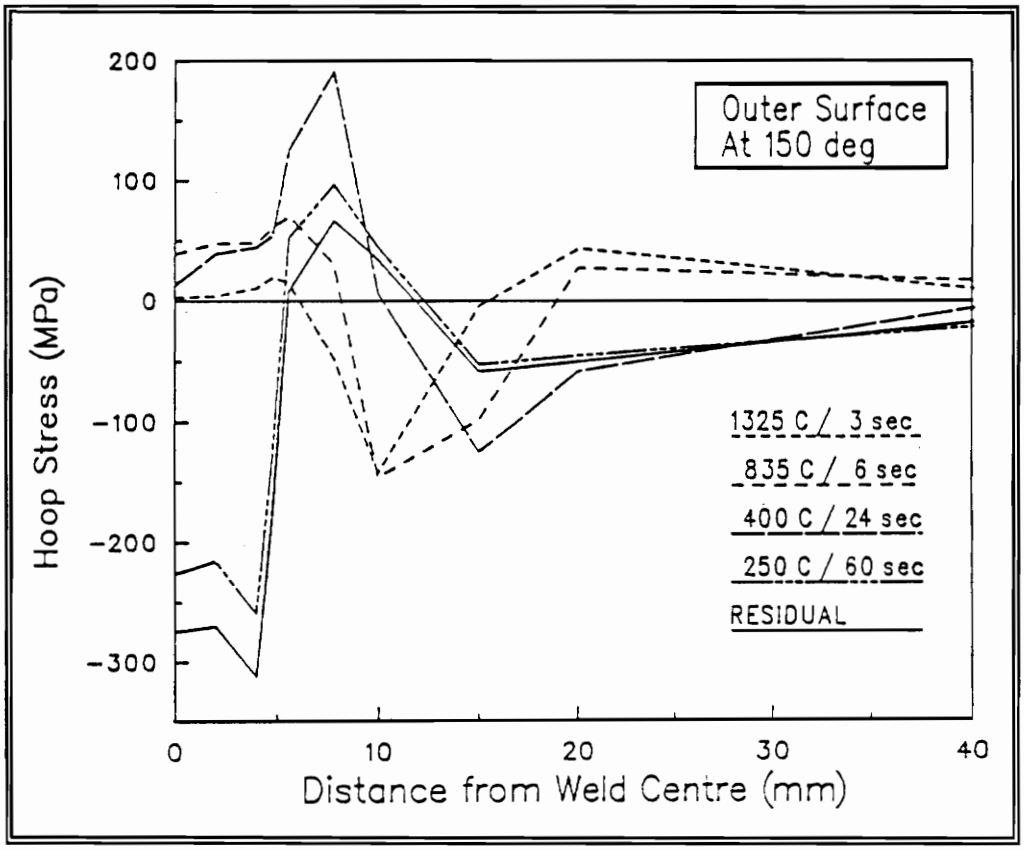

Figure 2-10 Hoop Welding Stresses On The Outer Surface Of A Cylinder With A Single Pass Butt Weld (By FEM)

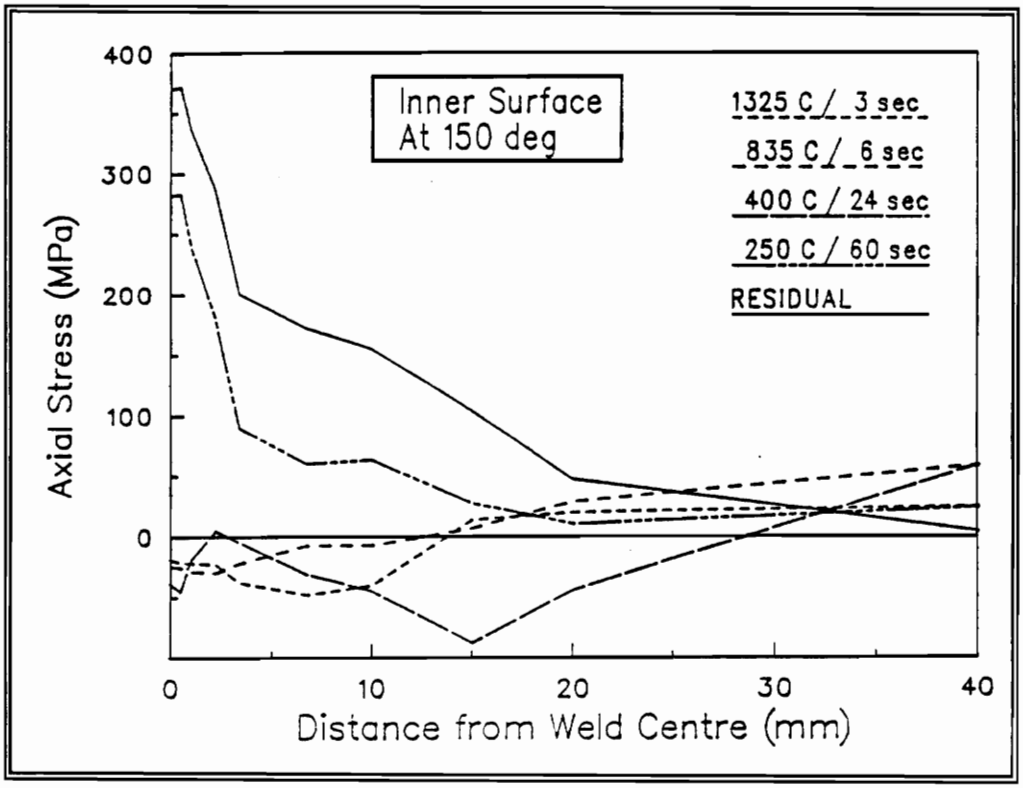

Figure 2-11 Axial Welding Stresses On The Inner Surface Of A Cylinder With A Single Pass Butt Weld (By FEM)

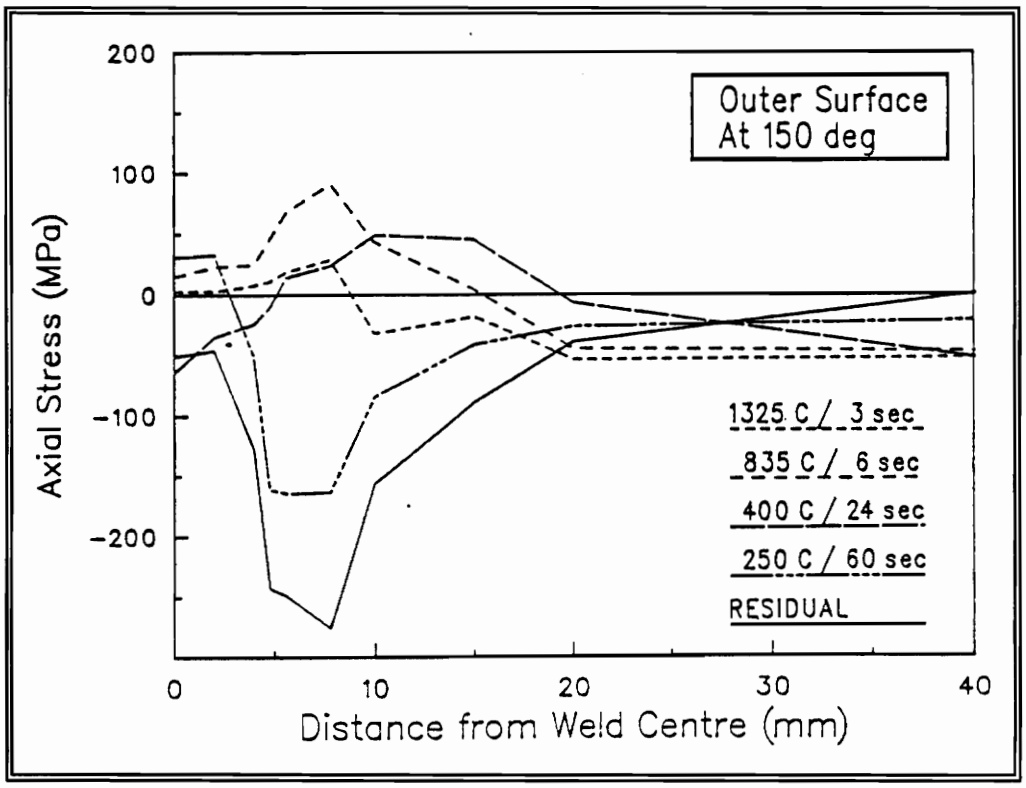

Figure 2-12 Axial Welding Stresses On The Outer Surface Of A Cylinder With A Single Pass Butt Weld (By FEM)

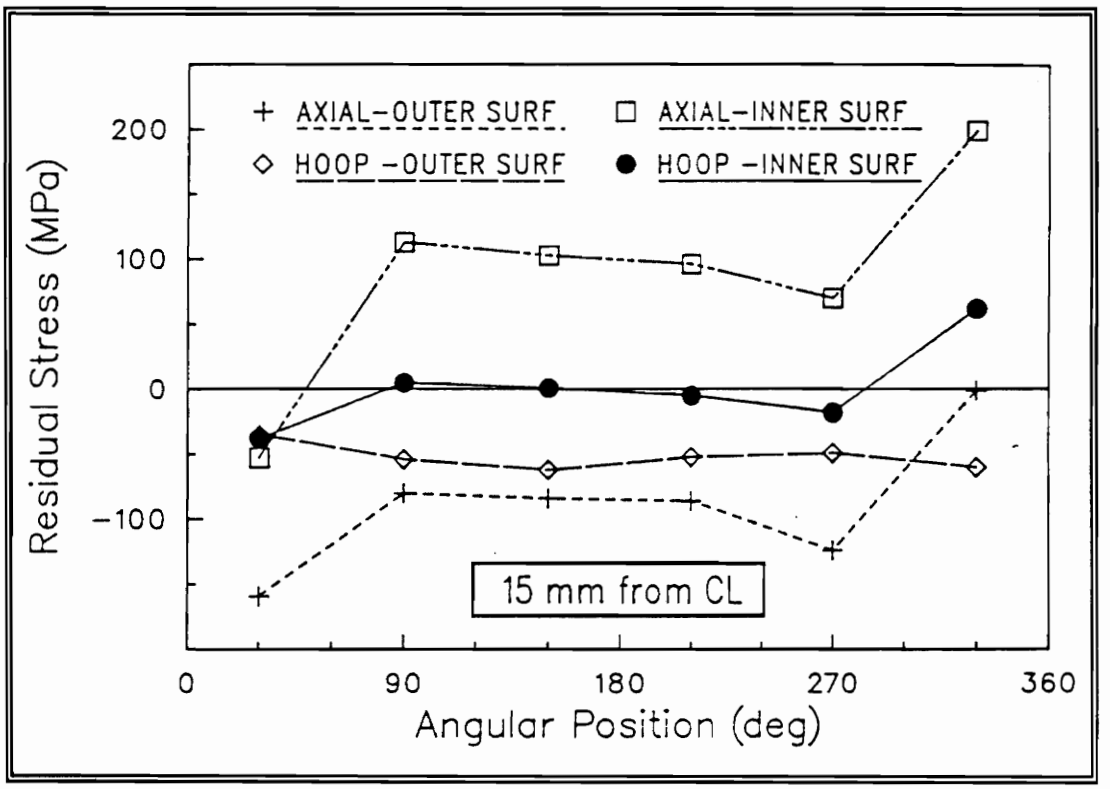

Figure 2-13 Axial And Hoop Azimuthal Residual Stresses For A Cylinder With A Single Pass Butt Weld (By FEM) CL Is The Center Line Of The Weld

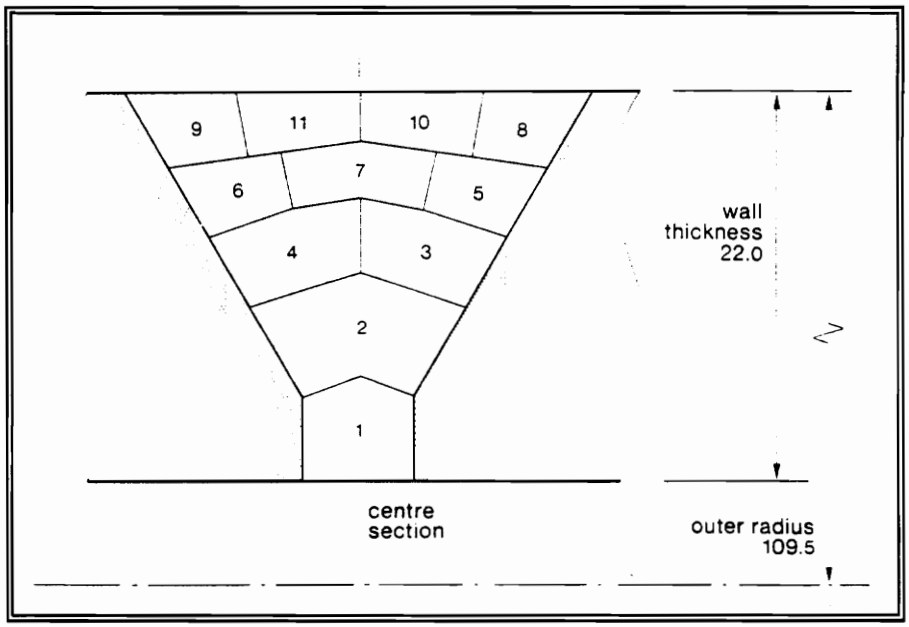

Figure 2-14 Idealized Weld Joint Of Eleven Passes In A Cylinder (mm)

T. Karlsson and Ellingson and Shack address multi-pass butt welds. T. Karlsson assumes axial symmetry to compare two welding geometries. A narrow gap (NG) and wider Single-U (U) grooves are examined. Calculations indicate that the last welding passes govern the final stress state. Figure 2-15 exhibits that the stresses are unevenly distributed through the wall thickness.(58) Case A and Case B refer to different FEM mesh densities. A narrow gap groove is advantageous because it requires less filler material and shorter welding times. The results show large deflections in the welding stresses as a function of thickness through the cylinder.

Ellingson and Shack experimentally measured the residual stress state in multi-pass stainless steel weldments. Stress was assessed on the inside of the pipe by first sectioning and then strain gages and hole-drilling. The dimensions of the schedule 80 type stainless steel pipe were a wall thickness of 8 mm and a outer diameter of 100 mm. The strain rosettes were placed every 45 degrees around the circumference. The interesting stress distributions are displayed in Figure 2-16.(61) The gage positions 1 and 5, 2 and 6, 3 and 7 are respectively 2, 7, and 14 mm on either side of weld metal. The average width of the weld is 4 mm. Bar refers to a whole section while strip is a 2 mm thick slice down the length of the bar.

No cases in this weld of seven passes exhibit axial symmetry. Some profiles appear periodic. Others are more irregular. The authors believe the distribution is induced by welding and is not a function of seamless pipe production. This is supported by the findings that deviations in the circumferential wall thickness do not resemble the residual stress contours. It is also noted that the stop and start position of the welding passes showed no correlation to the stress profile.(61) Another pipe with a

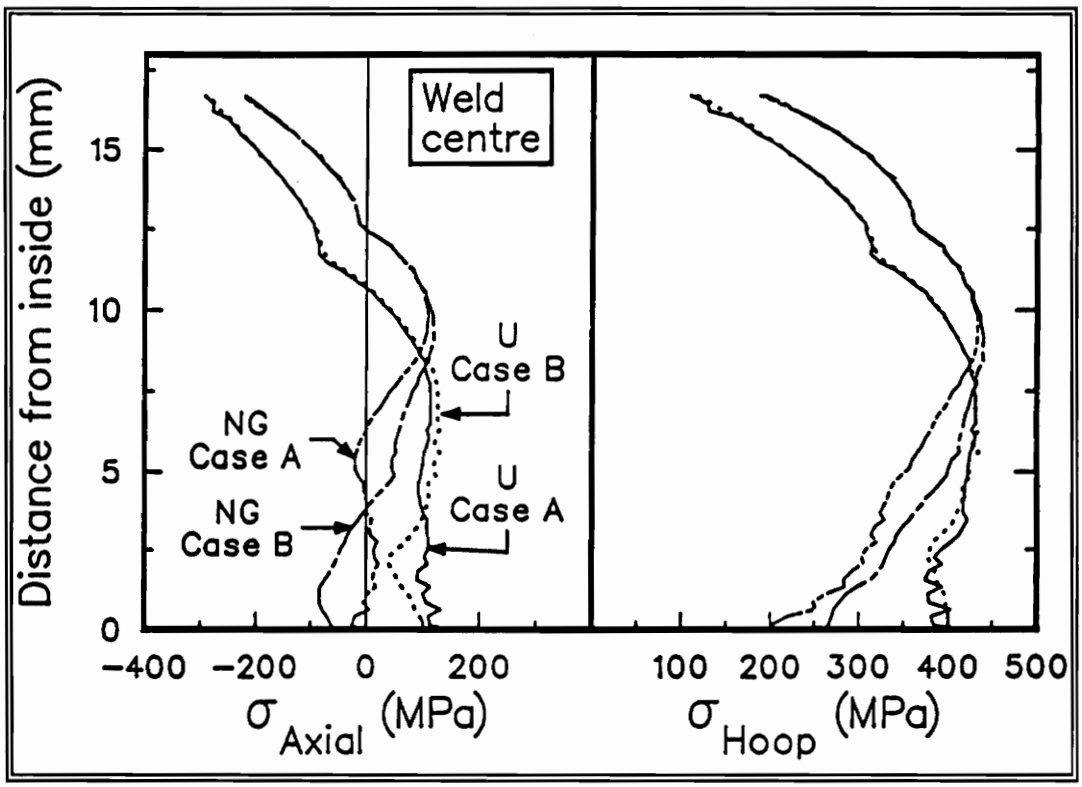

Figure 2-15 Residual Stresses Through The Thickness Of A Welded Pipe Case A and B Refer to Differing FEM Mesh Densities

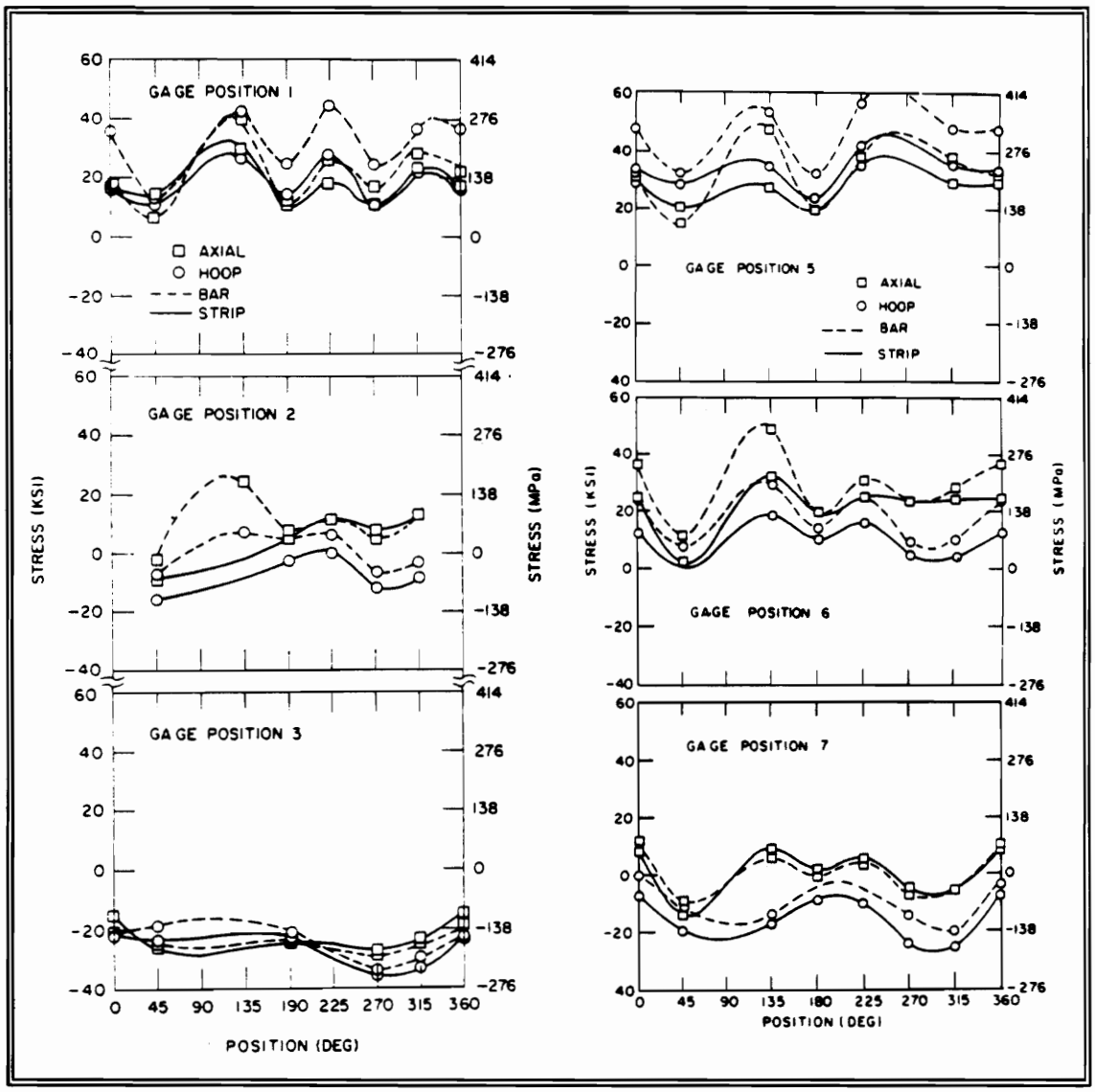

Figure 2-16 Axial And Hoop Residual Stresses At Various Gage Positions Around The Circumference Of A Cylinder Due To A Multi-Pass Butt Weld

larger diameter of 250 mm was similarly examined and had comparable but greater stress magnitudes.

These high tensile stresses on the inside surface are balanced by equal but compressive stresses on the outside surface of the pipe. When the stresses left by welding are unacceptability large, a stress relieving treatment is performed. Common for welded pipes is an induction heating stress improvement (IHSI). This routine changes the stresses by heating the outer surface of the pipe near the weld while cooling the interior with water. The final effect is to reverse the inside tensile stresses to compressive.(62)

2.7 Thermal Cycling of Small ΔTs

Almost all of the literature concerning thermal cycling revolves around large temperature variations ($\approx$ 1000° F - 1000° C). This is understandable because the larger the thermal gradients, the higher the potential for damage and failure. Also, the very common practices of quenching and welding generate these large temperature changes. However, small thermal gradients cannot be ignored especially in the light of Reference (25); that is, low thermal loadings can be sufficient for plastic collapse.

Works involving small ΔTs are now presented. Marsh cycled 304 and 316 stainless steel between differing temperatures to determine crack initiation time of thermal fatigue.(63) The smallest ΔT examined was 250° C to 100° C and the samples did not cleave in 100,000 applications. Ponter et al. studied the viscoelastic effect in copper cycled between 250° C and 50° C.(64)

The most interesting small ΔT experiment was performed to determine the cause of unexpected cracking discovered in a nuclear reactor's moderator circuit branch piping. At certain points colder heavy water at 140° C is introduced into the primary cooling circuit of 280° C. This causes a continuous thermal cycling of 140° C. The actual experiment was performed on the same material, AISI 347 stainless steel, cycled from 100 - 300° C in a servohydraulic universal testing machine with an imposed tensile load of 210 MPa. Crack initiation (0.2 mm) occurred in approximately 10^3 cycles.(65) This experiment exemplifies the damages possible with small range temperature cycling. With a temperature range of only 200° C and in a relatively small number of cycles, cracking occurred.

Small ΔT thermal cycling can give rise to heinous results and cannot be ignored, underestimated, or left un-investigated.

3.0 Principles of Residual Stress Determination By X-ray Diffraction

Methods for determining residual stresses differ in several respects. Some are destructive, and others are not. Most procedures are indirect and explore a parameter which is affected by the present state of stress. Such methods include hole-drilling, saw cutting, acoustic wave, and Barkhausen noise. Direct methods of residual stress determination are neutron and x-ray diffraction. Residual stress measurements are important to this project because residual stresses were monitored to determine the effects of thermal cycling.

3.1 Indirect Measurements of Residual Stress

Hole-drilling measures stress via change in local strain. As a small hole located between strain gages is drilled into the sample, material relaxes to compensate for that which has been removed. This results in a change of resistance in the strain gage and is related to the existing residual stresses.

Saw cutting qualitatively discloses the sign of the stress state. In this procedure a specimen is literally sawn in two. If the material closes around the blade, the material is in compression. The material is in tension if it opens or pulls away from the blade. This is a rough determination of stress. Saw cutting is very destructive as opposed to the moderate destruction of hole-drilling. Hole-drilling may be acceptable in some cases even though the hole is a stress raiser.

Acoustic waves gauge residuary stresses by sending waves through the material. The speed at which the wave can travel is affected by the state of stress. Compressive stress, a compacted matrix, impedes wave propagation. A drawback to this technique is that other sample factors, for example, multiple phases and inhomogeneities, also modify wave velocity.

Barkhausen noise is a technique only feasible for ferro-magnetic materials. Magnetic domains in a material can be flipped or realigned by a magnet. Residual stresses affect the ease of rotating these domains and thus present another parameter to investigate in determining residual stress.

3.2 Direct Measurement of Residual Stress

The only technique which measures strain instead a parameter influenced by residual stress is that of diffraction. X-ray and neutron are the two diffraction methods used in residual stress determination. Both measure the change in the lattice spacing in a crystalline solid and both are nondestructive. Although neutron diffraction is the most ideal technique because materials have a much smaller absorption coefficient for neutrons than for x-rays, meaning residual stresses can be measured through the thickness of the sample, x-ray diffraction is more commonly used. This fact is due to the unavailability of neutron diffraction facilities. In the United States neutron sources are found only in a few locations. While neutron diffraction reveals bulk residual stresses, x-ray diffraction discloses the stress states in a thin surface layer. Normally failures start on external surfaces so the residual stress state on the exterior is important information. Overall x-ray are fast, accessible, nondestructive, and even portable.

3.3 Bragg's Law

The d-spacing or distance between the crystalline planes is ascertained by the physical relationship defined by Bragg's Law, Eq. 3-1. Bragg's Law describes the

$$n\lambda = 2d_{hkl} \sin\theta \qquad \text{Eq. 3-1}$$

λ = incident x-ray wavelength
n = integer multiple of the radiation wavelength
d_{hkl} = the distance between planes with specified Miller indices hkl
θ = the angle of incidence of the x-ray to the hkl plane

action of an electromagnetic wave striking a crystalline lattice. Figure 3-1 displays this action.(66) When Bragg's Law is satisfied, the amplitude of the scattered radiation adds constructively, producing a diffraction peak. At any other angle the amplitudes add destructively, and no peak is produced. If the incident wavelength is primarily monochromatic and the incline angle is known, it is a simple calculation to determine the distance between the planes.

Stress, residual or applied, alters the spacing between the crystallographic planes from that of an unstressed lattice. An unstressed lattice has a d-spacing characteristic of that material. When the d-spacing decreases in size, this implies compressive stresses are pushing the atoms closer together. Larger d-spacings mean tensile stresses are pulling the atomic planes further apart. Figure 3-2 shows how the d-spacing shifts between a stressed and unstressed crystal.(67) Notice that if the lattice is viewed from the top, perpendicular to the line of the applied stresses, it seems that the d-spacing has increased due to the stress. However, if looked upon from a position parallel with the applied load it would suggest a smaller d-spacing and a compressive stress state. This exemplifies how important orientation is when

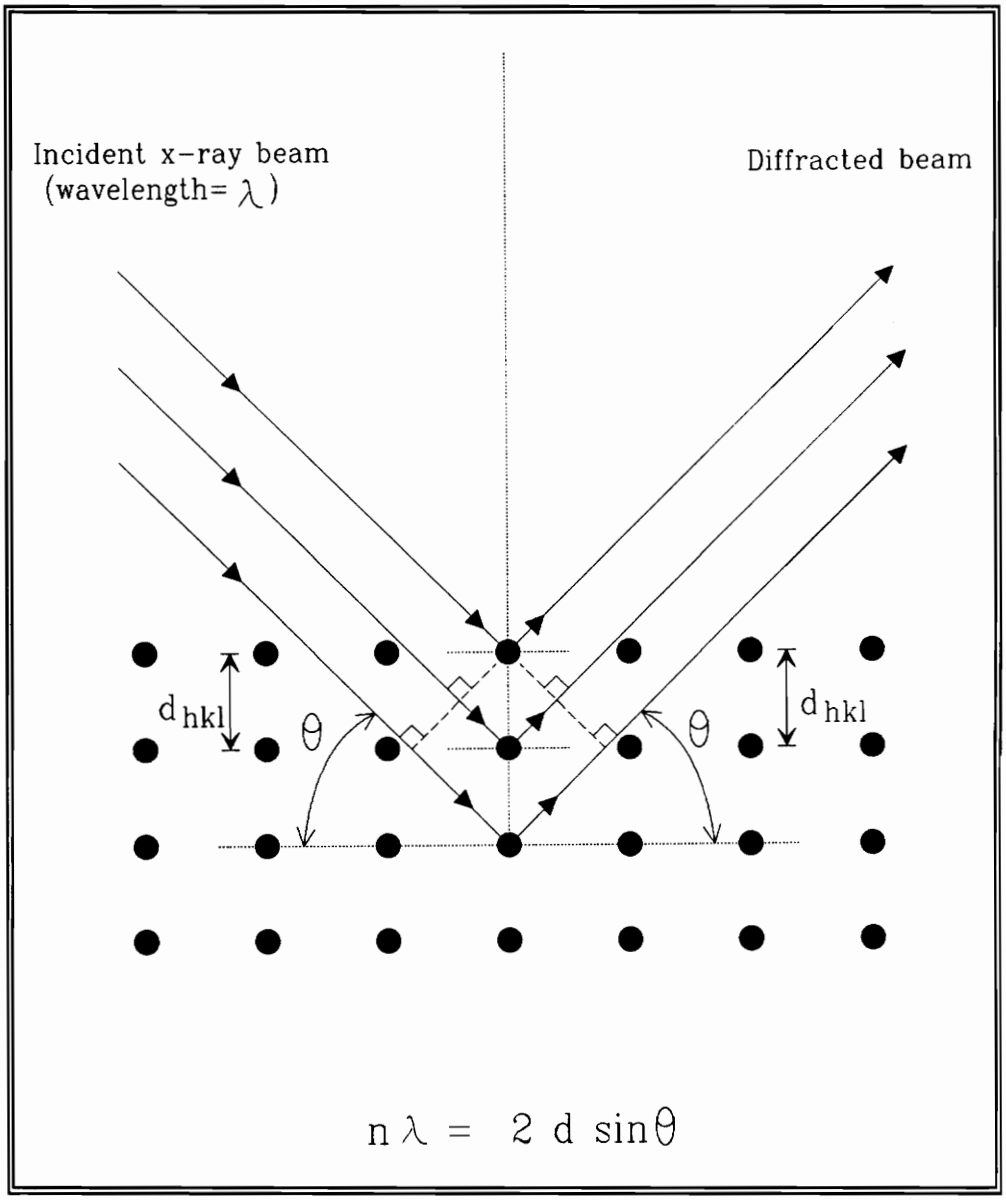

Figure 3-1 Diffraction Of X-rays By A Crystal Where Bragg's Law Is Satisfied

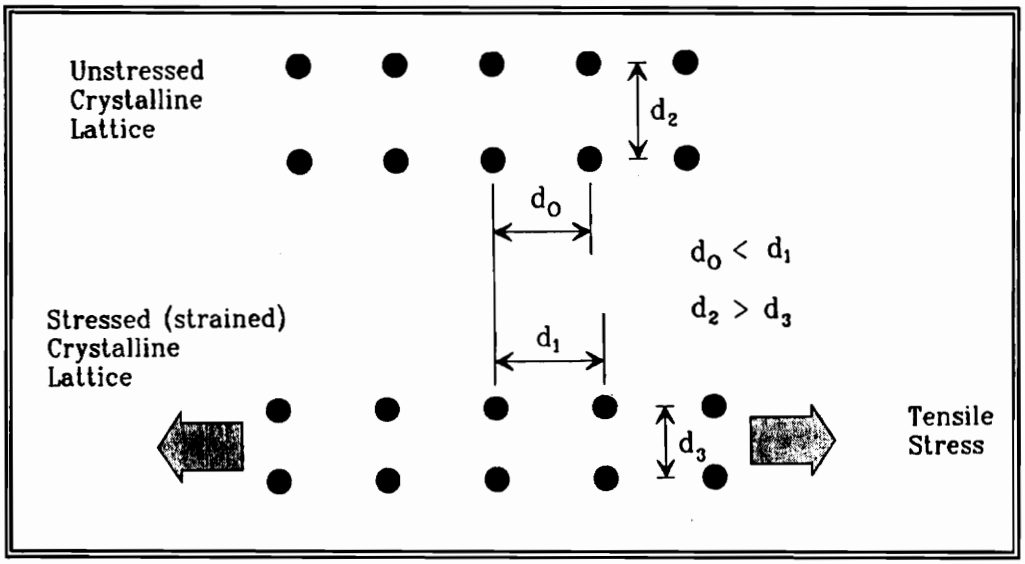

Figure 3-2 Unstressed And Stressed Crystalline Lattice

determining the d-spacing, and that by shifting one's orientation, the observable d-spacing changes.

3.4 Polycrystalline Materials

When an incident x-ray, λ, strikes a crystalline solid, the atomic planes which satisfy Bragg's Law diffract at angle θ. The distance between atomic planes is derived from the diffraction angle, θ, which is a function of the diffraction peak position. of this In a polycrystalline material with randomly oriented grains some grains will be aligned for diffraction; others will not. In an unstressed polycrystalline solid, regardless of the inclination of the incident x-ray, the d-spacings remain equivalent for similar planes. This is not so in a material under stress.

Stress applied to a polycrystalline material produces small changes in the d-spacing, the magnitude of which depend on the orientation between the stress field and an individual grain and the value of the stress. If this stressed polycrystalline material is subjected to x-rays from several angles, new grains with different d-spacings are brought into alignment to diffract. This means that the diffracted x-ray peak shifts as illustrated in Figure 3-3.(68) The amount and direction of the shift from that of an unstressed lattice is the basis for determining stress.

This technique is actually measuring the strain, not the stress. Strain is the change in length divided by the original length or, in this case, the change in d-spacing divided by the d-spacing of an unstressed lattice. Eq. 3-2 on page 49 is the equation for one dimensional strain. The geometry of a three dimensional system used in x-ray diffraction measurements is depicted in Figure 3-4.(68)

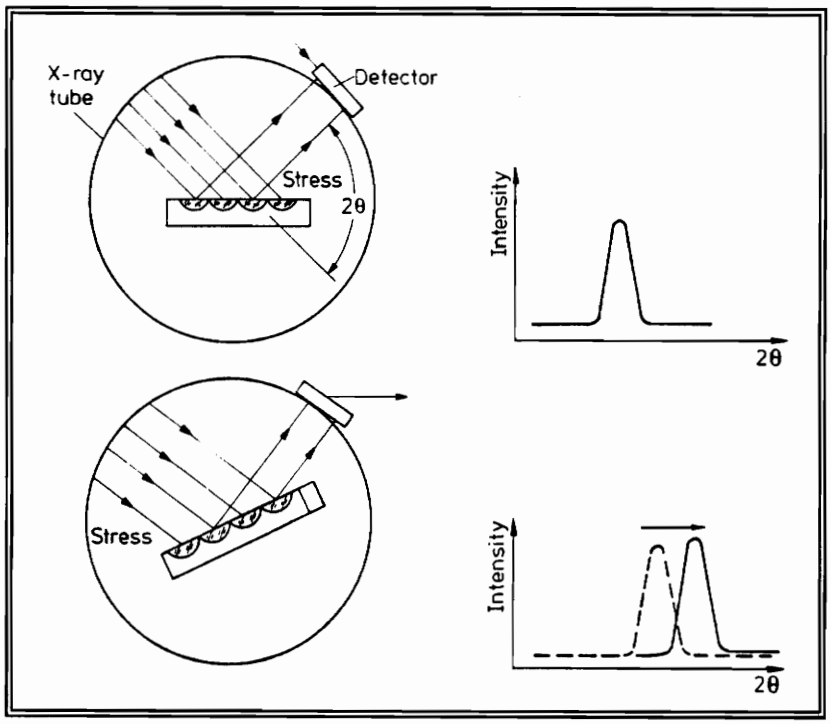

Figure 3-3 Shift In Diffraction Peak From A Strained Polycrystalline Solid Due To A New Orientation

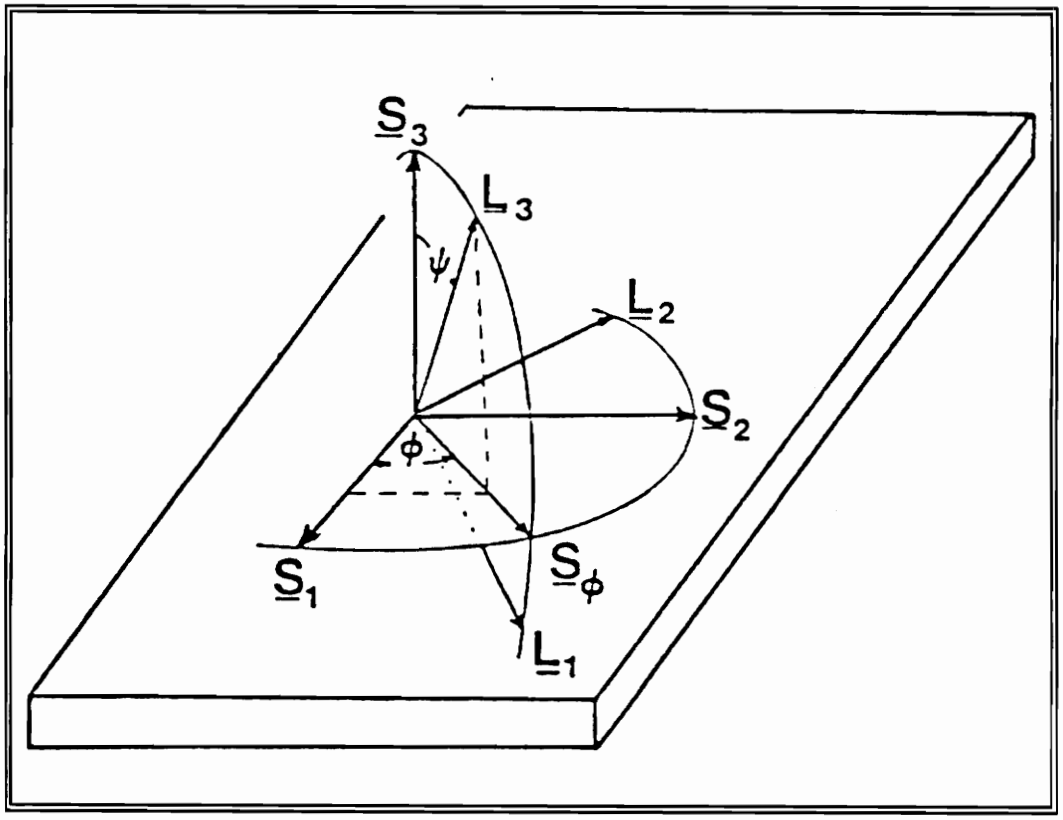

Figure 3-4 Three Dimensional Sample And Laboratory Coordinate Systems Used In X-ray Diffraction

From page 46

$$\epsilon = \frac{d_S - d_0}{d_0} \qquad \text{Eq. 3-2}$$

where

ϵ = strain,
d_0 = d-spacing of an unstressed lattice, and
d_S = d-spacing of a stressed lattice.

3.5 Stress-Strain Relations

S and L represent the two coordinate systems entailed in the residual stress measurements. S_1, S_2, and S_3 are the axes conveniently assigned to the sample, and L_1, L_2, and L_3 are the laboratory coordinates. L_3, located at an angle, ψ, from S_3, bisects the incident and diffracted x-rays and is perpendicular to the atomic planes satisfying Bragg's Law. The strain which is determined is the normal strain in the L_3 direction, ϵ_{33}. For convenience it is desirable to know the stresses in the directions of the sample coordinate system. This is acquired by translating the coordinate system, multiplying by the direction cosines, then invoking the stress-strain continuum relationships in a process developed by Dölle and shown below.(69)

$$(\epsilon'_{33})_{\phi\psi} = \frac{d_{\phi\psi} - d_0}{d_0} \qquad \text{Eq. 3-3}$$

$$= \epsilon_{11}\cos^2\phi\sin^2\psi + \epsilon_{12}\sin 2\phi\sin^2\psi + \epsilon_{22}\sin^2\phi\sin^2\psi + \epsilon_{33}\cos^2\psi + \epsilon_{13}\cos\phi\sin 2\psi + \epsilon_{23}\sin\phi\sin 2\psi$$

$$= \frac{1+\nu}{E}\left[\sigma_{11}\cos^2\phi + \sigma_{12}\sin 2\phi + \sigma_{22}\sin^2\phi - \sigma_{33}\right]\sin^2\psi + \frac{1+\nu}{E}\sigma_{33} - \frac{\nu}{E}\left[\sigma_{11} + \sigma_{22} + \sigma_{33}\right] + \frac{1+\nu}{E}\left[\sigma_{13}\cos\phi + \sigma_{23}\sin\phi\right]\sin 2\psi$$

In Equation 3-3 $d_{\psi\phi}$ is the d-spacing whose normal is oriented at angles ϕ and ψ from the sample coordinate system. E in these equations is the elastic constant particular to the certain set of hkl planes diffracting. The bulk elastic modulus cannot be used as, it is a conglomeration of all the lattice configurations, not just the set of diffracting planes.

3.6 Biaxial Stress Equation

The simplifying assumption of biaxiality is often adopted. This assumption is justified by the thinness of the layer penetrated by x-rays (for a Cr target incident on stainless steel ≈ 8μm). Consequently, the stress tensor, σ_{ij}, is zero if i or j = 3, and Eq. 3-3 is streamlined to the subsequent equation.

$$\frac{d_{\phi\psi} - d_0}{d_0} = \frac{1+\nu}{E}\sigma_\phi \sin^2\psi - \frac{\nu}{E}\left[\sigma_{11} + \sigma_{22}\right] \qquad \text{Eq. 3-4}$$

where

$$\sigma_\phi = \sigma_{11}\cos^2\phi + \sigma_{12}\sin 2\phi + \sigma_{22}\sin^2\phi - \sigma_{33},$$

and σ_ϕ is the stress component in the direction S_ϕ.

Eq. 3-4 can be further reduced because at $\psi = 0$

$$\frac{d_{\phi,0} - d_0}{d_0} = -\frac{\nu}{E}\left[\sigma_{11} + \sigma_{22}\right]$$

so the final form becomes Eq. 3-5.

$$\frac{d_{\phi\psi} - d_{\phi,0}}{d_0} = \frac{1+\nu}{E}\sigma_\phi \sin^2\psi \qquad \text{Eq. 3-5}$$

Eq. 3-5 predicts a linear relationship between d and $\sin^2\psi$. The slope, σ_ϕ, (dividing

out the elastic constants) is the residual stress in the volume of material irradiated by the incident beam. A minimum of two ψ tilt angles are required to determine the residual stress state, but for maximum accuracy and reliability in the d versus $\sin^2\psi$ equation more angles are better. The d-spacings obtained from multiple ψ angle diffraction peaks are linearly regressed versus $\sin^2\psi$ to identify the best fitting line. Figure 3-5 illustrates multiple angles and their diffraction peaks.(67)

The d versus $\sin^2\psi$ plot is not always linear. There are several possible explanations for the non-linearity. When there appears to be a split in $\psi > 0$ and $\psi < 0$ data, a shear stress is present. If no split is apparent but non-linearity is obvious preferred orientation, triaxial stresses, sample misalignment, or large grain size may be the cause.

For a more thorough explanation of residual stress determination by x-ray diffraction see References (68) and (70).

3.7 X-ray Residual Stress Analyzer

The residual stress measurements of this experiment were made with a Technology for Energy Corporation (TEC) Model 1610 Mobile X-ray Stress Analysis System. A few system specifics are a position-sensitive proportional x-ray counter, a low power x-ray tube, and a portable x-ray detector and electronics package. The system is shown in Figure 3-6.(67) More information can be found in the TEC operation manual.(71) A Cr x-ray target was engaged to produce the x-rays, CrKβ $\lambda = 2.08487$Å , which were directed through a 3mm circular collimator. The low power x-ray tube was maintained at 1.7mA and 35kV. Ten ψ angles were

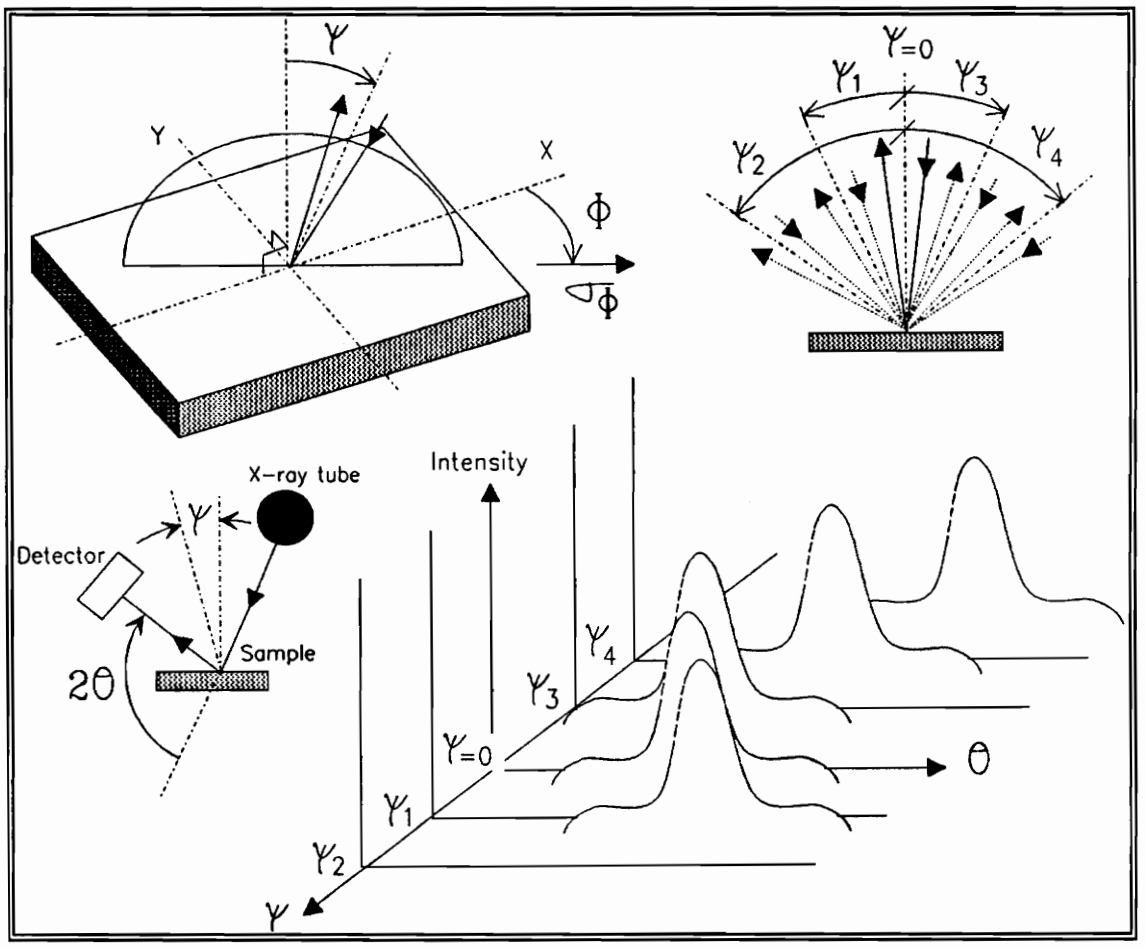

Figure 3-5 Multiple ψ Angles And Their Diffraction Peaks For Regression Of The Slope Equation

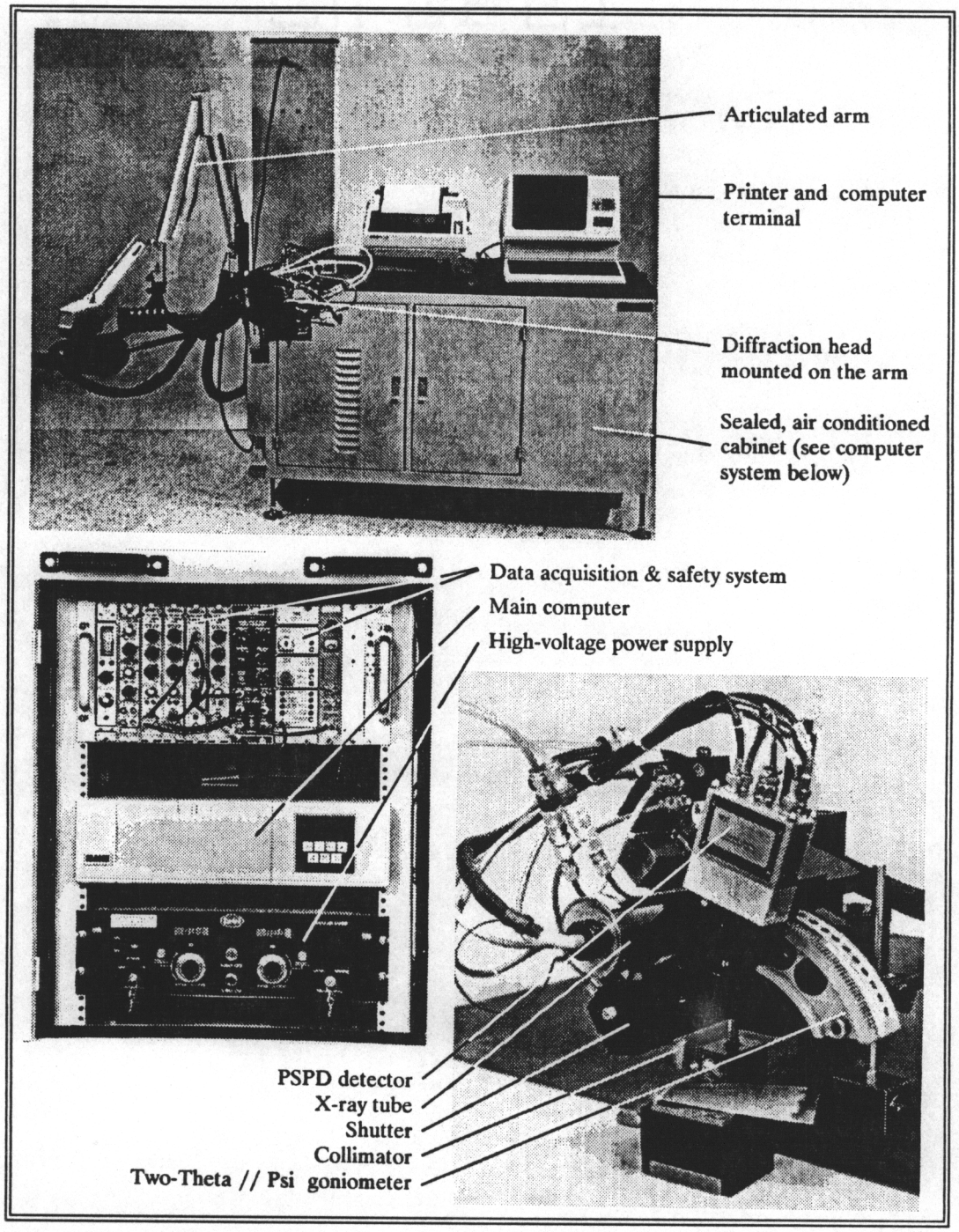

Figure 3-6 TEC Model 1610 Series X-ray Stress Analysis System

employed for the best accuracy possible in the d versus $\sin^2\psi$ regression. The TEC data analysis program acquires diffraction peak data as shown in Figure 3-7, adjusts for particular x-ray phenomena (absorption, Lorentz polarization, etc.), and then fits the peak to a parabola peak fitting program. From this the 2θ position is determined and the d-spacing calculated from Bragg's Law. The results of the internal calculations are shown in a typical TEC printout, Figure 3-8. The data are plotted assuming biaxial stresses as shown in Figures 3-9 and 3-10. The figures display data for a material which has compressive and tensile residual stresses, respectively. The residual stress is given along with error estimates due to counting statistics and goodness of fit. Note that there is no attempt to use multiple regression to recover any shear stresses present. However, as will be discussed in the Experimental Procedures, the data from the TEC print out can be input into a personal computer and fit to a multiple regression using the statistical program ABstat to recover any shear stresses.(72)

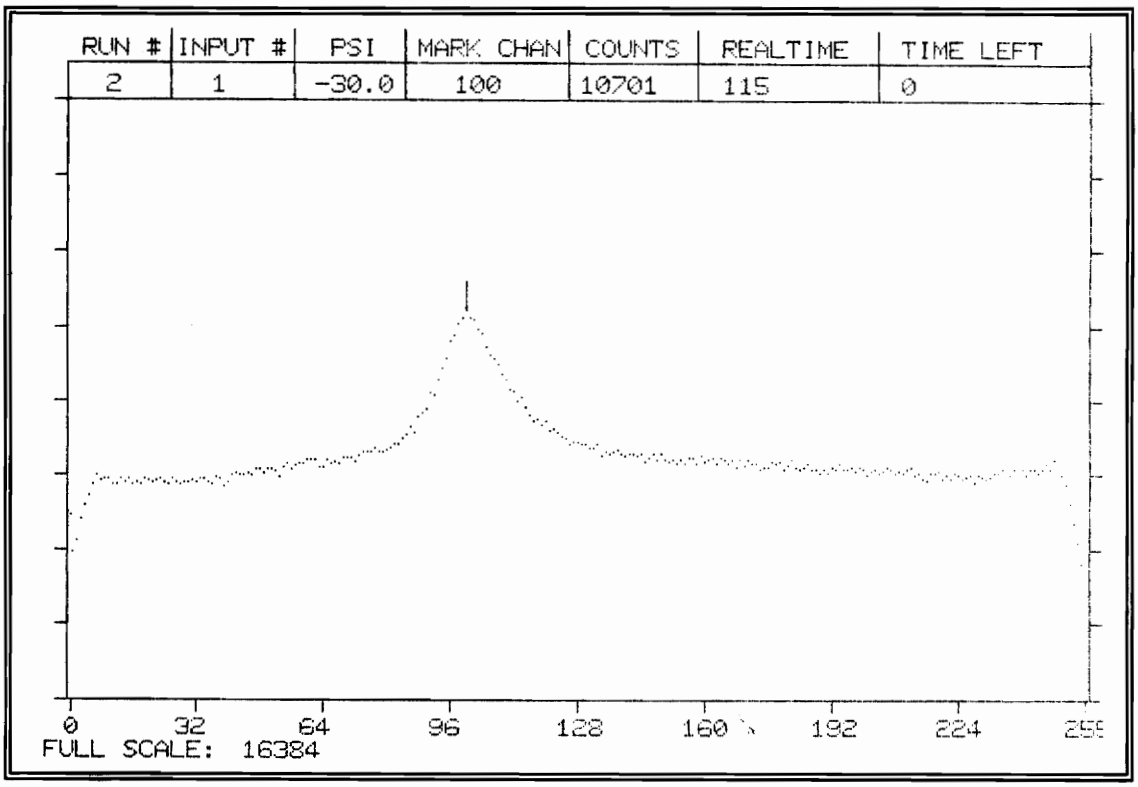

Figure 3-7 A Typical Austenite (311) Diffraction Peak From Uncycled 316L Stainless Steel Pipe

********** Residual Stress Analysis Report **********

Date: 21-NOV-89 Time: 16:13:42

Sample Description :
#1pipe,Cr,149,no filter, 20 thermal cycles
circle 1, postn 12

System Hardware Configuration :
Auto Psi Angle Drive
Psi Angle Position Encoder

ADC Channels Full Scale		256
Collimator Slit Type -	Round	3.00
X-ray Target Material and Wavelength	Manganese	2.1030
Detector Mounting Block Bragg Angle		149.00
Oscillating Psi Angle		0.00
High Voltage and Beam Current	35000.	1.70
Peak Bounding Range (percent)		20.
Material ID Number		80
Material Type	304 Stainless (Cr 220)	
Stress Spectra File Specifications		000572.SPC
Stress Spectra Acquisition Date:	25-SEP-89	01:05:17
Stress Spectra Count Time (sec)		100
Calibration File Specifications		CLH2CR.149

Detector Calibration Coefficients
A 0.602618E-08 B 0.357926E-05 C 0.0589044 D 141.3375

Psi	Sin^2(Psi)	Pk Chan	Intens	FWHM	Kalp Cor	2-Theta	D Spacing	St. Dev.
-41.5	0.42649	104.61	738.3	2.66	0.00000	147.55	1.095160	0.000040
-30.0	0.23868	103.68	680.8	2.55	0.00000	147.49	1.095314	0.000038
-22.0	0.13085	102.40	757.8	2.27	0.00000	147.41	1.095529	0.000038
-12.0	0.03734	100.21	716.2	1.99	0.00000	147.28	1.095896	0.000031
0.0	0.00021	100.90	392.6	2.12	0.00000	147.32	1.095779	0.000048
10.0	0.03506	102.45	740.9	2.22	0.00000	147.42	1.095520	0.000036
15.0	0.07444	101.09	624.2	2.53	0.00000	147.33	1.095749	0.000041
25.0	0.18911	102.96	813.2	2.14	0.00000	147.45	1.095435	0.000033
35.0	0.34109	104.36	623.4	2.05	0.00000	147.53	1.095201	0.000032
41.5	0.45178	104.42	759.4	1.78	0.00000	147.53	1.095192	0.000026

Fitted Delta D vs Sin^2(Psi) Data

D Spacing Intercept		1.095756
Slope of Fitted Line		-1.447791E-03
Material Stress Constant		4.950000E-08
Residual Stress	-26.7 ksi	-184.0 MPa
Counting Statistics Stress Error (+/-)	1.3 ksi	9.2 MPa
Goodness of Fit Stress Error (+/-)	4.7 ksi	32.3 MPa
Total Stress Error (+/-)	4.9 ksi	33.6 MPa

Figure 3-8 TEC Data Printout Of A Stress Measurement

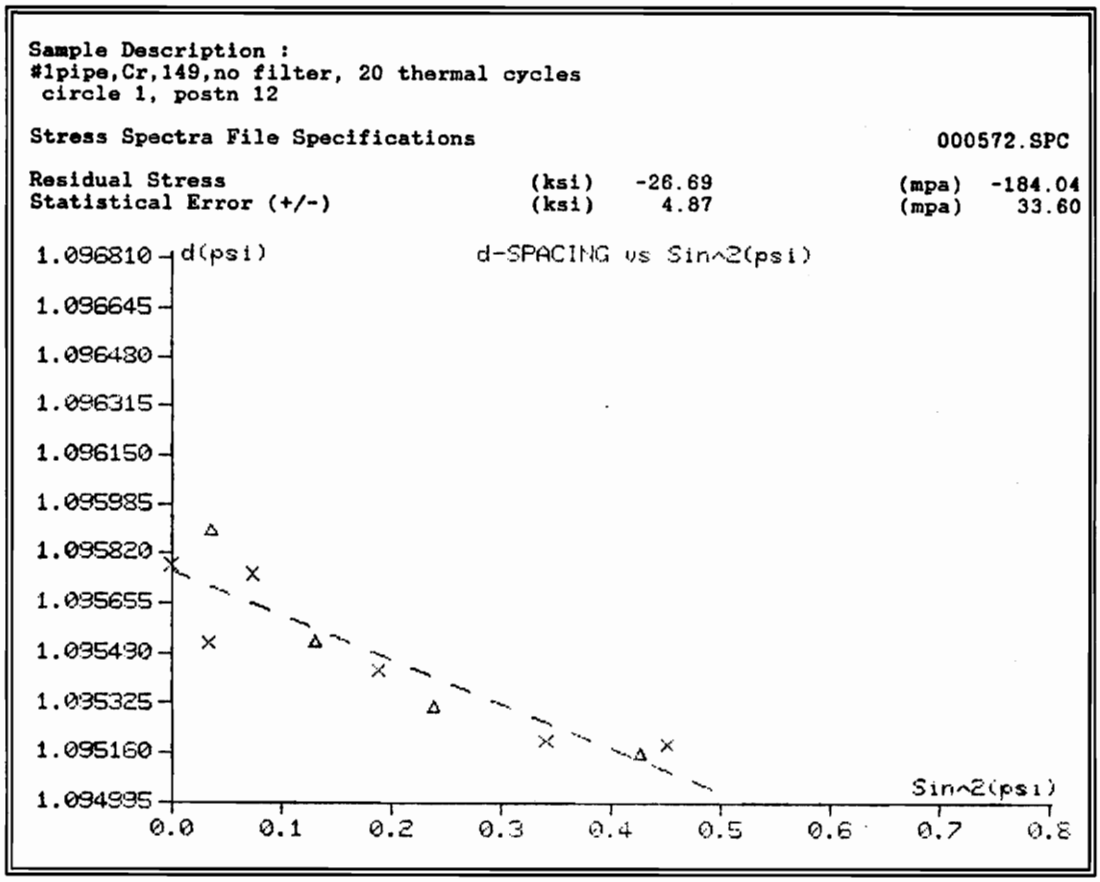

Figure 3-9 TEC Printout Of Compressive Residual Stress In A Material

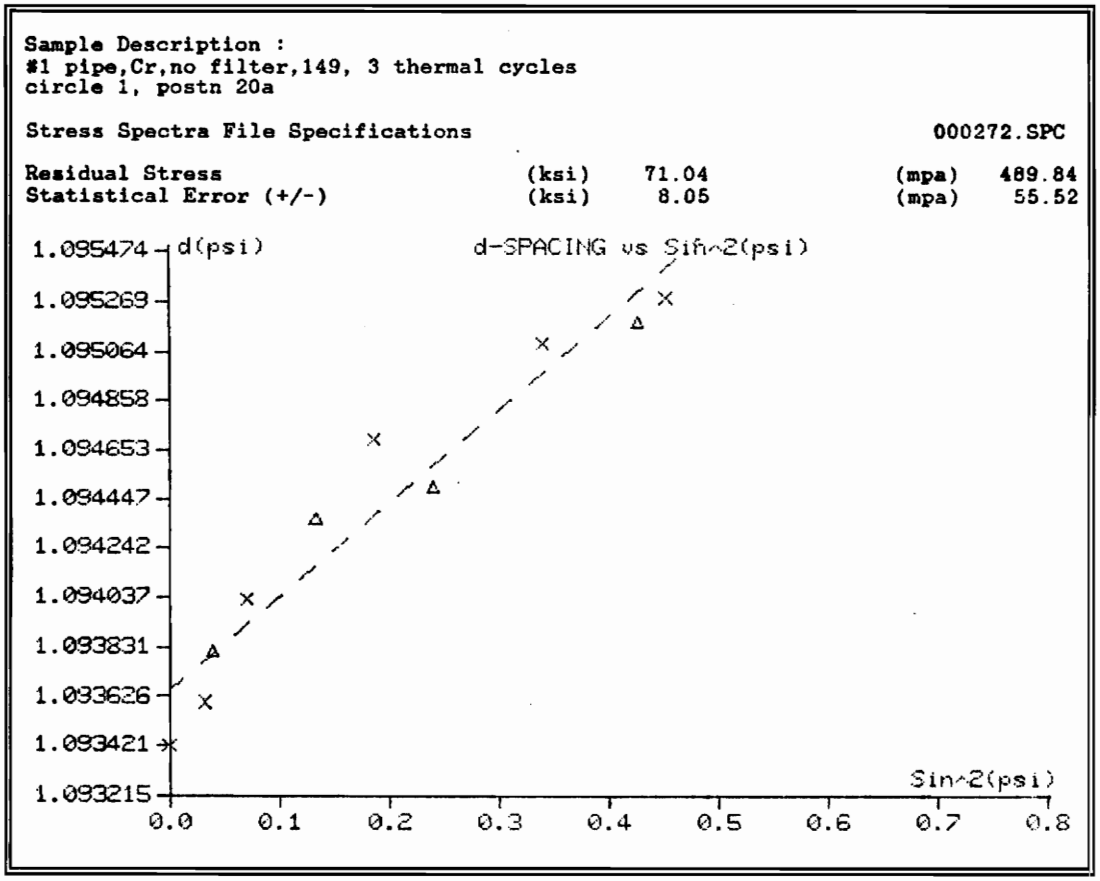

Figure 3-10 TEC Printout Of Tensile Residual Stress In A Material

4.0 Materials

The type of material used in this experiment was 316L austenitic stainless steel. Austenitic stainless steels have been in use about 70 years. They are valued for many applications because of their superior resistance to corrosion and high temperature oxidation. Their properties also include good fabricability, weldability, and essential physical and mechanical properties. Austenitic stainless steels are used extensively but especially in the power and chemical industries. Additional information on stainless steels can be found in References (73), (74), and (75).

4.1 Material Specifications

Only one specimen is used in the bulk of this experiment. This solitary specimen is a new section of thick-walled stainless steel pipe from of a food processing plant. The pipe is seamless and has a multi-pass circumferential butt weld, ground flush, at its center. A picture of the pipe is shown in Figure 4-1. The sample has the following dimensions:

- inside diameter - $3^{2}/_{16}$ inches,
- outside diameter - $4^{8}/_{16}$ inches, and
- length - 24 inches.

4.2 Chemical Analysis

Chemical analyses on the piping material was performed and provided with the piping section. Two tests on the 316L stainless steel elemental alloying compositions were made and are listed in Table 1. The numbers indicate weight percent and the balance is iron.

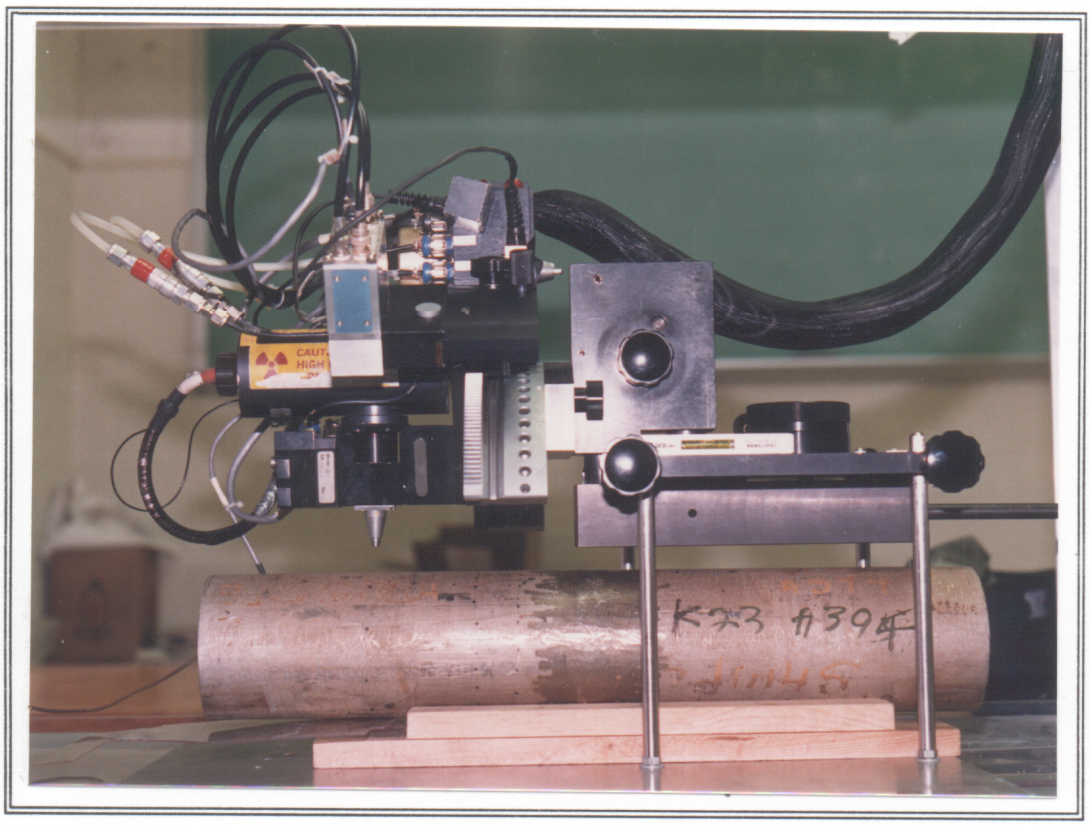

Figure 4-1 The 316L Thick-Walled Pipe In The Hoop Orientation Under The X-ray Stress Analyzer

Table 1 Chemical Analysis

	Cr	Ni	Mo	C	Mn	P	S	Si	Al
#1	16.53	11.30	2.08	0.015	1.73	0.024	0.026	0.38	--
#2	16.44	11.22	2.01	0.019	1.72	0.025	0.030	0.41	--

4.3 Material Properties

The chemical composition of the piping material is most important as the physical properties result from the chemistry along with production history. Two important physical properties presented now are the mechanical and temperature related properties.

4.3.1 Mechanical Properties

Along with the chemical analysis, data on the mechanical properties of the piping material were provided. Five tests on annealed specimens were performed. These results are listed in Table 2.

Table 2 Mechanical Properties

.02% yield strength	tensile strength	% elongation
34.0 ksi	79.8 ksi	70.0
34.0 ksi	81.0 ksi	70.0
36.0 ksi	81.0 ksi	71.0
36.0 ksi	79.0 ksi	74.0
36.0 ksi	81.0 ksi	70.0

Technically, austenitic stainless steels are not hardenable alloys. This statement is in reference to alloys such as carbon steel or aluminium which can be heat treated to

enhance strength. However, austenitic stainless steels do have the nature of stain- or work-hardening.(76)(77)(78) This characteristic of increasing stress versus strain behavior can be especially prevalent in 316L. The degree of work-hardening greatly depends on the application of the strain, and 316L will respond differently based on the size and frequency of the applied strain. An example of differing cyclic and monotonic responses for annealed 316 stainless steel is shown in Figure 4-2.(79)

4.3.2 Temperature Related Properties

Austenitic stainless steels have good high temperature resistance. However, a very relevant drawback to austenitic stainless steels is their poor thermal shock resistance. This behavior is due to stainless steel's relatively low thermal conductivity combined with a high linear expansion coefficient. This combination makes thermal cycling more of a concern in stainless steels than some other materials.

Another important property at high temperatures is the ability to resist creep. Generally creep properties are not a consideration at temperatures below about one third the melting temperature in kelvin, however, 316L stainless steel has shown some tendencies for low temperature logarithmic creep.(21)(22)(26)(80) Because of the short time the pipe was heating in the furnace, creep is not considered to be a factor in the experiment.

At room temperature austenite is technically not a metallurgically stable phase, as martensite is at a lower energy state. Of course, there must be some driving force to encourage the transition from one phase to another. Two common modes of driving this reaction are a temperature drop or low temperature coupled with deformation.

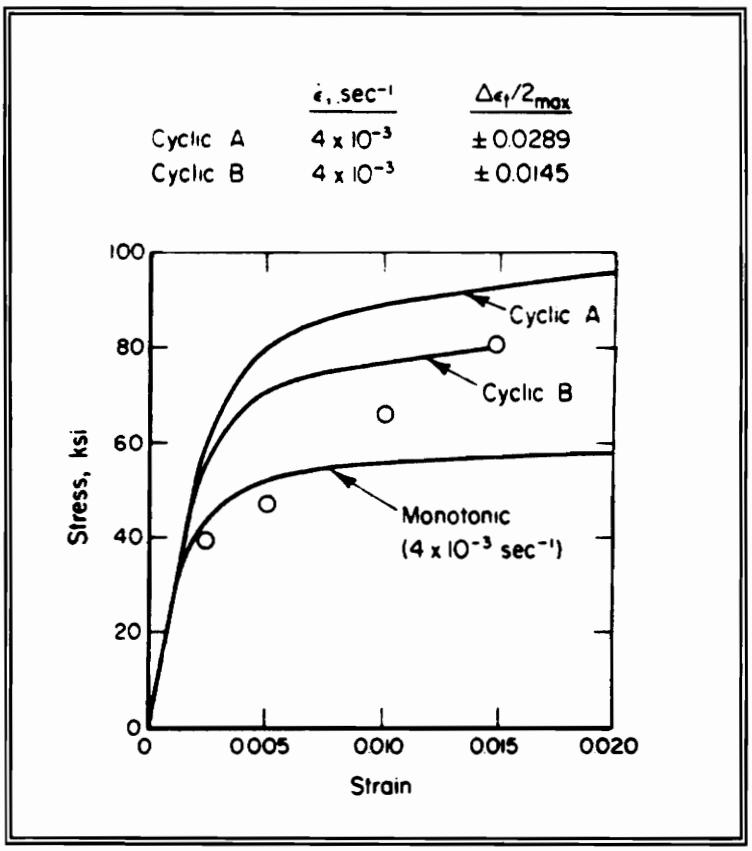

Figure 4-2 Behavior Of Annealed 316 Stainless Steel Under Differing Strains At 70° F, The Monotonic Curve Is The Standard Tensile Test, The A And B Curves Are Cyclical Reverse Loadings At Different Strain Rates, The Open Circles Represent Stress Behavior Versus Constant Strain

Equations based on composition have been developed to predict the temperature at which this transformation takes place. The martensitic transformation temperature equation is:(73)

$$M_S(^\circ C) = 1305-61.1(\%Ni)-41.7(\%Cr)-33.3(\%Mn) \quad \text{Eq. 4-1}$$
$$-27.8(\%Si)-1667\%(C+N).$$

Given the pipe's composition, the temperature at which martensite would start to precipitate, M_S, is below -150° C, nowhere in the region of temperatures involved with the quenching in this experiment. An equation to forecast temperature and deformation effects is:(74)

$$M_{d30}(^\circ C) = 497-462\%(C+N)-9.2(\%Si)-8.1(\%Mn) \quad \text{Eq. 4-2}$$
$$-13.7(\%Cr)-20(\%Ni)-18.5(\%Mo).$$

M_{d30} stands for the temperature at which 50% martensite is attained under a true strain of 0.3. From Equation 4-2 this temperature would be around -18° C. The effect of deformation transformation is unlikely to play a role in the experiment because -18° C is well below the quenchant temperature but also because 30% strain is very high and more along the lines of something seen in rolling or a similar deformation process. See Figure 4-2 for comparative engineering strain values. In conclusion, phase transformation is not expected.

4.4 Sample Fabrication

Sample fabrication is most important to a component's behavior and properties. Unfortunately, there was almost no information available about the production history of the pipe. Other than the composition and mechanical properties listed in Tables 1 and 2 and the knowledge that the weld had no post weld heat treating, nothing except visually gathered information was known at the time of the thermal

cycling and x-ray diffraction measurements. After cycling the pipe was dissected for microstructural evaluation.

4.4.1 Seamless Pipe Fabrication

An obvious feature of the pipe was that is was seamless. Production of seamless pipe varies from process to process and mill to mill, but some of the basics are included here. A solid cylindrical rod is heated to approximately 1200° C. The heated material is forced forward and encounters a centered piercing mandrel which forms a cavity in the rod. See Figure 4-3.(81) On the outside two or three rollers conform the tube. This shell is usually reheated for further fabrication, perhaps a second piercing. The next process is the reeling mill (similar to the piercing mill) where the wall thickness is slightly reduced. After being reeled the tube is sized in several passes similar to the reeling mill. Various annealing and surface finishing techniques exist.(81)

4.4.2 Circumferential Butt Weld

With no knowledge of the welding parameters except the lack of post weld heat treatment, all information known about the weld was determined after the thermal cycling when the pipe was sectioned for microstructural evaluation. All of the microstrucural analysis was performed courtesy of Oak Ridge National Laboratory.

A cross-section of the pipe and weld area is presented in Figure 4-4 at 2x magnification. The multi-pass butt weld consists of approximately twenty passes. The microstructure shows duplex austenite and delta ferrite phases. The measured 8 to 10 percent ferrite is a common phase in austenitic stainless steel welds. The

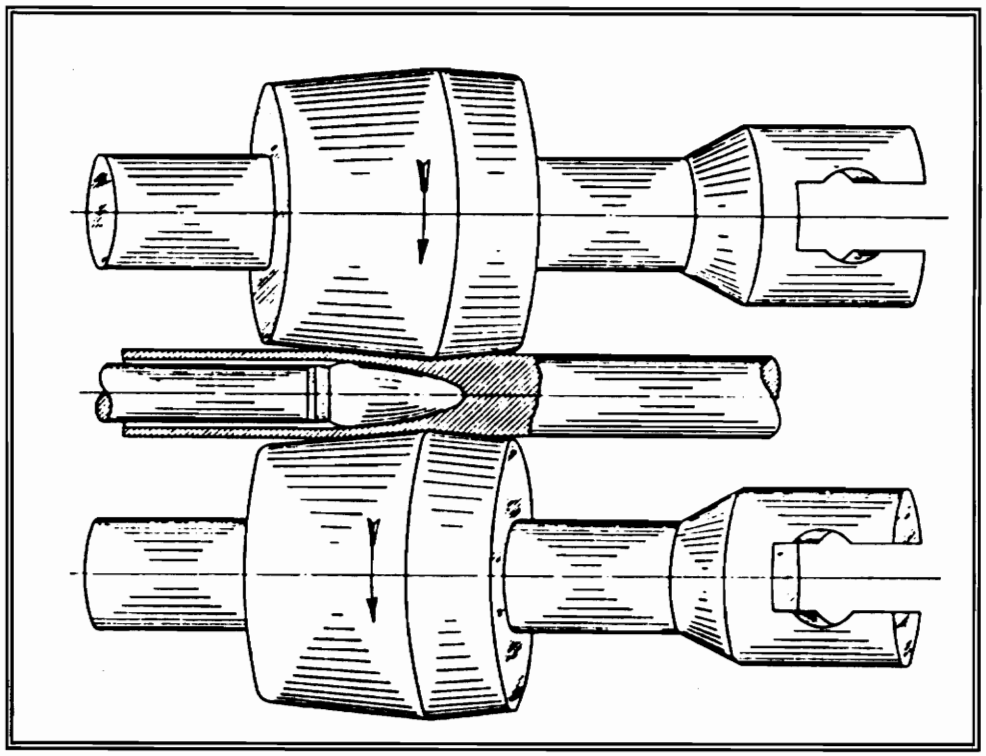

Figure 4-3 Sketch Of Seamless Pipe Piercing Mill

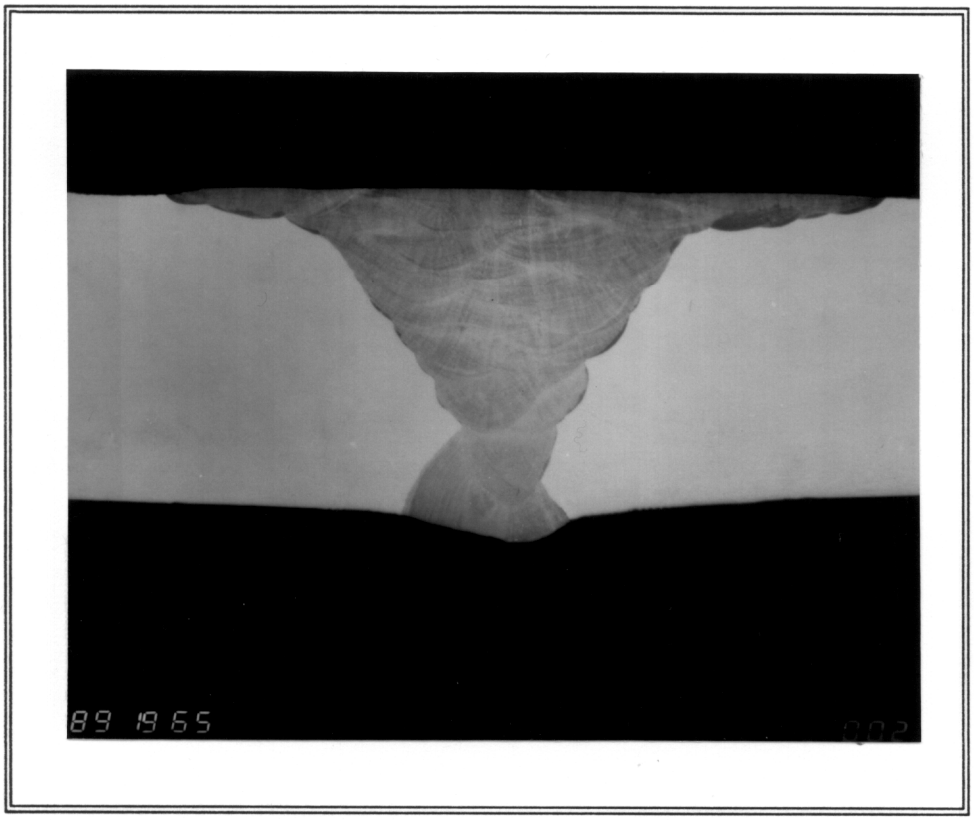

Figure 4-4 Transverse View Of The Weld And Wall Section Magnification Of Two

presence of ferrite in the microstructure helps to minimize the tendency of austenitic stainless steel for hot-cracking during the welding process. This percentage is the recommended amount of ferrite for an as-welded microstructure.(74)(82) The microstructure of the weld fusion line is exhibited in Figure 4-5 at 200x. The right side of the photograph faintly shows the base metal structure in the stainless steel wall material. A few black stringers, usually residual ferrite, are visible but generally the wall material is very clean. On the left side of Figure 4-5 is the fusion zone showing a matrix with delta ferrite in the structure. The microstructural features and ferrite content of the weld material vary depending on the position examined. Ferrite morphology varies from the top pass to the root pass. Variations are due to solidification rates and latter thermal cycling due to subsequent weld passes.(83)(84) Figure 4-6 reveals a crown, mid, and root pass. In the root pass dissolution of the ferrite takes place due to the heat effects of the subsequent passes. In the crown pass large columns of ferrite are visible. The mid-pass structure is between the other two.

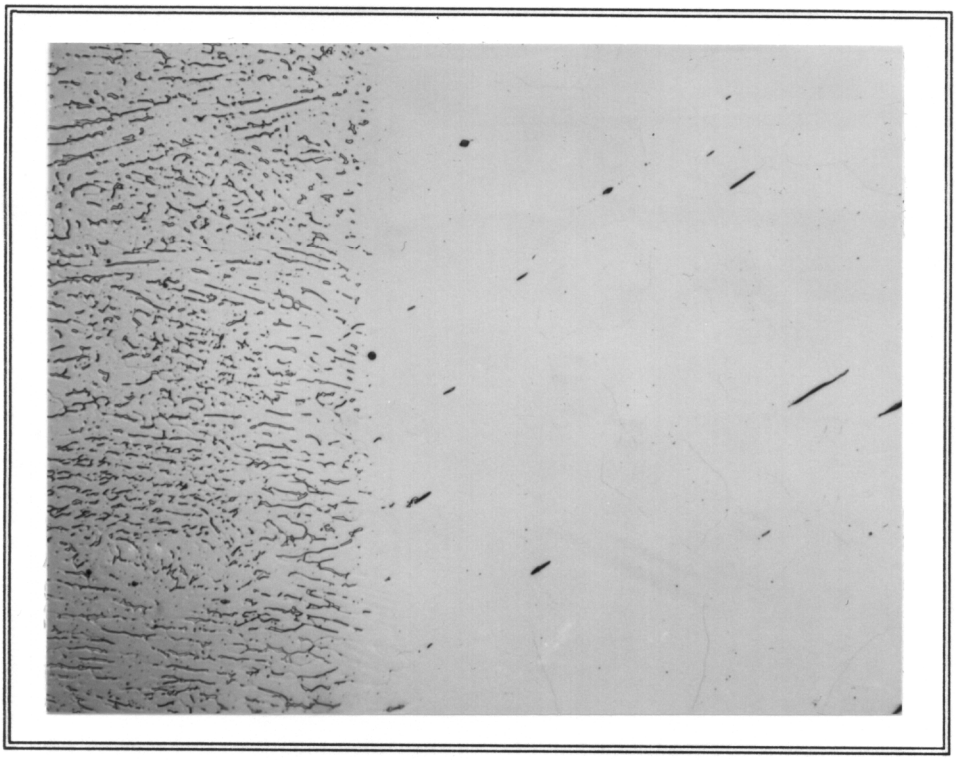

Figure 4-5 Weld And Wall Area Fusion Zone
Magnification Of 200X

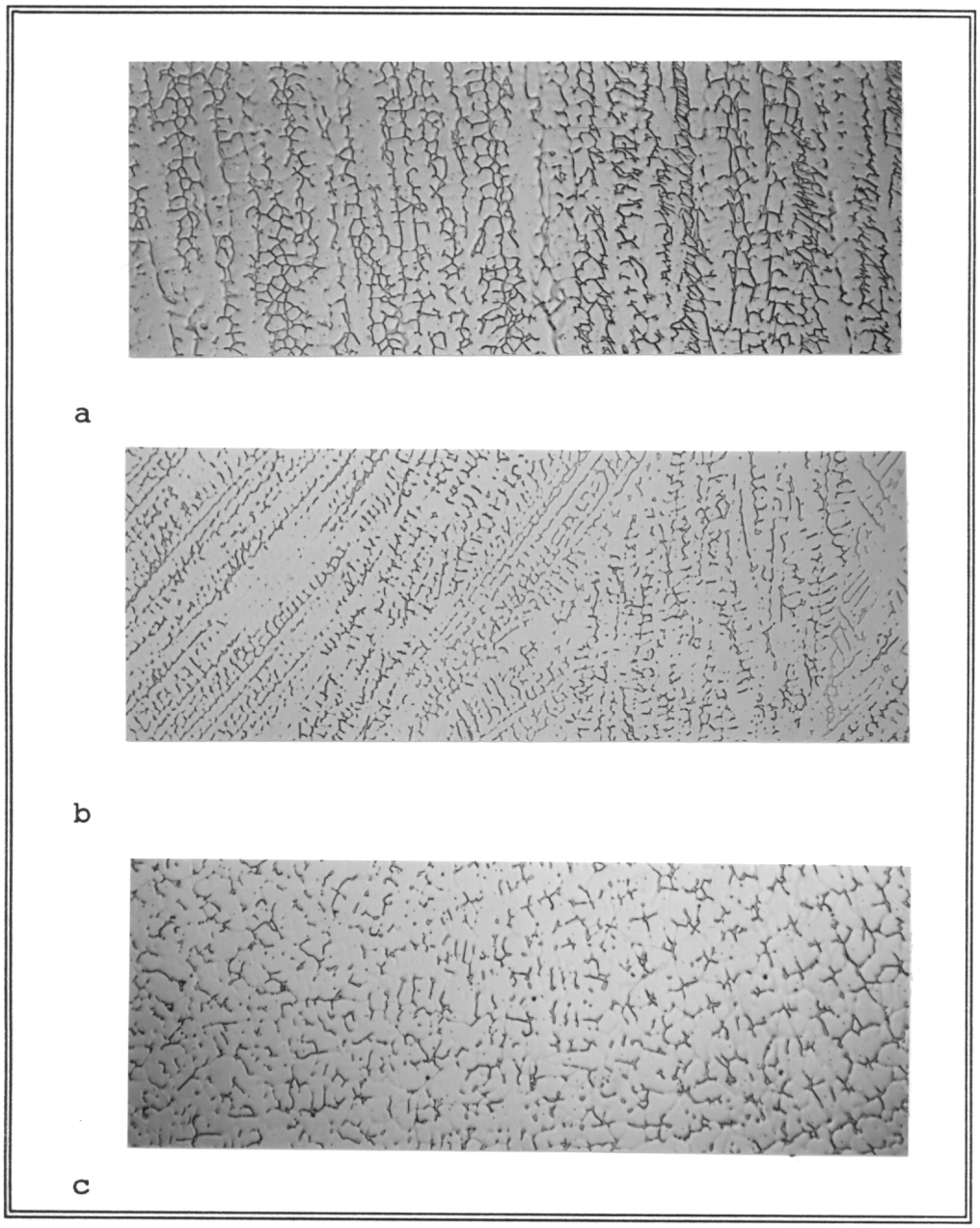

Figure 4-6 Crown (a), Mid (b), And Root (c) Pass Weld Microstructures Magnification is 200X

5.0 Experimental Procedures

The experimental procedures employed to study the effects of thermal cycling on residual stresses were devised for simplicity and practicality. The initial step was to determine the stress state as-received in the pipe. The as-received stress state was examined on the surface and into the pipe wall. Next, the pipe was thermally cycled and the residual stresses remeasured. These steps were repeated and constitute the bulk of this project. A more through and detailed explanation is contained in the following sections.

5.1 Initial Stress State

The initial experiment after receiving the piping section was to determine the as-received stress state in the pipe wall and also in the weld area which had been ground. Several variations in the x-ray diffraction technique were made to determine the best parameters for measuring stress in this stainless steel pipe. The chosen parameters were cited in Section 3.7.

A total of 93 locations at which to measure residual stress were chosen. These points consist of three circles around the circumference of the pipe and three lines along the length of the pipe. Figure 5-1 shows the placement of these measurement locations. The pipe is represented unrolled, two dimensional, as a rectangle. The positions were arbitrarily chosen, and an unequal number of locales exist in the circles and lines. Each line includes points in the ground weld area while the circles are to one side of the weld and outside the ground area. Figure 5-1 also includes a

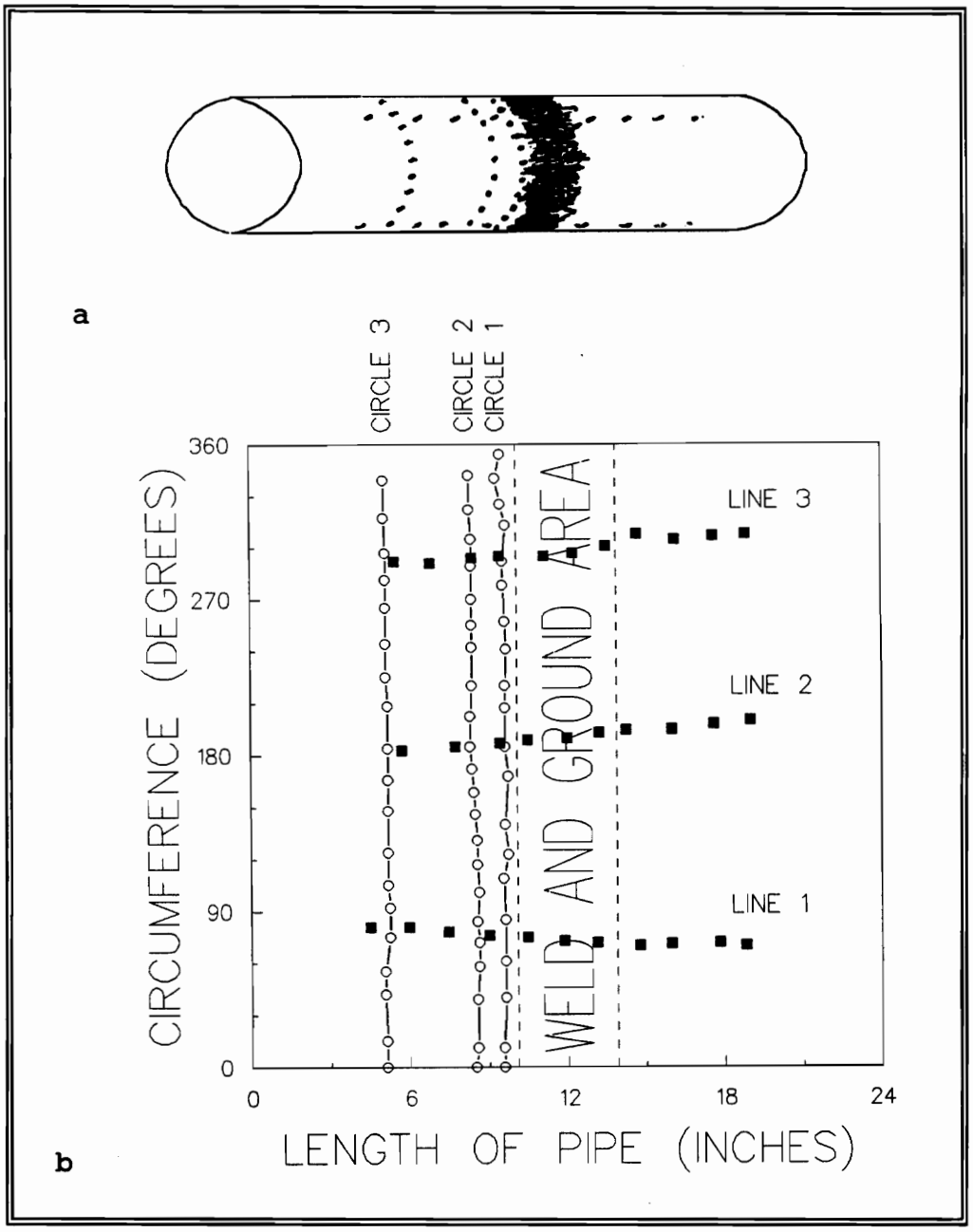

Figure 5-1 The Positions Of The Three Circles and Three Line Of Measurement Locations On (a) A Three Dimensional Sketch And (b) A Two Dimensional Rectangle Representing The Pipe Unrolled

three dimensional sketch of the pipe with the lines and circles of measurements shown. All measurements were made on the exterior surface.

Measurements were not made near the ends of the pipe so as to avoid edge effects. Many researchers assume the St. Venant principle as a guideline for figuring edge effects.(18)(42)(85) This principle limits the edge effects region to a distance from the edge equal to a fundamental dimension of the component. For a cylinder the usual premise is that end effects cease at a distance approximately equal to the diameter. Ericsson and Hildenwall(42) and Fletcher and Lewis(50) suggest this distance to be even less.

Each location was examined in two orthogonal directions in order to acquire both the hoop and longitudinal (long.) stresses. Pictures of the hoop and longitudinal x-ray diffraction setups are shown in Figures 4.1 and 5.2, respectively.

5.2 Stress Gradient

Since x-ray diffraction provides only a surface residual stress measurement, it was desirable to know if a stress gradient exists. Two techniques were incorporated to divulge the stress versus depth profile-- electropolishing and hole-drilling.

5.2.1 Electropolishing

In order to employ electropolishing, a procedure for controlled material removal was first developed. Multiple electropolishings were performed on 316L stainless steel flat plates. For this process a Proto Manufacturing Model 8818 portable electropolisher was operated at 1.0 ampere and ~60 volts. The electrolyte of 10%

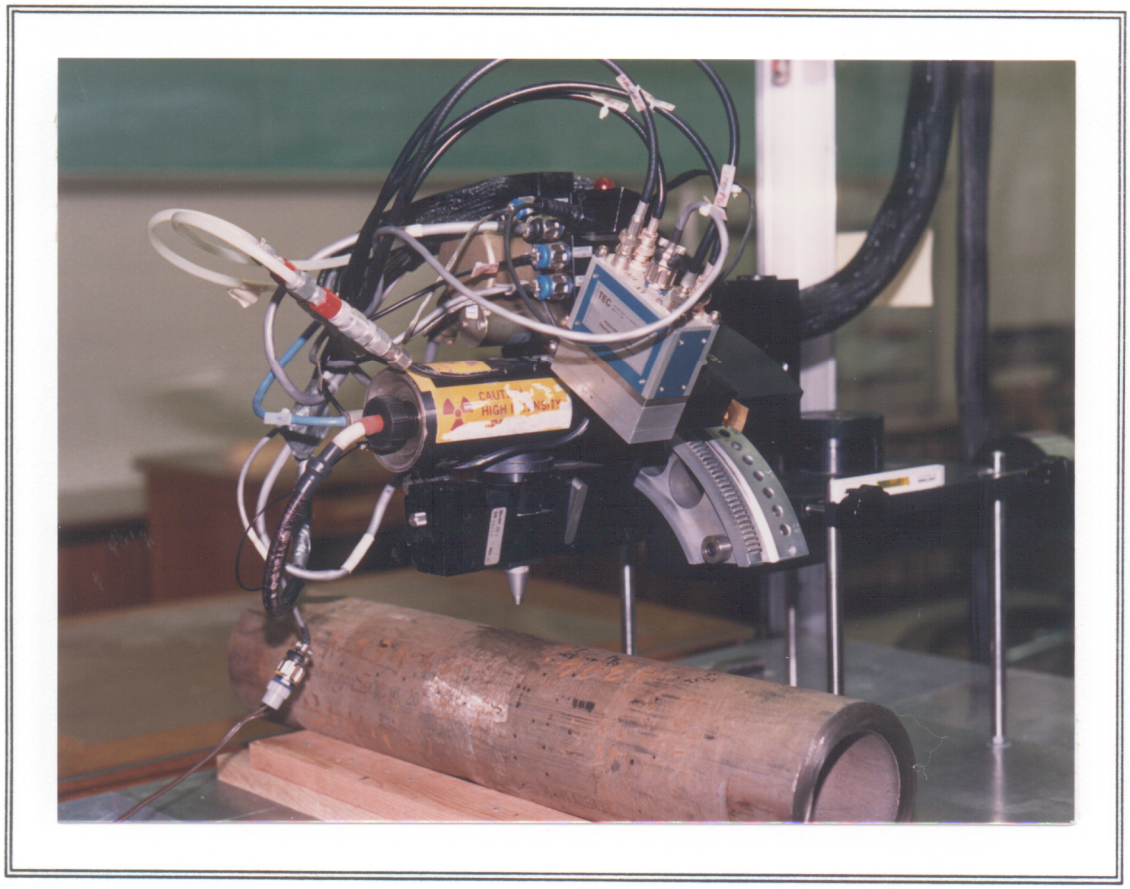

Figure 5-2 Longitudinal Stress Measurement Setup

perchloric acid and 90% ethanol was maintained at 10° C. The depth of removed material was gauged for each polishing period of three minutes. Depth measurements on the flat plate were made with a Taylor-Hobson Taly Surf 4 profilometer. Also, to facilitate smooth planer removal, the electropolishing probe was rotated a quarter turn each three minute period. Figure 5.3 shows that the depth versus electropolishing time plot is quite linear and regresses to the given equation. The regression equation was then used to determine the polishing time needed for a particular depth removal on the pipe. Measuring electropolishing depth directly on the pipe was not possible due to pipe's size and weight.

A position 4.375 inches from the end of the pipe, near Circle 3, was selected to measure the stress gradient. Only one location was investigated due to the destructive nature of the test. Controlled thin layers 0.002 inches deep were electropolished away. X-ray measurements were made after each layer removed. At a depth of 0.008 inches hole-drilling was initiated at the same location.

5.2.2 Hole-drilling

The hole-drilling strain gage method of residual stress measurement relies on stress/strain relaxation and redistribution as material is removed from a body. By noting the change in strain via resistance in a strain gage rosette, the stress values can be calculated from continuum equilibrium equations. Additional information on the hole-drilling method can be found in References (86) and (87).

A Measurement Group TEA-06-062RE-120 strain gage rosette was applied on the electropolished area described above. Measurement Group Model P-3500 and

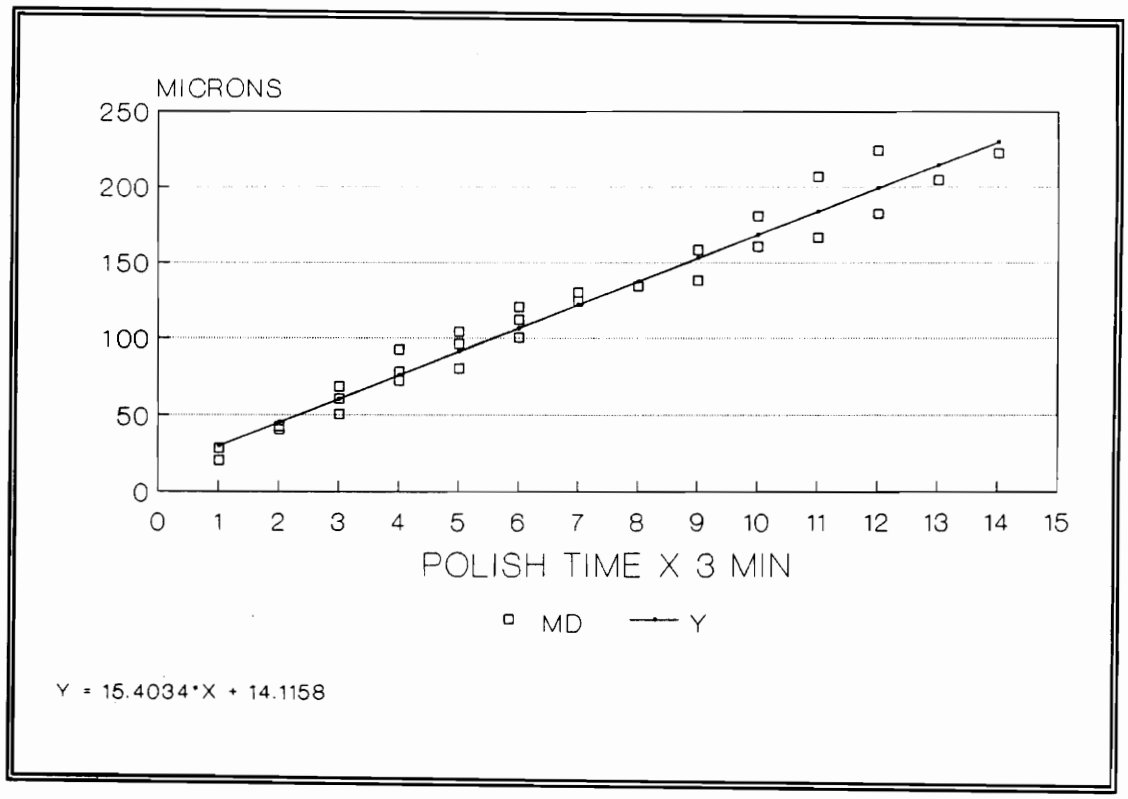

Figure 5-3 Depth Versus Electropolishing Time

Measurement Group Model SB-10 apparatuses were used to calibrate the strain readings and indicate the strain adjustments. A Measurement Group Model RS-200 milling guide was centered above the area to be drilled and cemented to the pipe. This houses the 0.0625 inch diameter milling cutter. Pressurized nitrogen gas was attached to rotate the drill. Procedures for hole-drilling followed the ASTM Standard Method E837.(88) The error estimate on hole-drilling measurements is approximately ± 5%. Figure 5-4 is a detailed schematic of the hole-drilling procedure.

Data gathered from both electropolishing and hole-drilling were combined to define the stress gradient. A mathematical correction was applied to amend the stress values for the extracted layers of material.(89) The electropolishing and hole-drilling site is revealed in Figure 5-5. The true size of the electropolished area is one inch in diameter. After the stress profile was determined, thermal cycling was initiated.

5.3 Thermal Cycling

Modes for thermal cycling were greatly hampered by the dimensions and weight (60 pounds) of the pipe. Other considerations included simplicity and economics. The process developed involved heating the pipe in a large furnace, quickly extracting the pipe from the furnace, and quenching it in an icy brine bath. All of the thermal cycling was performed at Oak Ridge National Laboratory (ORNL) through a Materials Science Summer Study Program sponsored by ORNL, the Southeastern Universities Research Association, and Oak Ridge Associated Universities and funded by the Department of Energy.

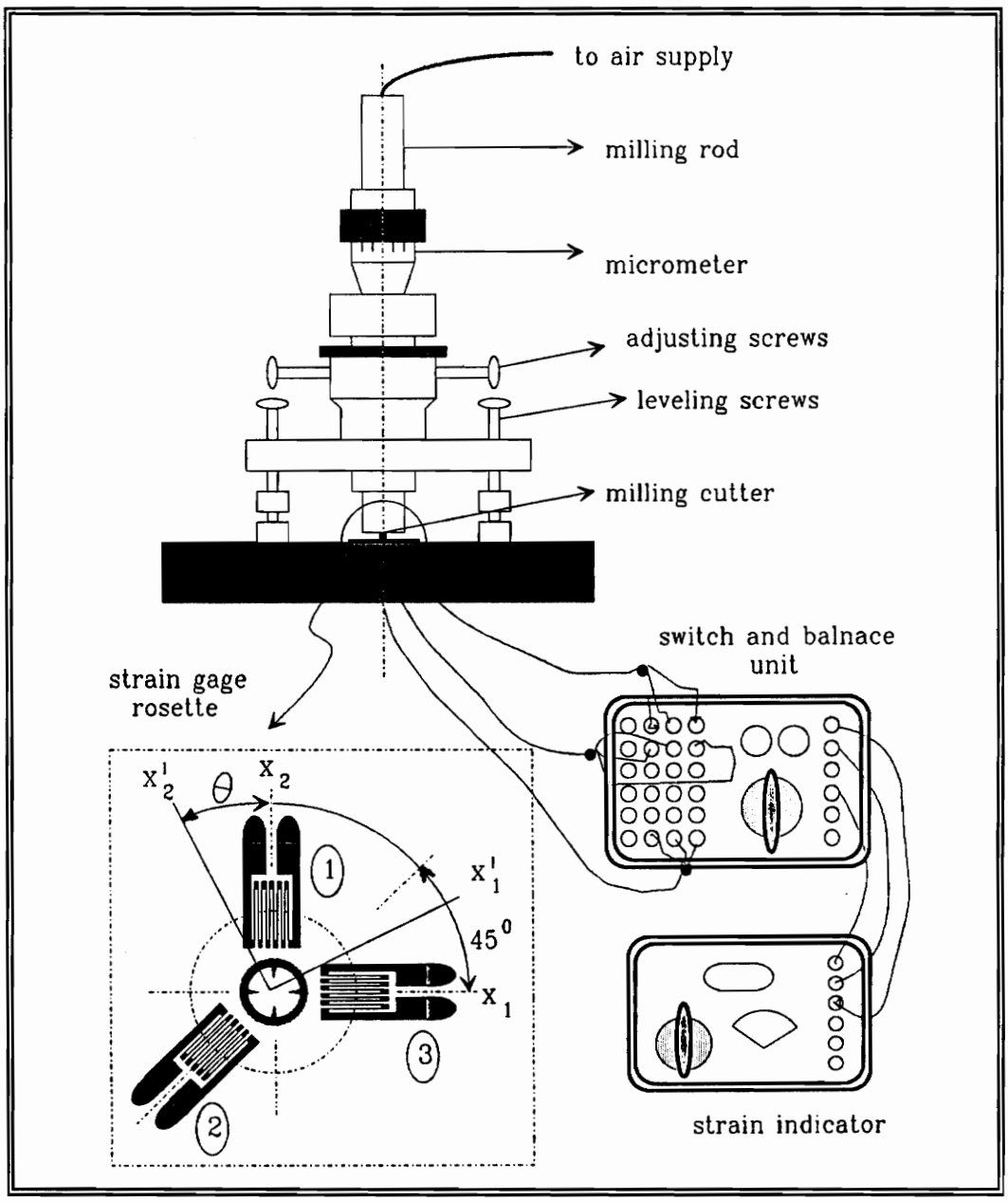

Figure 5-4 Detailed Schematic Of The Hole-Drilling Procedure

Figure 5-5 Electropolishing And Hole-drilling Site
Electropolishing Hole Diameter Equals One Inch

The thermal cycling setup is shown in Figure 5-6. In the background is the Blue M Furnace used to heat and equilibrate the pipe to 300° F. A forklift with angle iron extensions was utilized to extract the pipe and plunge it into the icy brine bath positioned beneath the furnace door. The cooling quenching was performed on the exterior surface only, the open ends of the pipe being closed with large rubber stoppers. The quenchant of 10 weight percent NaCl, balance water, was contained in a 55 gallon drum and maintained between 21 and 23° F. Dry ice dropped into the brine sustained the low temperature. Frozen condensation is observable on the drum's exterior. Upon quenching the bath's temperature rose approximately five degrees.

Three iron-constantan thermocouples were attached to monitor the pipe's temperature change. One was placed on the inside surface, one was anchored to the outside surface, and another was wedged between the pipe and its holder. The thermocouples were soldered to the pipe in two different fashions. The first series of solderings left the thermocouple tip uncovered. The last cycles were performed with the tip covered with solder. In both instances the thermocouples were flush with the pipe's surface. A Yokogawa Model 4153 3-Pen Model chart recorder was used to register the temperature changes.

X-ray residual stress measurements were performed after a total of one, three, eight, and twenty thermal cycles at each of the locations described in Figure 5-1. Between each set of quenches the thermocouples were removed, and the pipe was transported back to Blacksburg, VA, for the x-ray analyses. During the measurements after the first thermal cycle, it was decided not all the measurement locations were necessary

Figure 5-6 Apparatus Of The Thermal Cycling Process (ORNL)

to obtain any higher accuracy. The even positions of Circle 2 and Circle 3 were eliminated.

Subsequent to the final x-ray measurements the pipe was cut for metallography, also carried out at ORNL. The metallography of the pipe was presented in the previous chapter.

6.0 Results and Discussion

The objective of this project was to evaluate the role of relatively small thermal cycling in developing residual stresses in a section of thick-walled stainless steel pipe. During this experiment tremendous amounts of x-ray diffraction data were acquired. Some analysis was performed to identify bad data and eliminate it. This is addressed in Section 6.1. The as-received stress state is described in Section 6.2. The stress versus depth profile is contained in Section 6.3. In Section 6.4 a quenching temperature profile is shown and compared with a FDM calculation for thermal stresses in Section 6.5. Sections 6.6 and 6.7 contain the effects of thermal cycling on the stresses. Lastly, an analysis of the influence of the initial stress state is given in Section 6.8.

6.1 Data Assessment

Since the generation of the d versus $\sin^2\psi$ regression equation is performed automatically in the TEC instrument, analysis must be performed to affirm its validity. Review of the data included auditing the assumption of a biaxial state of stress. The data from the TEC machine was input into a personal computer and multiple regression statistical analyses were accomplished using ABstat which verified that there were no significant shear stresses. This is not surprising as most of the d versus $\sin^2\psi$ plots both in the wall and weld area were "wavy". An example of this is shown in Figure 6-1. Preferred orientation is usually detectable by waviness or crossing of the d versus $\sin^2\psi$ data. Conversely, when shear stresses are present there is a splitting between the positive and negative ψ angles data.(68)(70)

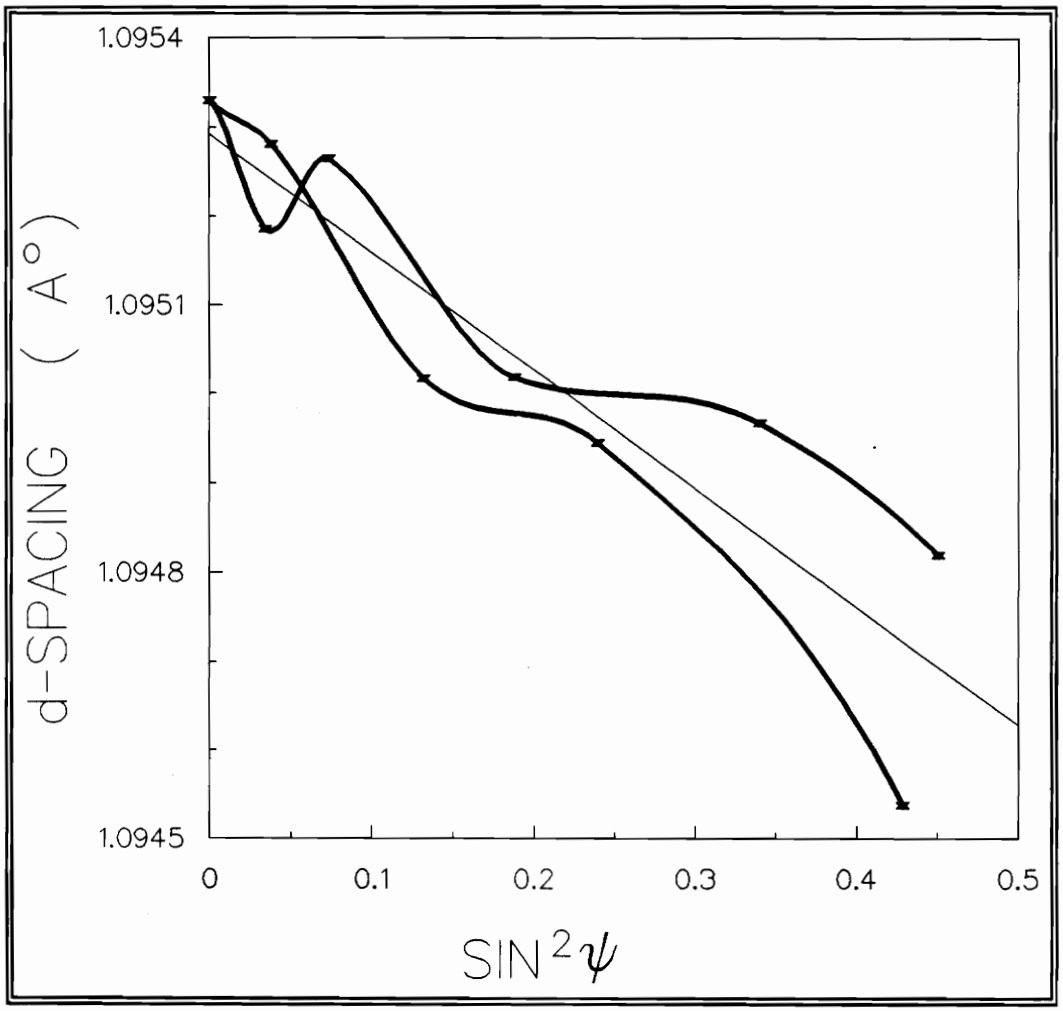

Figure 6-1 Sample d Versus Sin$^2\psi$ Plot Exhibiting Preferred Orientation

Stainless steels often exhibit preferred orientation either from preferred crystalline growth or deformation planes. Preferred orientation causes difficulty in obtaining x-ray data. Materials with texture can produce diffraction peaks with great variation in intensity which can lead to inaccurate d-spacings and an erroneous regression equation. In this experiment diffraction peaks were discarded if they fell in one of three cases: the peak's intensity was very low or very high, the standard deviation was extremely large in the peak measurement, or the point was obviously apart from the other data so as to be suspect. Of the 8240 diffraction peaks measured, only 1.6% were considered faulty and rejected. When a diffraction point was eliminated, a new d versus $\sin^2\psi$ equation was regenerated on Abstat.

6.2 The Initial Residual Stress State

Since this project studied the effects of thermal cycling via changes in the stress state, it was important to document well the initial residual stress state. The residual stress values in the as-received pipe are presented in Figures 6-2 through 6-10. The zero degree position of the circles was arbitrarily chosen and has no significance, but is the same for each circle as was shown in Figure 5-1. Measurements around the circumference of the pipe are displayed in both degrees and inches. The zero position is the same for both.

6.2.1 Stresses Along the Length of the Pipe

The hoop and longitudinal stresses of Line 1, Line 2, and Line 3 are shown in Figures 6-2 through 6-4. The points along the three lines which lie in the ground area of the weld exhibit extremely high tensile stresses. It should be noted that although the yield stress for this material in the annealed condition is 35 ksi, 316L

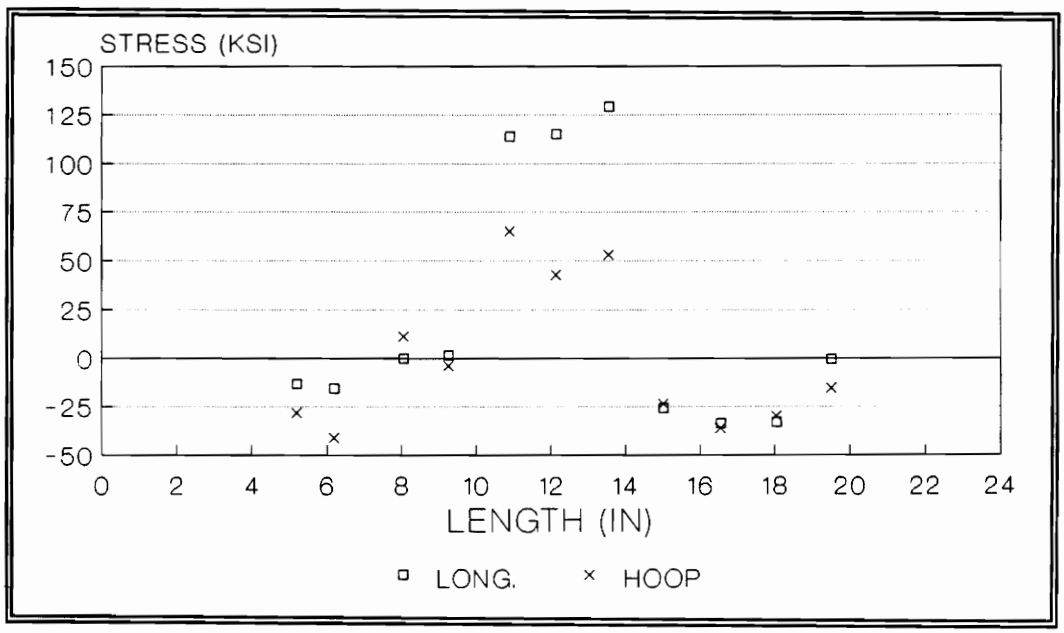

Figure 6-2 Line 1 Long. And Hoop Initial Stresses

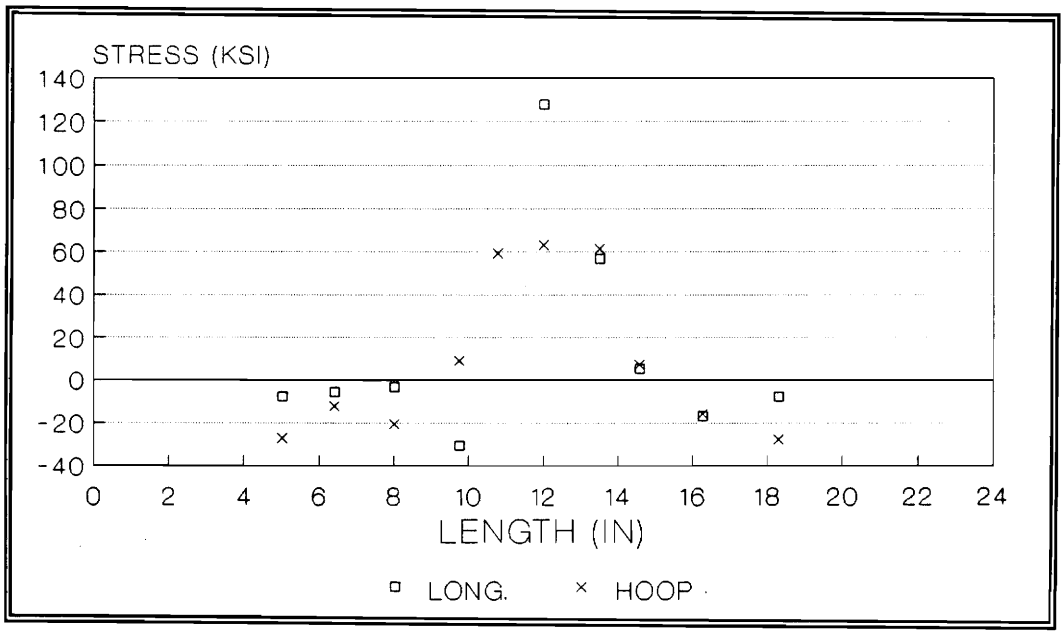

Figure 6-3 Line 2 Long. And Hoop Initial Stresses

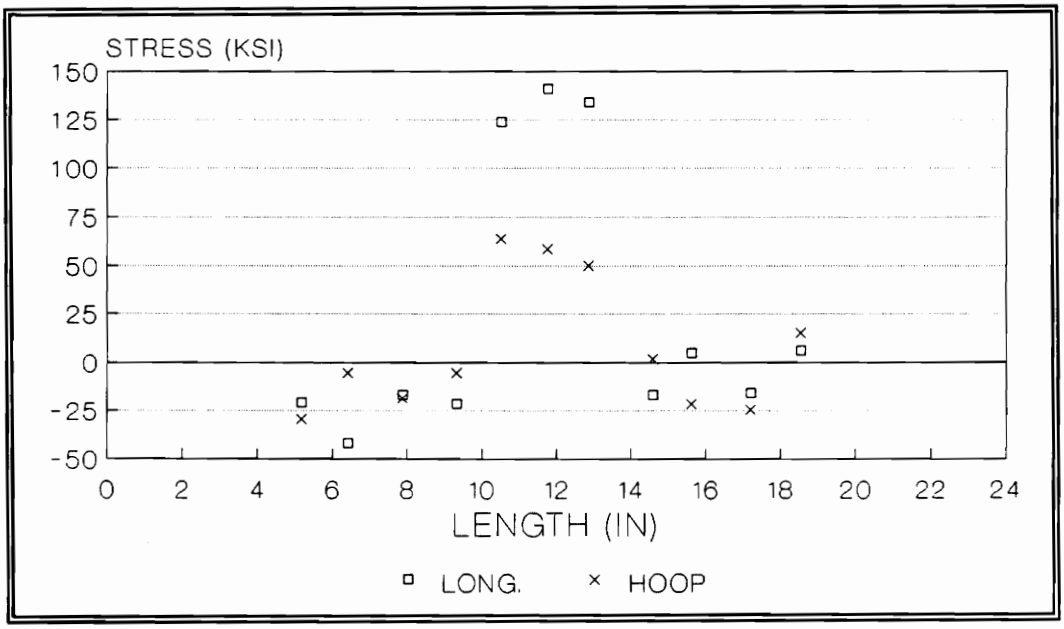

Figure 6-4 Line 3 Long. And Hoop Initial Stresses

stainless steel has the ability for extreme work-hardening. Thus, the high residual stress values detected in the ground regions of the weld are believed to be reliable. Similarly high stress values for 304 and 316 stainless steel have been reported by others.(62)(84)(90)(91) Obviously, grinding of the weld bead induces the observed stresses. Our original intention to ascertain stress values in the heat affected zone (HAZ) of the weld was abandoned due to the completely overwhelming residual stresses caused by grinding. Outside the ground area the stresses varied and range between -30 and +20 ksi approximately.

6.2.2 Stresses Around the Circumference of the Pipe

The initial hoop and longitudinal stresses around the circumference of the pipe are shown in Figures 6-5 through 6-7. The first and last locations of Circle 1, which was closest to the weld, (Figure 6-5) are highly tensile and fall on grinding nicks. As previously mentioned, in most stress analyses of cylindrically shaped objects the stress patterns are assumed to have azimuthal symmetry. This clearly is not the case in the section of pipe studied here. The data of Figures 6-5 through 6-7 reveal both periodic- and random-looking data. Using the statistical program COSTAT, these data were fitted by least squares to second order Fourier series.(92) All of the longitudinal stresses were statistically significant and the Fourier coefficients are given in Table 3. The phase angle shift of the first harmonic between Circles 1 and 2 is much greater than between Circles 2 and 3 even though Circles 1 and 2 are closer together. If the residual stresses were a consequence of the pipe manufacturing process, one would expect the phase angles to vary linearly with distance along the pipe. Such is not the case. Only the hoop stresses of Circle 3 fit significantly to a second order Fourier equation. Figure 6-8 shows the Fourier fit to Circle 1 data.

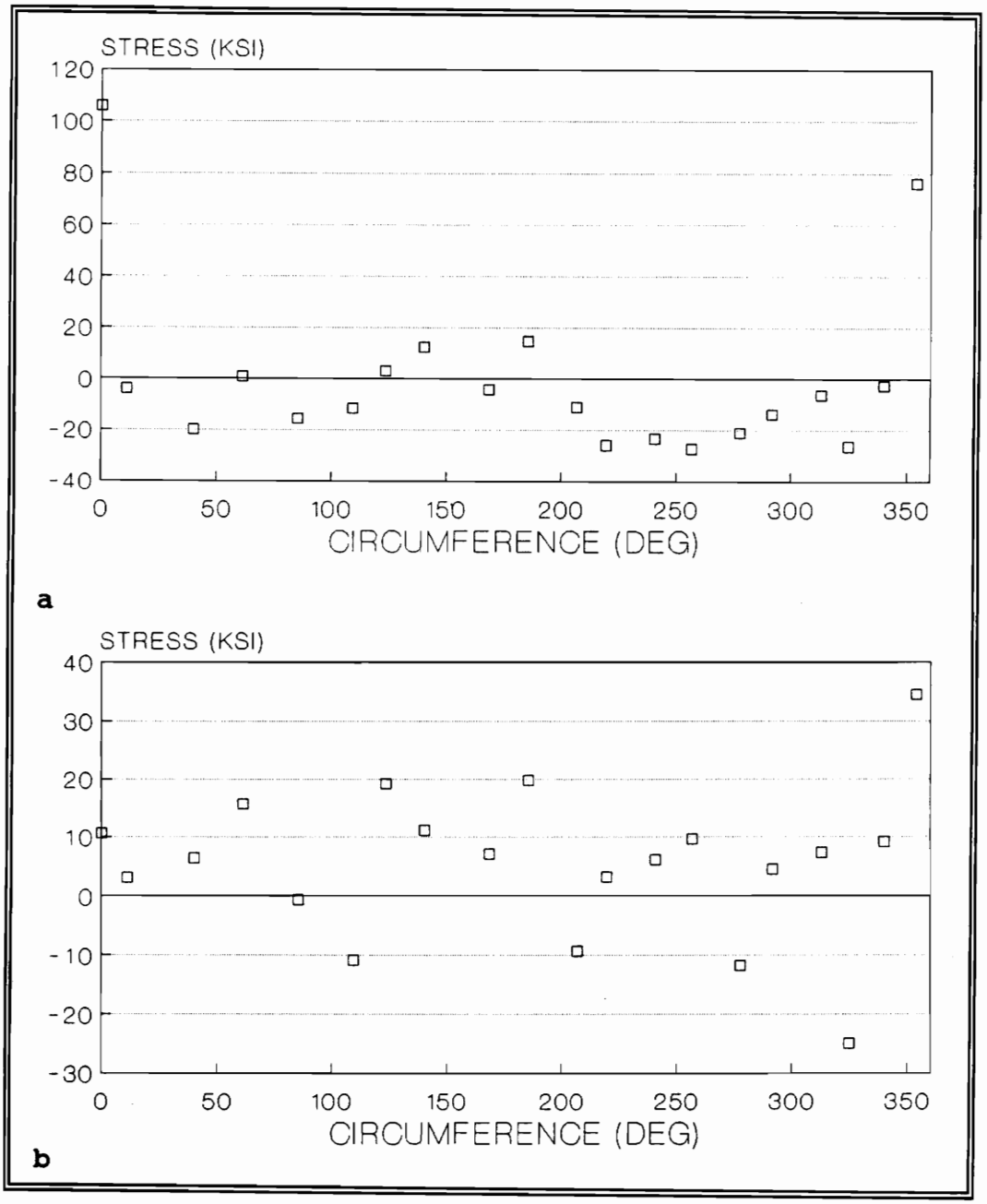

Figure 6-5 Circle 1 Long.(a) And Hoop (b) Initial Stresses

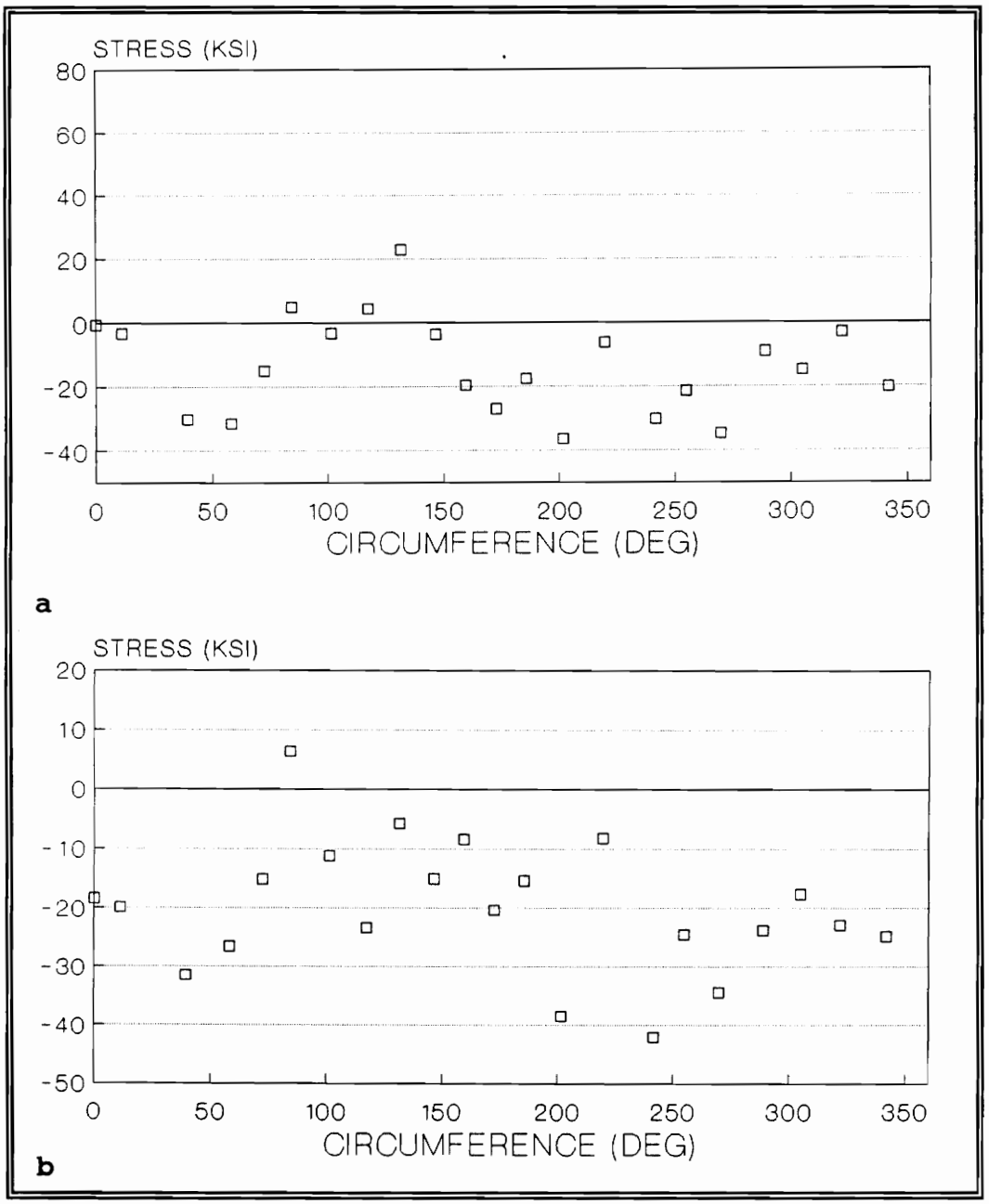

Figure 6-6 Circle 2 Long.(a) And Hoop (b) Initial Stresses

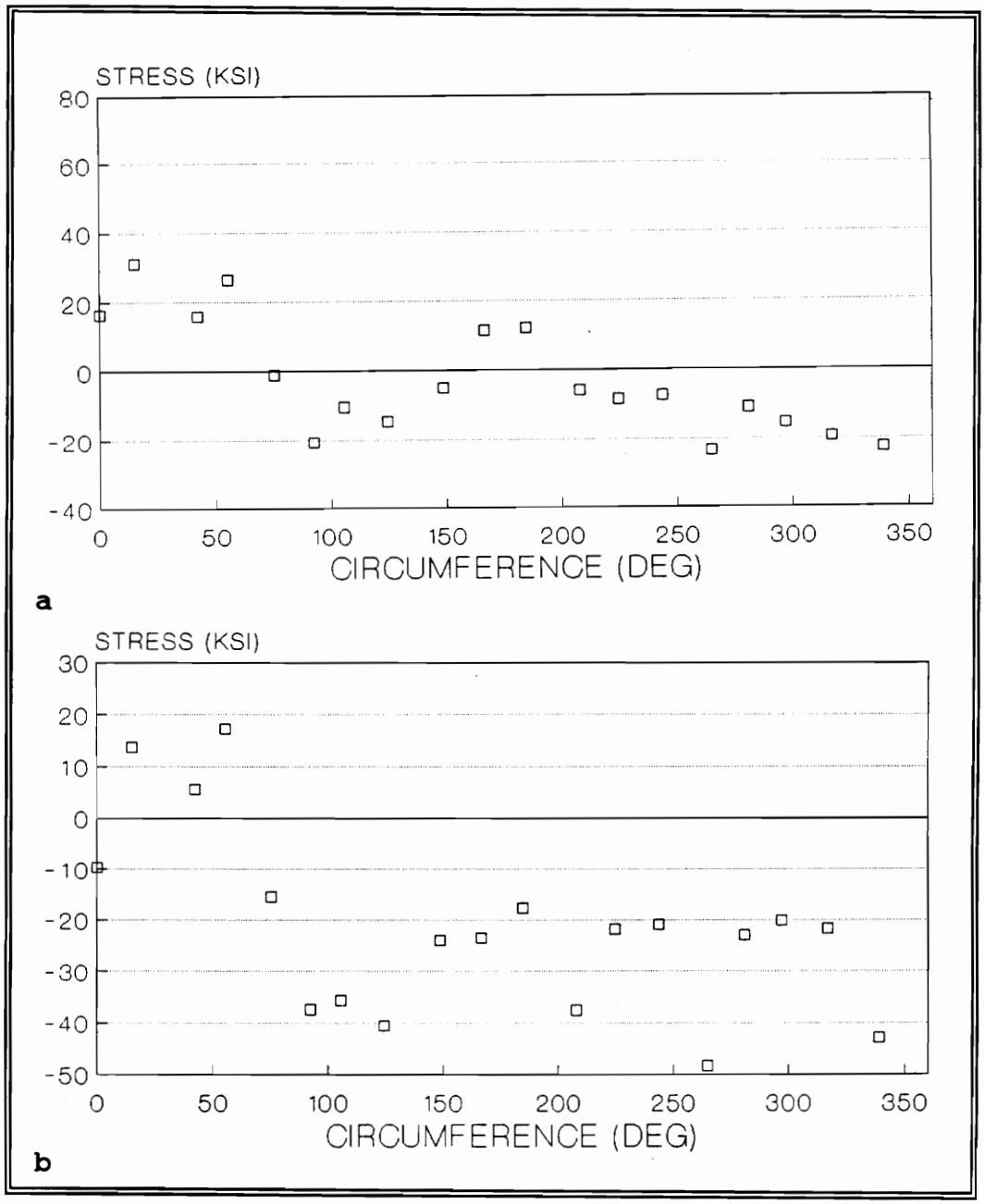

Figure 6-7 Circle 3 Long.(a) And Hoop (b) Initial Stresses

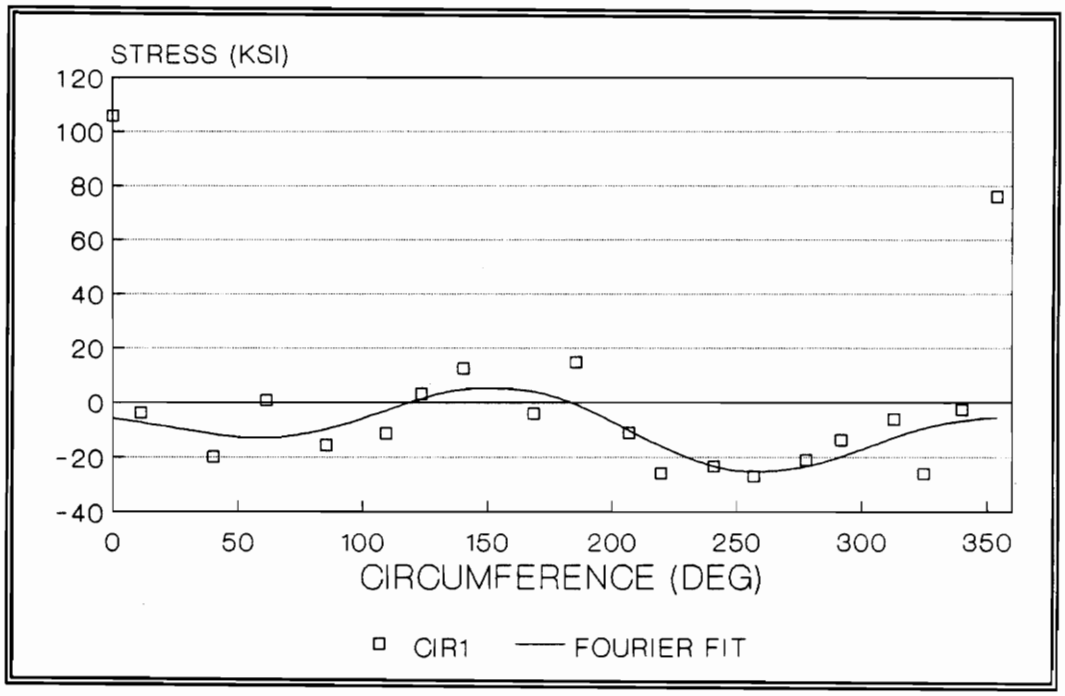

Figure 6-8 Fourier Fit To Circle 1 Long.

Table 3 Fourier Coefficients For Significant Fits Of Circles

	Phase Angle	Amplitude	
CIR 1 Long.	115.77 321.81	8.93 9.71	Harmonic #1 Harmonic #2
CIR 2 Long.	78.86 260.91	7.67 11.24	Harmonic #1 Harmonic #2
CIR 3 Long.	61.98 143.96	9.22 16.29	Harmonic #1 Harmonic #2
CIR 3 Hoop	27.23 60.80	12.67 13.68	Harmonic #1 Harmonic #2

The cause of the circumferential variation in residual stress appears to be the multi-pass butt weld. This premise is partially supported by the phase angle data above but primarily by the other investigations reported in the Literature Review. T. Karlsson, R. Karlsson, and Jonsson and Josefson reported comparable stress oscillations from butt welding. It is understandable that welding can cause these oscillations in residual stresses around the circumference. First, welding introduces severe thermal gradients. The large, sharp temperature gradients are sufficient to produce residual stresses. Second, by welding in a rotational manner around the pipe, it is reasonable that this circumferentially moving heat source could produce stresses which vary around circumference. Stresses are especially developed when the ends of the pipe are constrained as mentioned in the Literature Review.

As in the Lines' data, the Circles show a great degree of variation in magnitude axially and aximuthally. Three dimensional projections of the Circle's data, Figures 6-9 and 6-10, vividly depict these characteristics. The axes for each graph have been

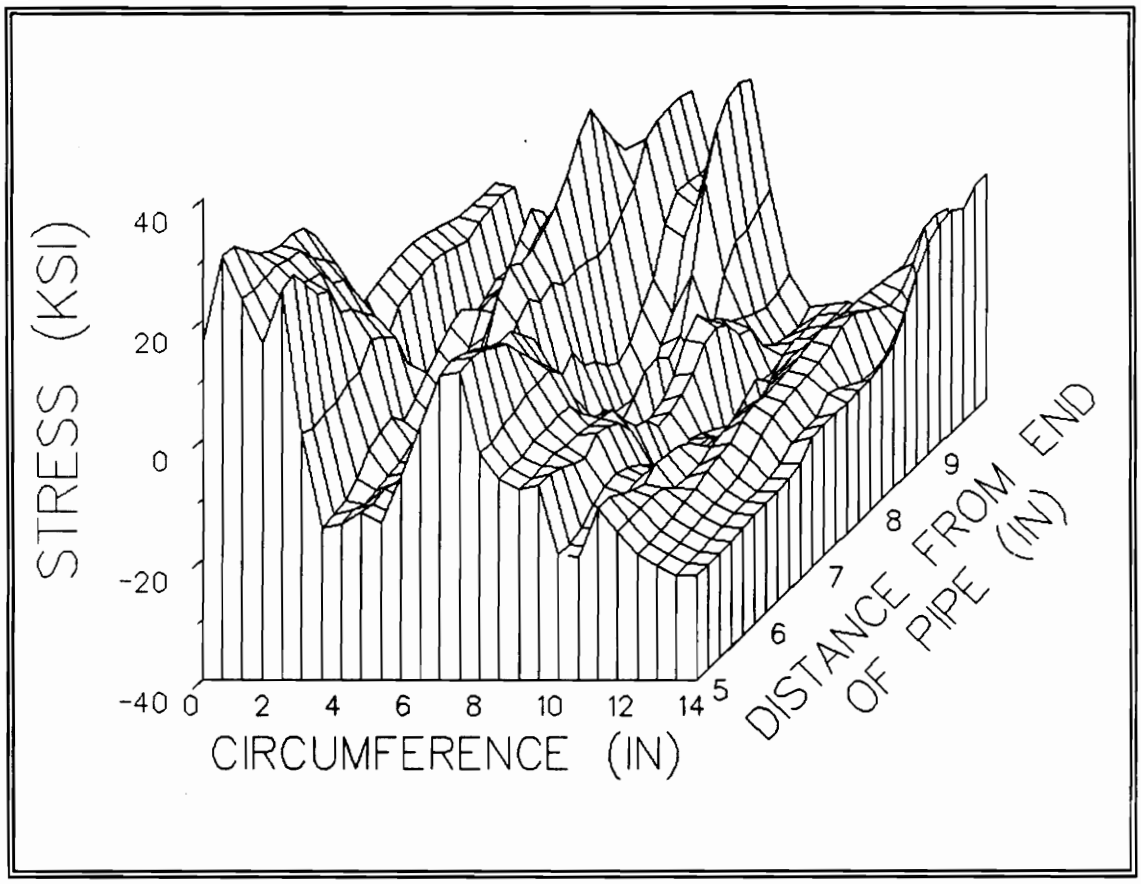

Figure 6-9 Three Dimensional Projection Of The Initial Long. Stress (Weld Is 12 Inches From End Of Pipe)

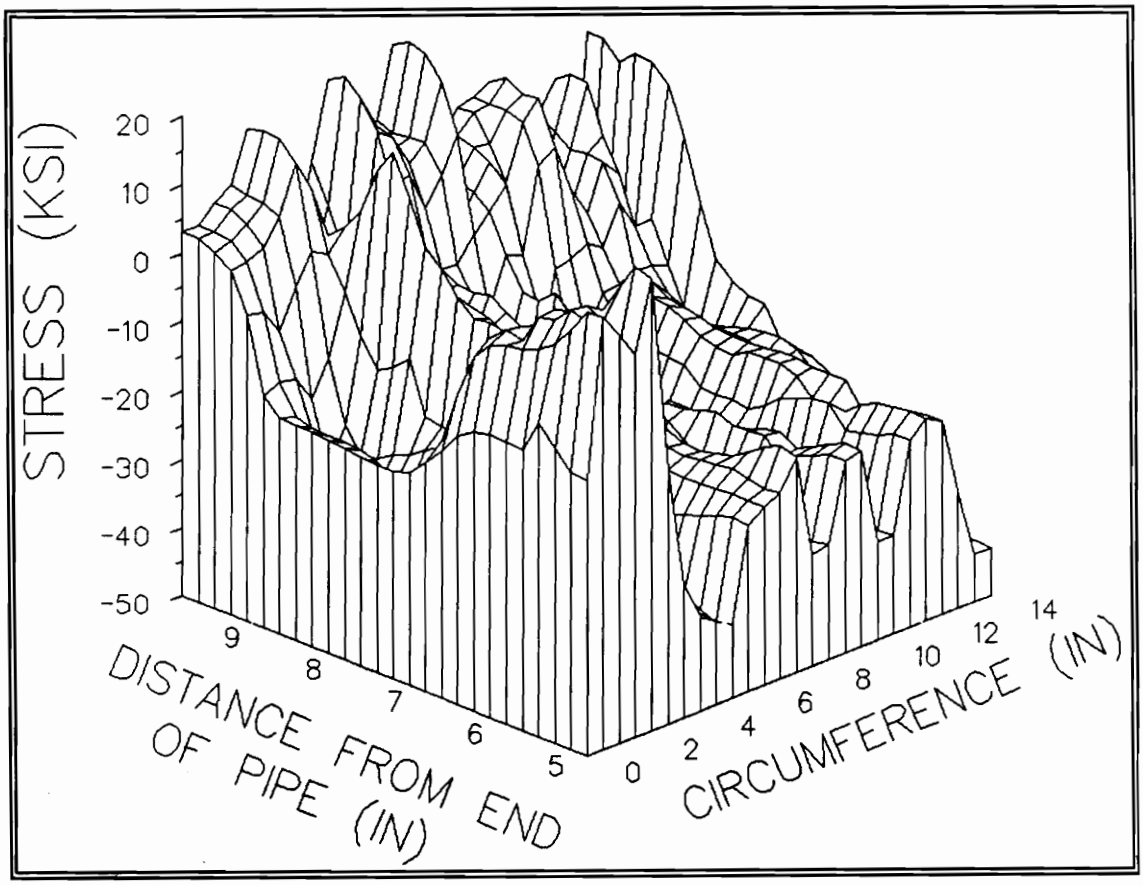

Figure 6-10 Three Dimensional Projection Of The Initial Hoop Stress (Weld Is 12 Inches From End Of Pipe)

arranged for the best perspective of the stresses. The weld is not part of these figures but would be located at 12 inches from the end of the pipe. The ground area extends several inches around the weld (See Figure 5-1). The two points of Circle 1 which fell on grinding nicks were not included in the generation of the graphs. Figure 6-11 was constructed from the three Fourier series fitting to the longitudinal data.

6.3 The Stress Versus Depth Profile

An important question arises with the discernment of the as-received stress state. Are these stresses just a surface phenomena? To determine the stress versus depth profile the techniques of electropolishing and hole-drilling were prescribed as earlier discussed. The as-received stress versus depth profile is illustrated in Figure 6-12. The filled squares are the longitudinal stresses while the open circles are the hoop stresses. At one of the locations the two coincide. The measurements at depths greater than 0.008 inches are by hole drilling, while those below 0.008 are x-ray diffraction. Near the surface there is a gradient in both the hoop and longitudinal stresses, but both level out to about -25 ksi at about 0.025 inches below the surface.

These data must be corrected for the effects of material removed by electropolishing. To do this Moore and Evan's mathematical correction developed for layer removal was employed.(93) Figure 6-13 contains the corrected results for the longitudinal stresses. It can be seen that the correction due to material removal is minuscule. This is understandable as the total amount of material removed by electropolishing was only 0.008 inches, and the hole-drilling data were observed to a depth of 0.048 inches. Correction for the hoop stresses were not calculated.

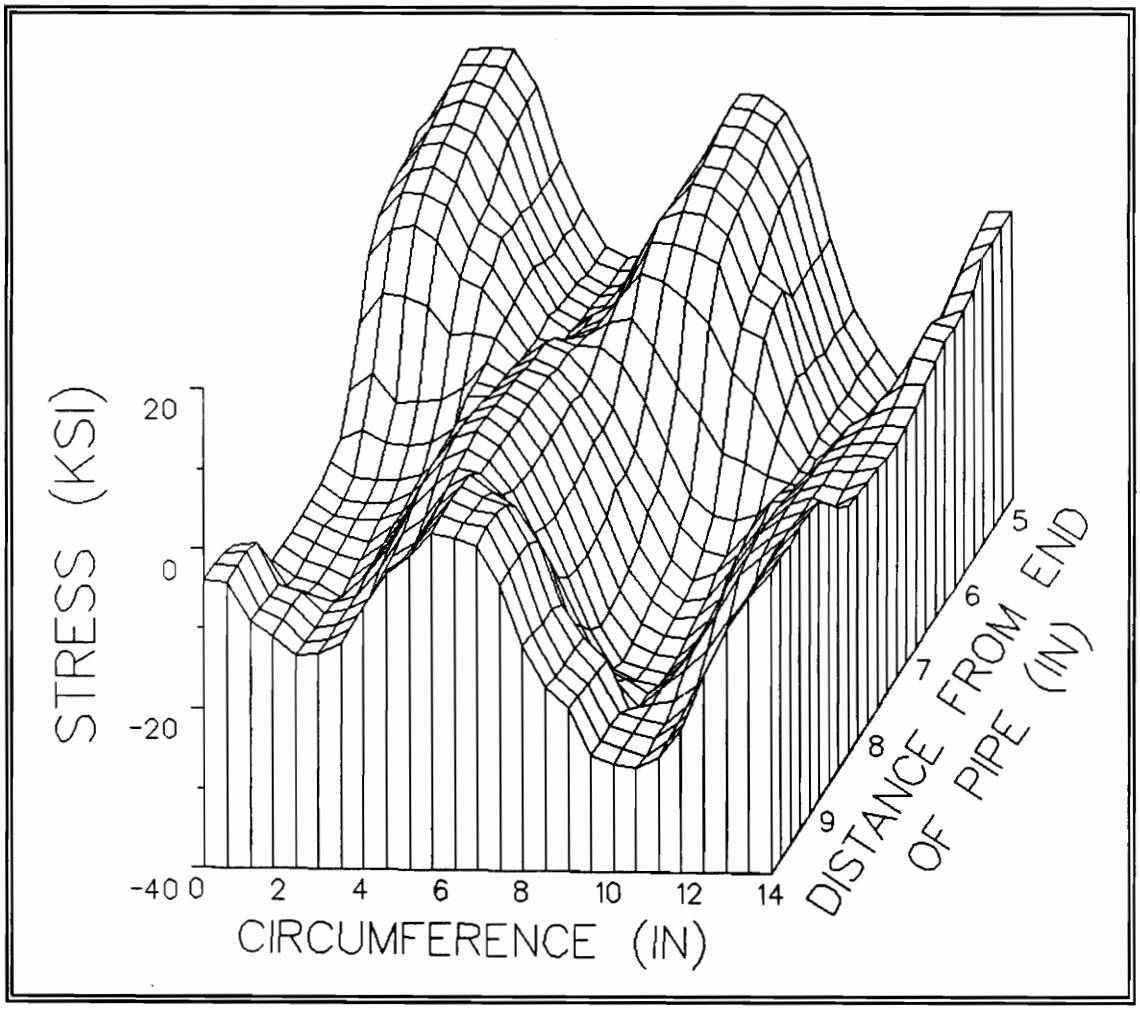

Figure 6-11 Three Dimensional Projection Of The Fourier Fits To The Long. Circle Stresses

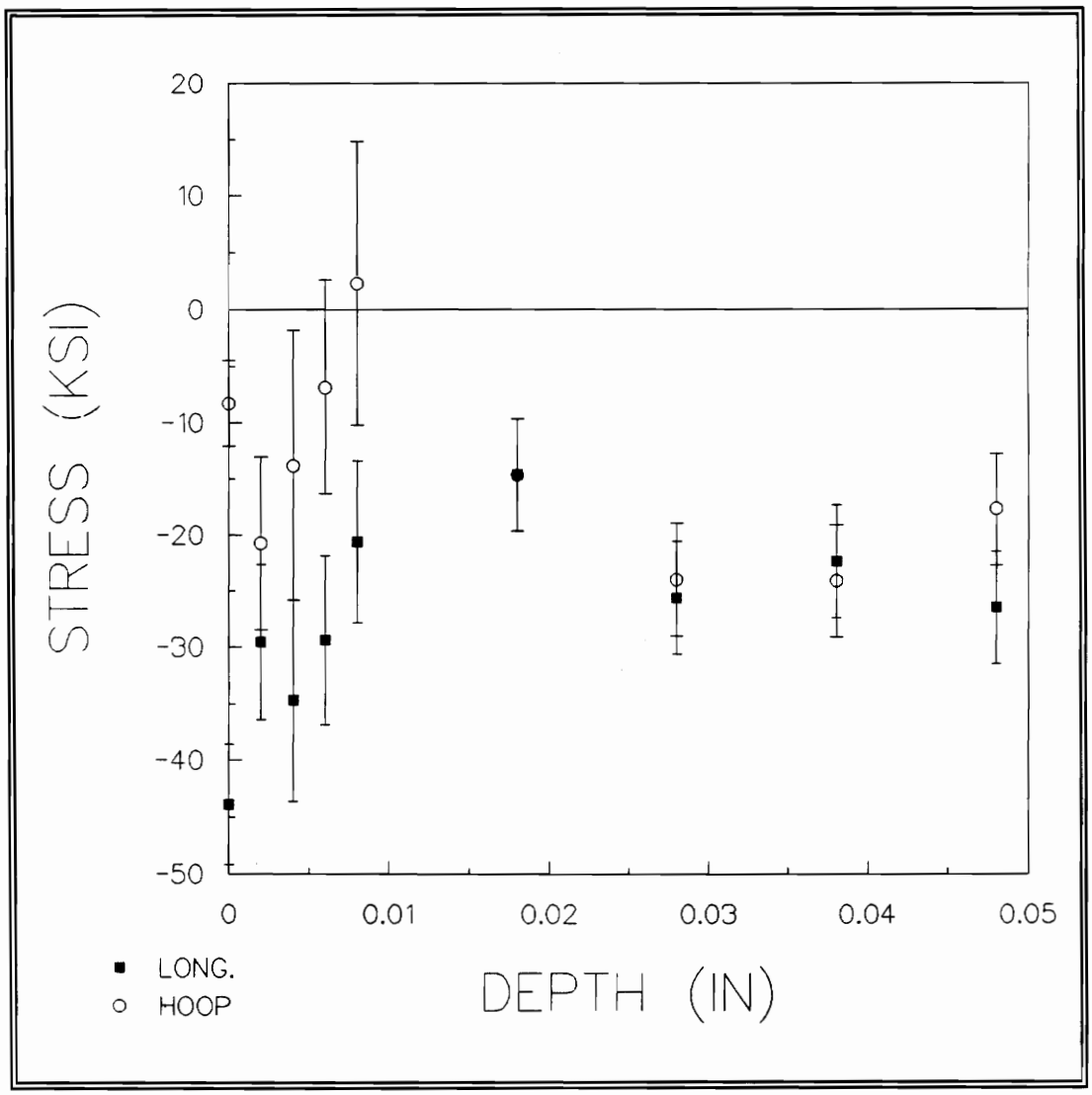

Figure 6-12 Stress Versus Depth Profile By Electropolishing And Hole-Drilling Black Squares Are The Longitudinal Stresses And The Open Circles Are The Hoop Stresses

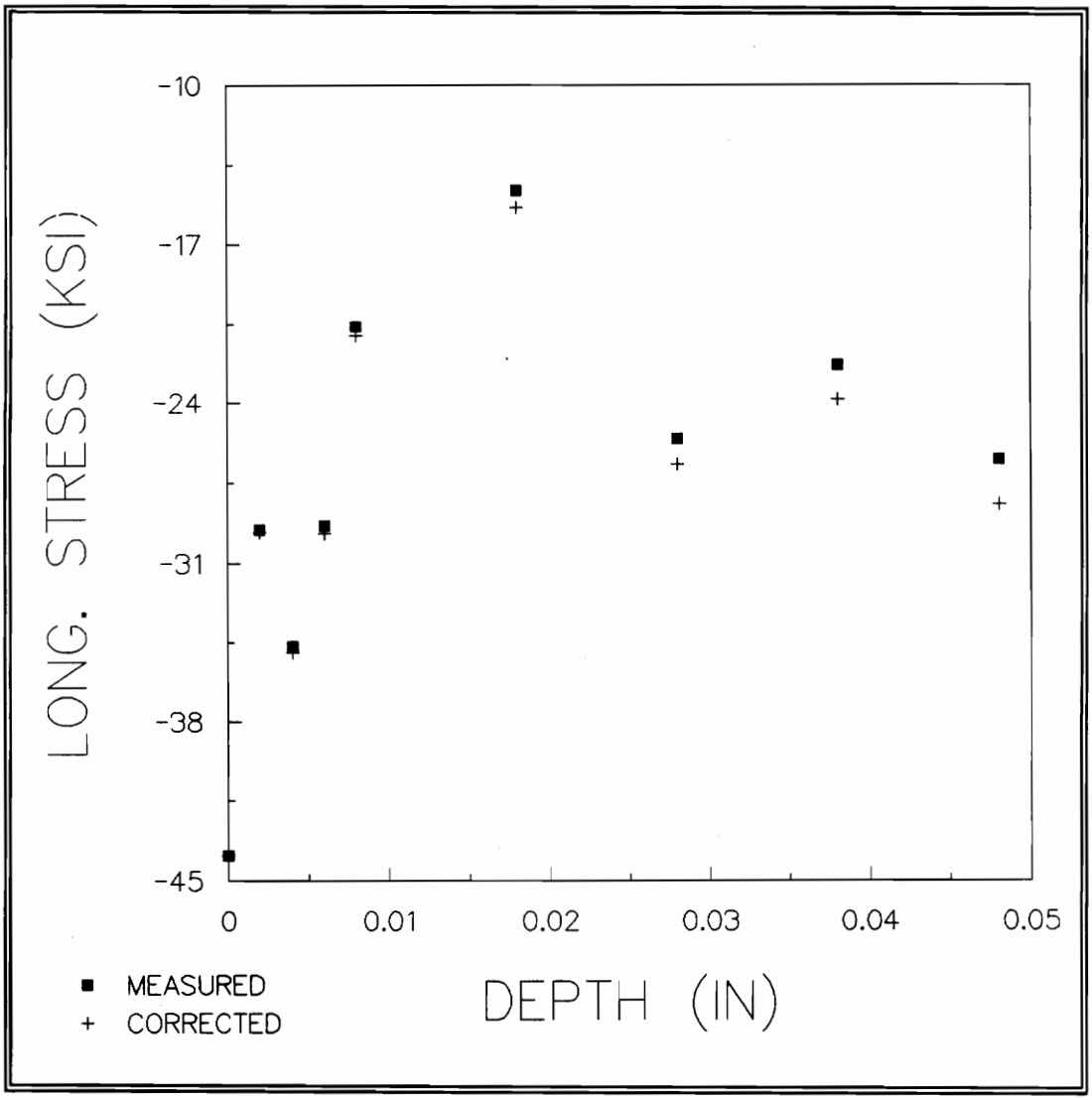

Figure 6-13 Corrected And Measured Longitudinal Stress Values For Material Removed By Electropolishing

While the exact stress profile near the surface is somewhat clouded by the large error bars (a result of stainless steels' preferred orientation and difficulty with the x-ray measurements), several observations are apparent. The residual stresses exist not only on the surface but are also present in the bulk of the pipe. It is important to remember that over the entire volume of the pipe, the sum of the residual stress must equal zero. Therefore, the compressive stresses measured here must be balanced by tensile residual stresses elsewhere in the pipe. Along with stresses in the bulk, the surface stresses must be balanced. Overall, the surface stresses contain large variations in the circumferential and lengthwise directions. These variations exist in both the hoop and longitudinal stresses. The highly tensile stresses in the ground area may be cause for concern due to the frequent occurrence of stress corrosion cracking in stainless steels. High tensile stresses are also a negative factor for fatigue resistance. Now that the as-received stress state has been determined, the plan to monitor the residual stresses as the pipe is thermal cycling was implemented.

6.4 Thermal Quenching Profiles

To study the residual stresses, the pipe was thermally cycled and measurements were made after a set number of cycles. The thermal cycle was achieved by means of a down quench. The quench introduces a temperature differential between the rapidly cooled exterior and the slow cooling interior. This differential in temperatures is the cause for concern with thermal cycling as discussed in the Literature Review.

6.4.1 Finite Difference Model

Dr. George Swift of the Engineering Science and Mechanics Department at Virginia Tech developed a finite difference model to calculate the quenching stresses induced in a cylindrical member.(94) The program allows data input for varying situations. For example, one could calculate the stresses for an inner diameter on a hollow cylinder or outer diameter stresses in a solid specimen. Dr. Swift's program was used to predict the quench rate and induced stresses of the experimental process.

Of the material and experimental constants need for the FDM, two were hard to determine. These were the convective film coefficient and the yield stress in pure shear. Convective film coefficients are generally difficult information tocome by because they are hard to measure. The shear yielding stress is difficult to determine in this material because it is dependant on how much work hardening has taken place and will vary across the surface of the pipe. Temperature and stress profiles were generated using different constants to determine the sensitivity of the FDM to these two constants. These are shown in Figure 6-14 and Figure 6-15.

Figure 6-14 shows the dependance of the temperature profile on the convective film coefficient. The film coefficient was changed from 0.09 to 0.28 BTU/in^2.° F.min. Even though the coefficient has been more than doubled there is almost no difference in the initial cooling curve. After the film coefficient has been tripled there is a split in the lines, but it really there is not that significant a difference in temperatures. However, the yield stresses tell a different story.

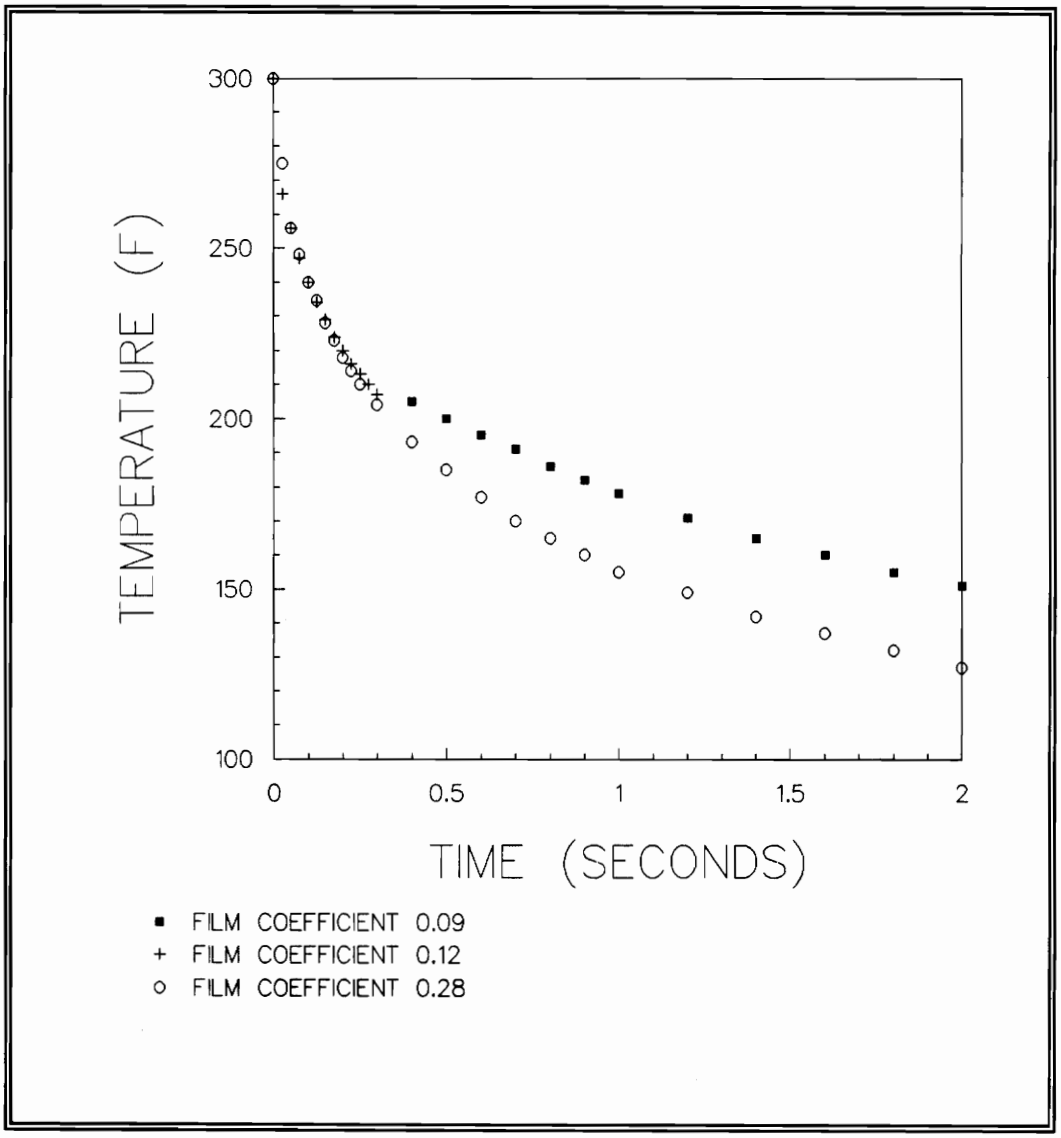

Figure 6-14 Finite Difference Model Of Temperature Profiles Dependant On The Convective Film Coefficients (FDM)

The yield stresses will not effect the temperature profile, but the generation of stress. Figure 6-15 shows the effect of three different yield stresses in pure shear, 25 ksi, 40 ksi, and 58 ksi. Each curve has a different maximum stress and a different final stress value. In the case of 58 ksi the calculations were stopped because the material never yielded. Both the 25 and 40 ksi cases yielded in tension and then upon cooling become compressive. One predicts a final residual stress around -35 ksi and the other at -5 ksi, so as the yield stress varies so will the amount of plastic deformation. In a material like 316L stainless steel which work hardens, or increases its yield stress, with repeated strain loadings, eventually, the yield stress will reach a level to arrest plastic deformation. However, at least the FDM gives a prediction of a thermal tensile stress of 45 to 65 ksi and a residual stress of 5 to 35 ksi compressive for similar input values.

It is important to note two differences in the model and the real material. The FDM program assumes no residual stress and starts at zero stress. Also, the calculations assume an elastic-perfectly plastic material. Because of the work hardening in 316L a bilinear or parabolic model more closely fit the material's response to loading. (see Figure 4-2).

6.4.2 Other Stress Predictions

Other predictions can be made besides the finite difference model. For example, from Eqs. 2-5 and 2-6 in the Literature Review the thermal stress can be calculated. Plugging the material constants, the temperature difference, and the pipe's dimensions in Eq. 2-5 or 2-6 predicts a tensile thermal stress of 42.5 ksi on the exterior surface.

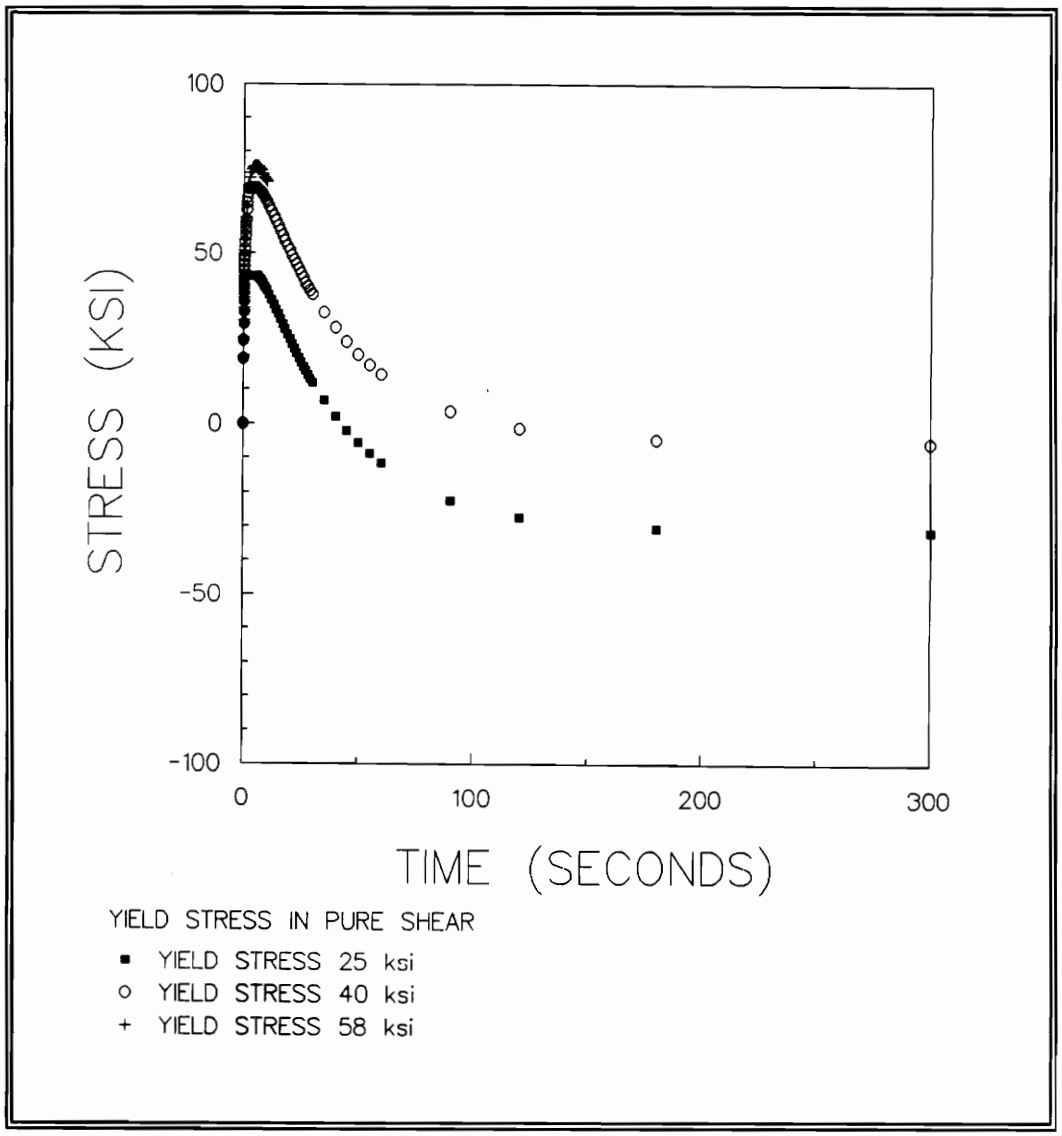

Figure 6-15 Comparison Of Stress Profiles For Different Levels of Shear Yield Stress (FDM)

6.4.3 Experimental Profile

A representative temperature profile of the thermal cycling is shown in Figure 6-16. The temperature drop on the outside was very rapid as expected. The interior of the pipe wall cooled quite slowly taking over five minutes to reach 40° F. Thus the thermal gradient has been injected. The comparison between the finite difference program and the thermocouple chart recordings is also shown in Figure 6-16 (the FDM uses a film coefficient of 0.28). Both the covered and uncovered thermocouple readings are drawn because the true temperature change should be between the two. The average of the two is indeed close to the calculated profile. Differences in the beginning inflections may be response delays in the chart recorder.

6.5 Residual Stresses After Thermal Cycling

Along with the initial residual stress measurements (0 cycles), measurements were made after one, three, eight, and twenty thermal cycles. Different notation was used to distinguish between the different sets of x-ray diffraction data. The system of labeling is given:

CIRX - initial longitudinal stress values of Circle X or the compilation of all Circle X's long. cycling data, and

CIRXH1 - initial hoop stress values of Circle X or the compilation of all the Circle X's hoop cycling data.

(X = 1, 2, and 3)

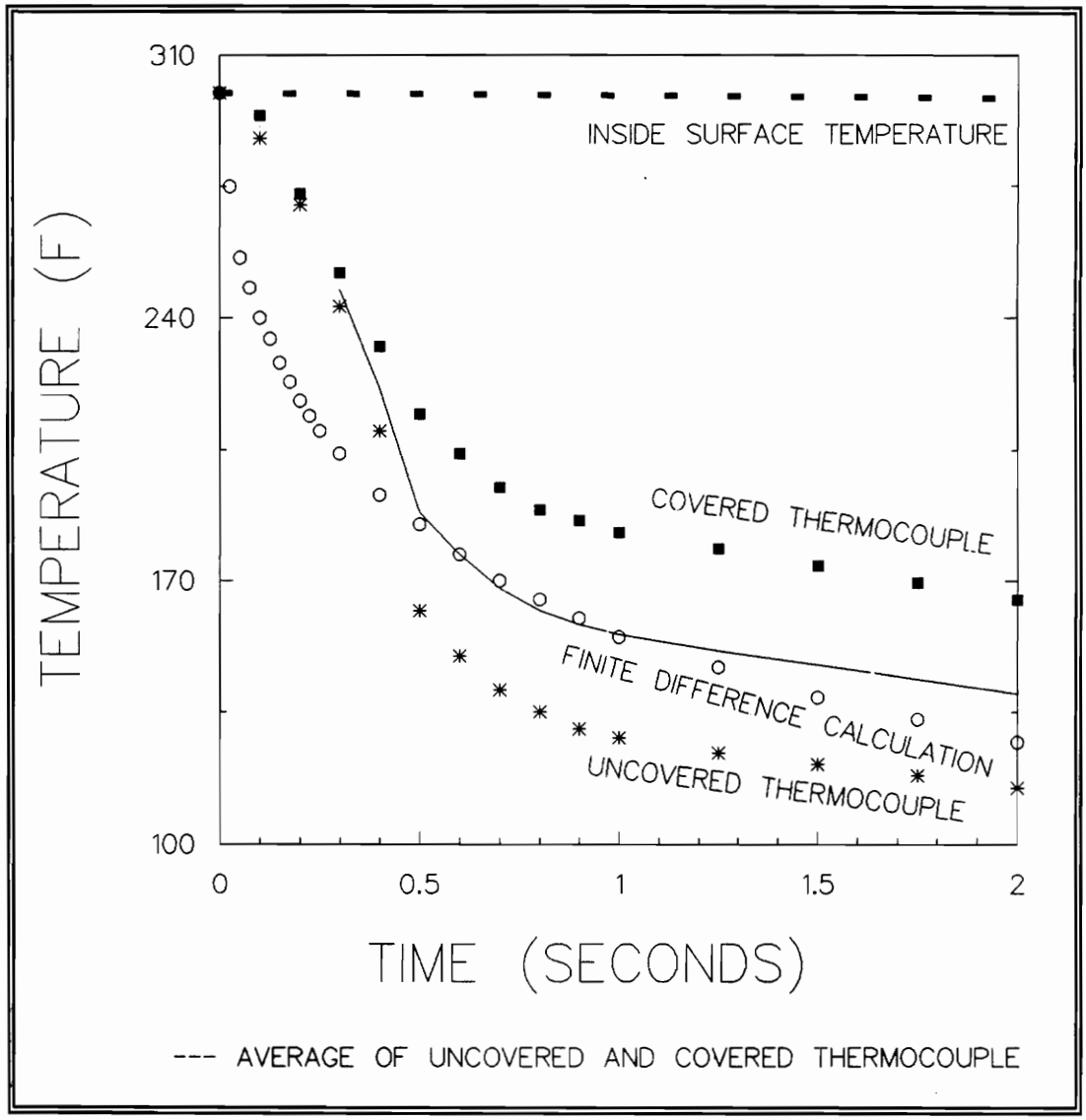

Figure 6-16 Temperature Profiles For The Experimental Quench On The Inside And Outside (Covered And Uncovered) Compared To The Finite Difference Calculation (Film Coefficient = 0.28)

The rest of the data fit into the following matrix.

$$\left\{ \begin{matrix} \text{CIR} \\ \text{LN} \end{matrix} \right\} \text{i} \quad \left\{ \begin{matrix} \\ \text{H} \end{matrix} \right\} \text{j}$$

CIR and LN distinguish between the Circle's and Line's data. The second set of brackets tells where the stresses were hoop (H) or long. ( ). Note that only the hoop stresses have a marking. The i tells which circle or line it is, and j is the number of thermal cycles. The initial stress state is not marked with a 0 as above explained. Some examples are CIR2, CIR28, CIR2H3, CIR33, LN1, LN1H1, and LN320.

6.5.1 Changes in Stress Values Between 0 and 1 Thermal Cycles

The longitudinal stress values of 0 and 1 thermal cycle of Circle 1 are compared in Figure 6-17. For clarity the error bars are drawn on the 0 thermal cycles data only. CIR11 values have similar standard deviations. Certainly the stresses become more compressive after one thermal cycle though individually every location does not comply. The standard deviations may overlap, but note that the CIR11 data are almost always below CIR1 points not evenly distributed above and below. The mean value of the CIR1 data is -10.2 ksi while the mean of CIR11 is -20.6 ksi, a 10 ksi change. Figures 6-18 through 6-20 represent the changes in 0 and 1 thermal cycles in the other Circle's data and demonstrate that in all cases a more compressive stress develops. Table 4 contains the means between 0 and 1 cycle.

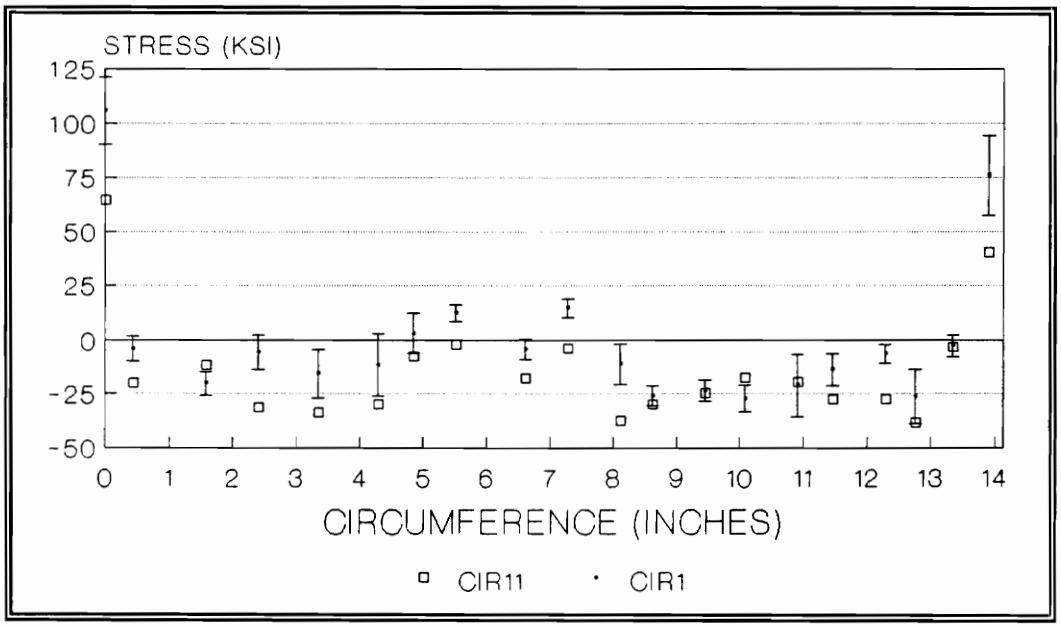

Figure 6-17 Circle 1 Long. Stresses
Initial (With Error Bars) And One Thermal Cycle

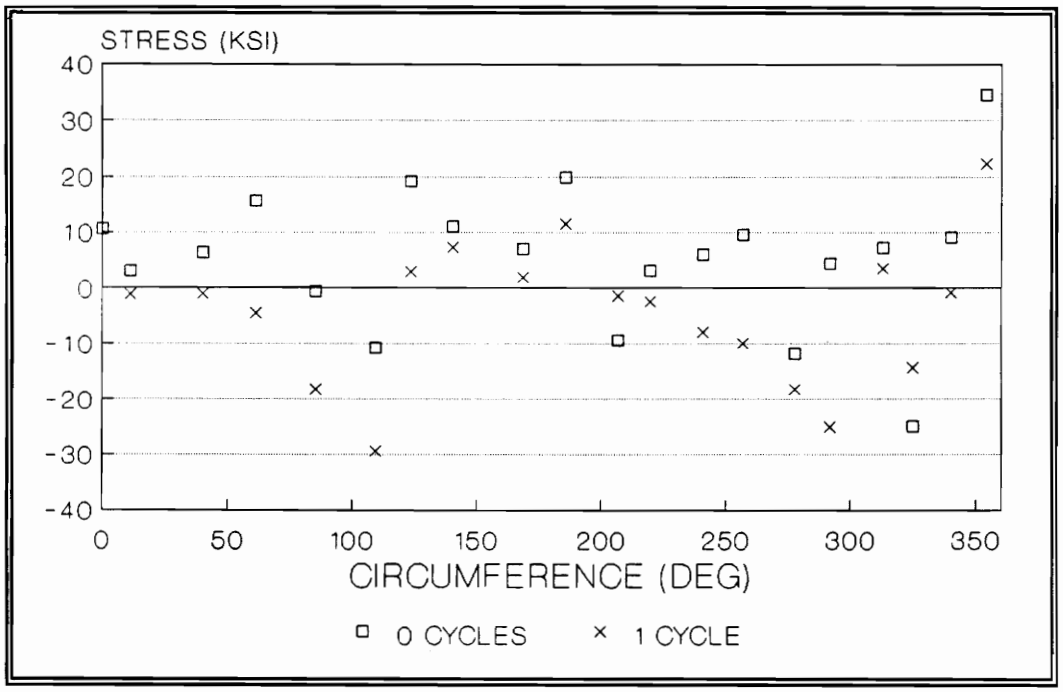

Figure 6-18 Circle 1 Hoop Stresses Initial And One Thermal Cycles

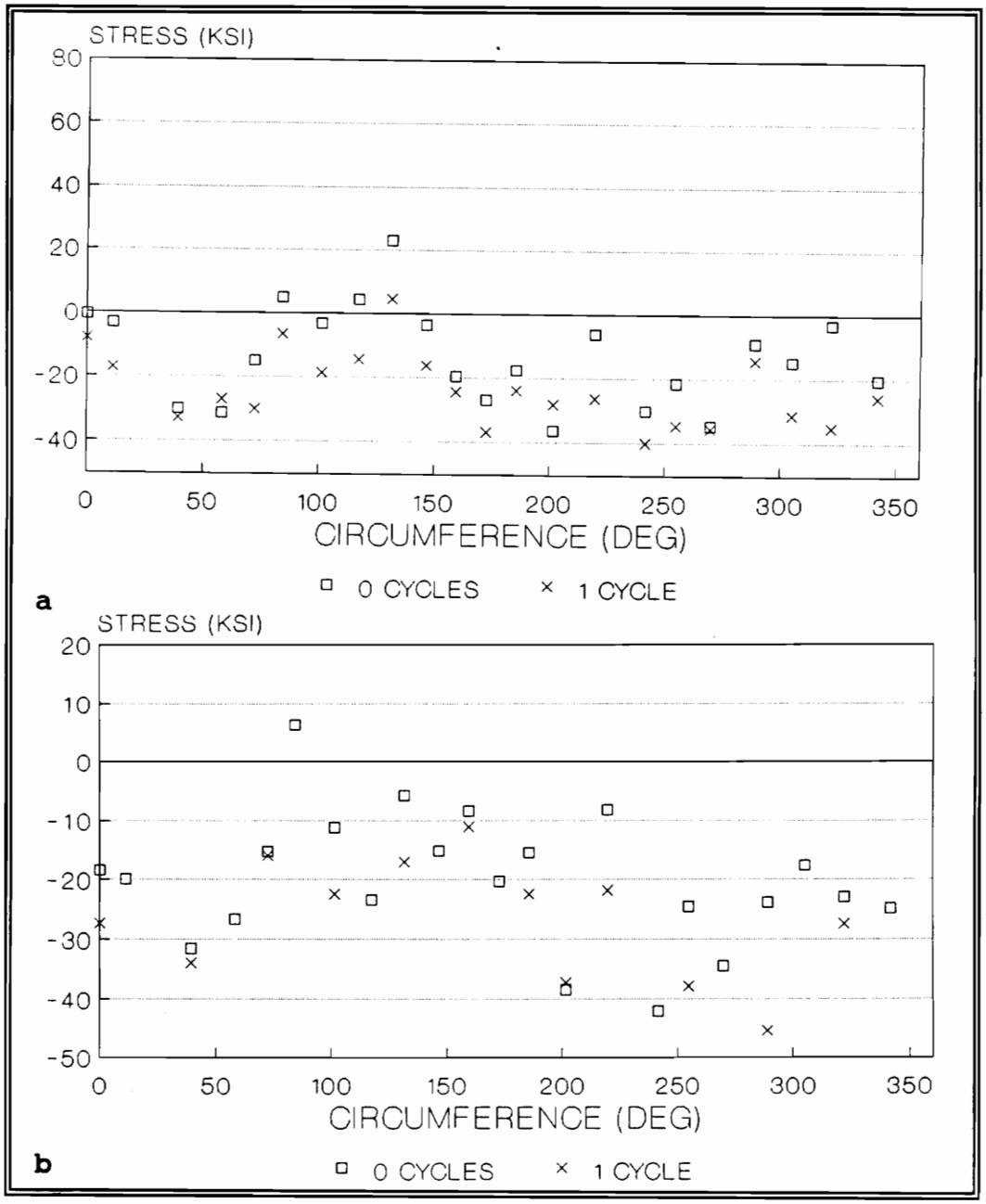

Figure 6-19 Circle 2 Long.(a) And Hoop (b) Stresses Initial One Thermal Cycle

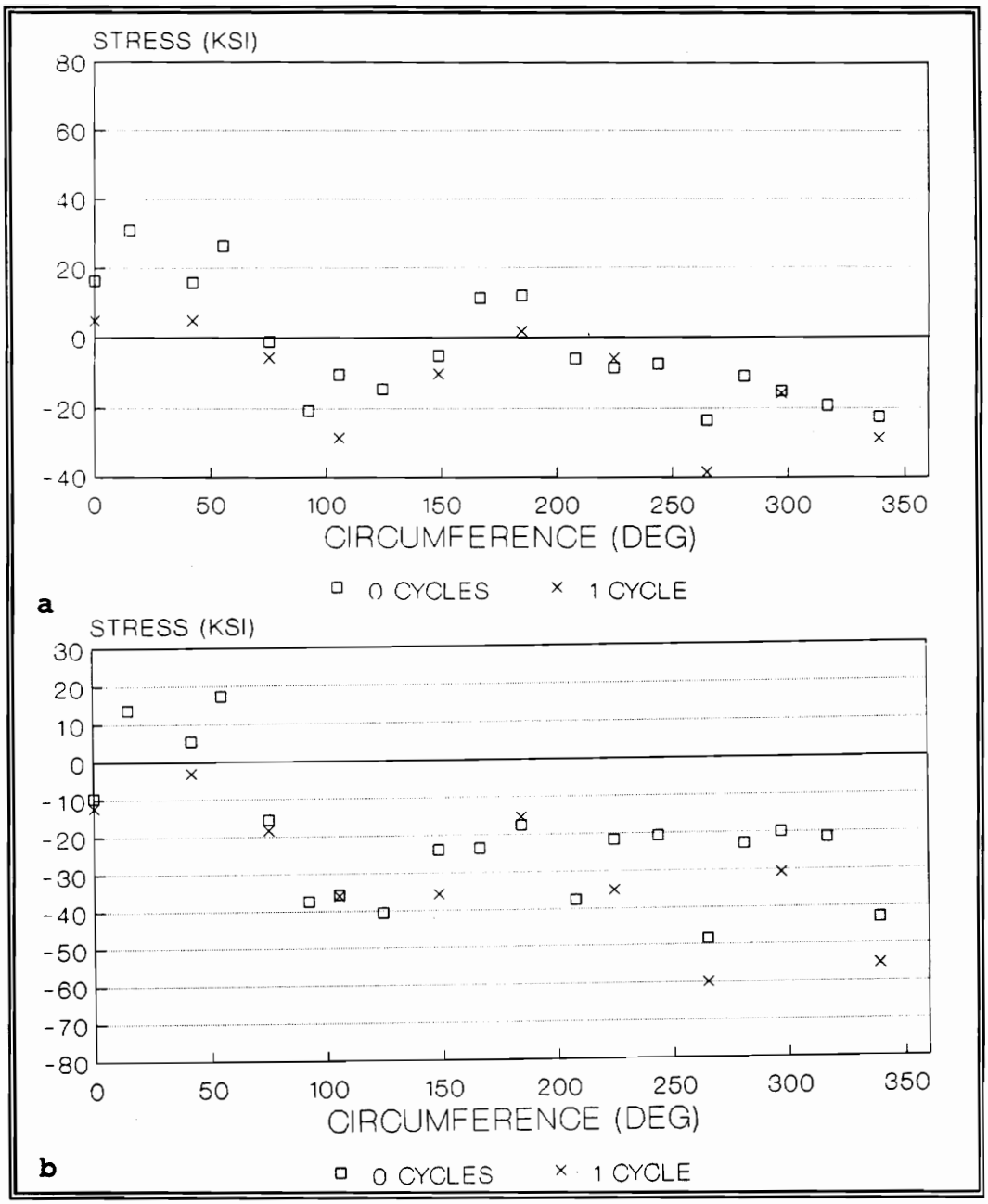

Figure 6-20 Circle 3 Long.(a) And Hoop (b) Stresses Initial One Thermal Cycle

Table 4 Circle Stress Means For 0 and 1 Cycles (ksi)

	CIR1	CIR2	CIR3	CIR1H	CIR2H	CIR3H
Initial Stress Mean	-10.18	-13.46	-2.82	3.55	-20.15	-21.30
Stress Mean For 1 Cycle	-20.55	-23.84	-12.20	-5.98	-26.69	-30.30

The fact that the stresses become more compressive residual stresses is not surprising. As explained in the Literature Review, this is expected. The pipe yields in tension but results in compression after the interior cools. Even with the assumptions in the finite difference model, an average of -10 ksi falls in the range of values predicted by the two curves which did yield. Furthermore, the change in the stresses does indicate that the thermal stresses induced by the quench are sufficient to cause yielding. Many would believe such a small temperature differential, only 280° F (≈ 155° C), is inadequate for plastic deformation. This is not the case as the stress values did change. Interestingly enough after the first thermal cycle the data which previously fit to second order Fourier series were no longer statistically significant at the 95% level even though the data still appear oscillatory. The thermal cycle damped the oscillatory nature of the stresses around the circumference of the pipe.

The Lines' values were not plotted but exhibit shifts analogous with the Circles except for LN1. See Table 5. The Circles' information was considered more significant for two reasons and subsequently less focus was placed on the Lines. The reasons to emphasize Circles were, first, because most researchers assume azimuthal

symmetry, and second, because the data shed light on the effects of the welding process. Measurements on Line 2 were not continued because of the above reasons and to reduce the days needed for the diffraction measurements. One stress value requires a minimum of one half hour to acquire and often can be much longer. The Lines data are be presented in Appendix A.

Table 5 Line Stress Means For 0 and 1 Cycle (ksi)

	LN1	LN3	LN1H	LN3H
Initial Stress Mean	-15.22	-15.57	-20.88	-11.17
Stress Mean For 1 Cycle	-12.51	-25.31	-25.22	-21.72

Contour maps of the Circles' data were devised for a pictorial comparison of the initial residual stresses with those after one thermal cycle. In the color maps of the longitudinal stresses, Figures 6-21 and 6-22, each color represents 6.7 ksi. The lighter the color the higher (tensile) the stress and, conversely, the darker the color the lower (compressive) the stress value is. Changes to a more compressive residual stress state are delineated by the darker colors in Figure 6-22. For contradistinction a contour of the Fourier equations is included in Figure 6-23.

6.5.2 Subsequent Stress Changes With Continued Cycling

All of the longitudinal stress measurements of Circle 1 are shown in Figure 6-24. With the individual variation at a location it was decided the most effective method to analyze the data was to average the stresses for each circle and cycle set and determine how the means vary (since the Fourier coefficients were not significant).

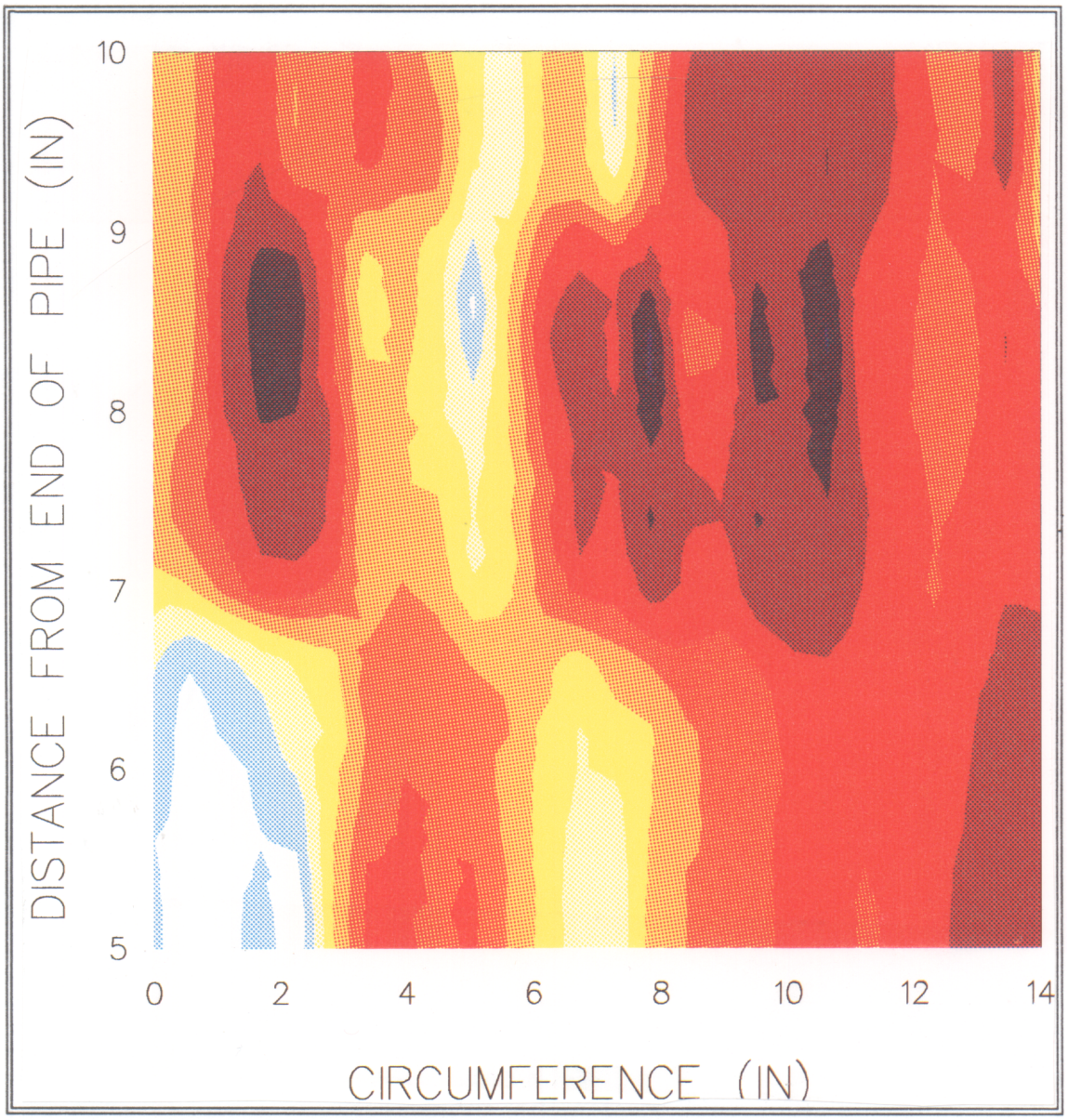

Figure 6-21 Color Contour Map Of Initial Long. Stresses
Each Color Equals 6.7 ksi

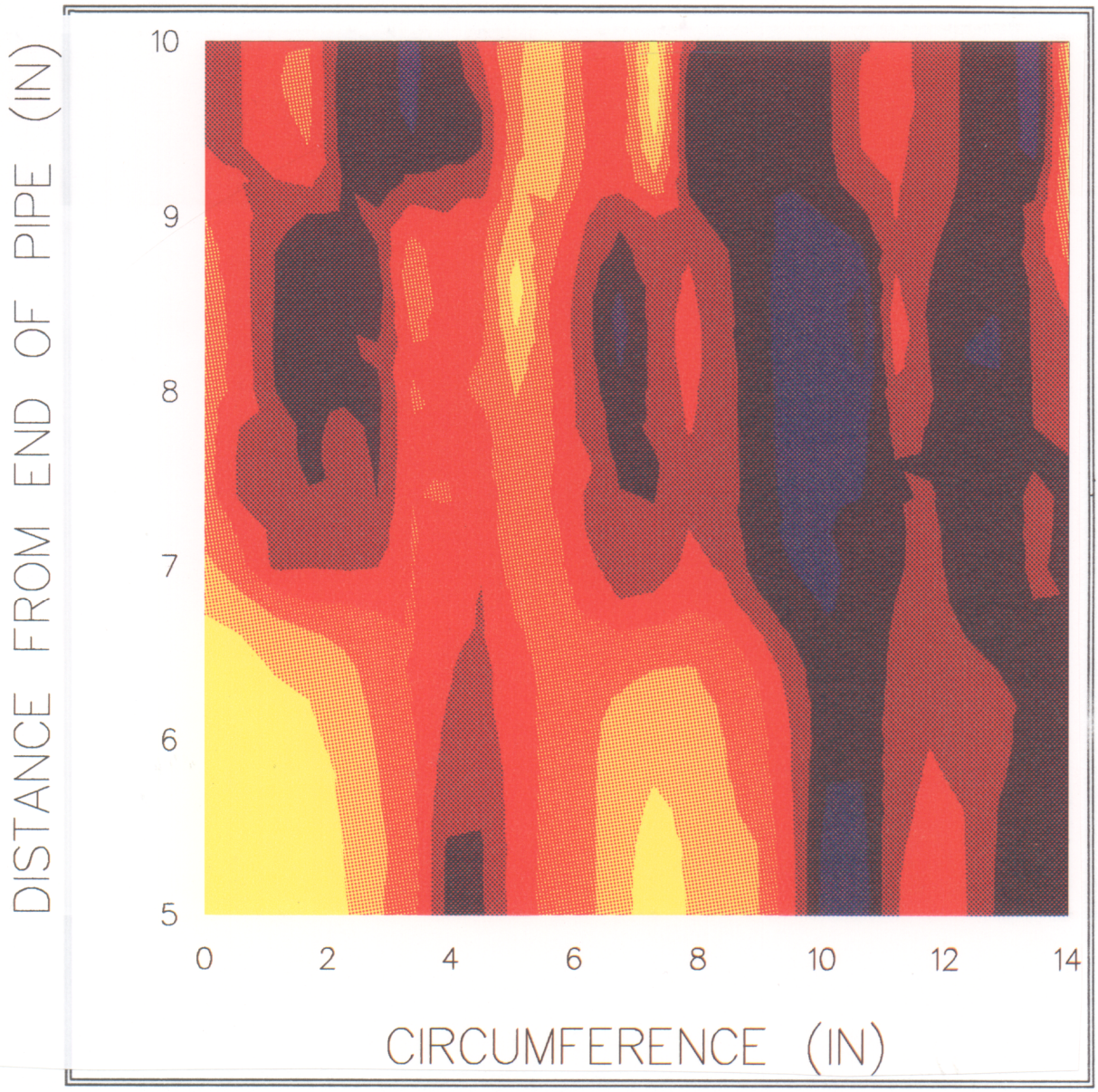

Figure 6-22 Color Contour Map Of Long. Stresses After One Thermal Cycle Each Color Equals 6.7 ksi

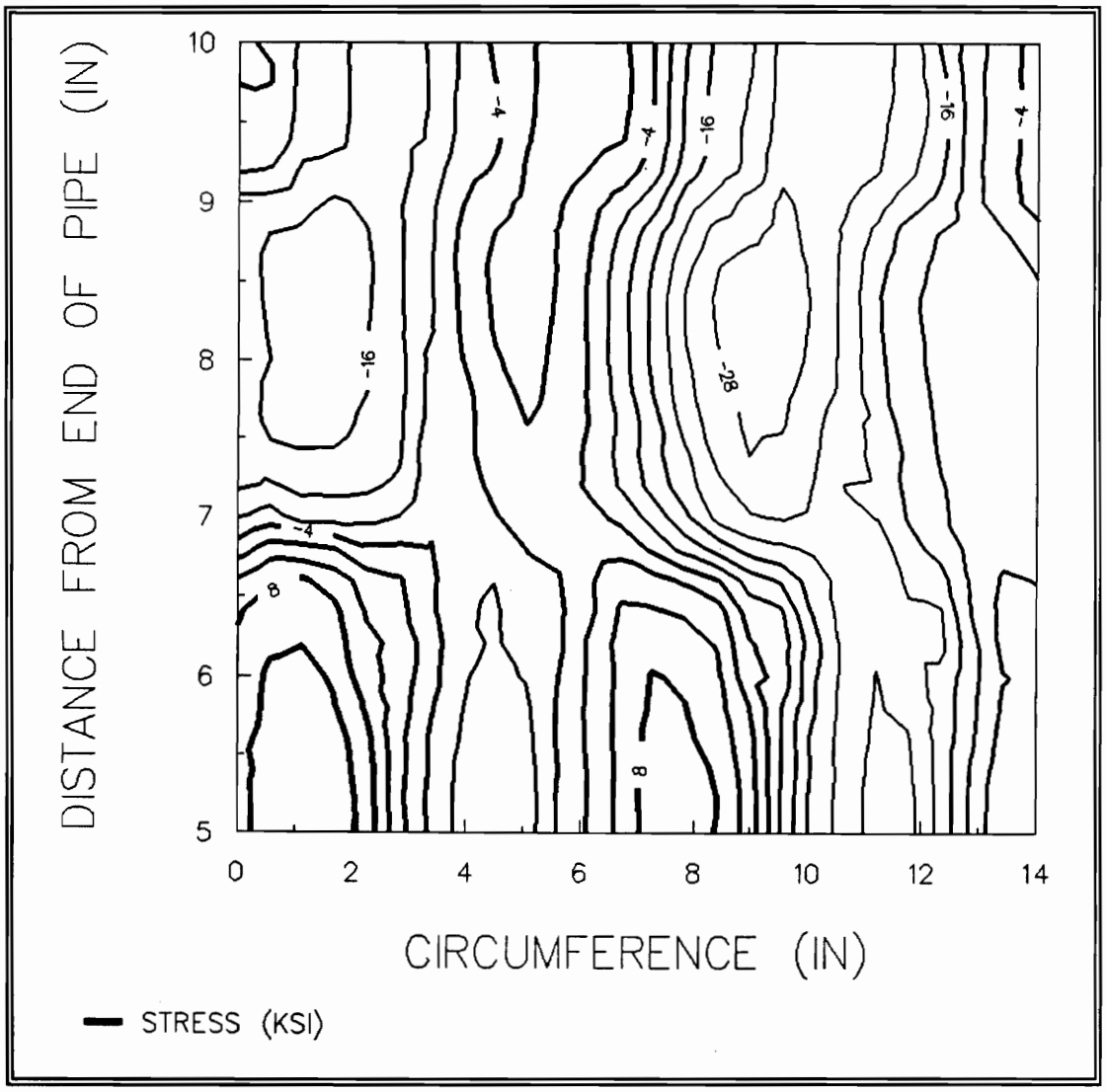

Figure 6-23 Contour Map Of The Fourier Fit To Circles' Long. Stresses

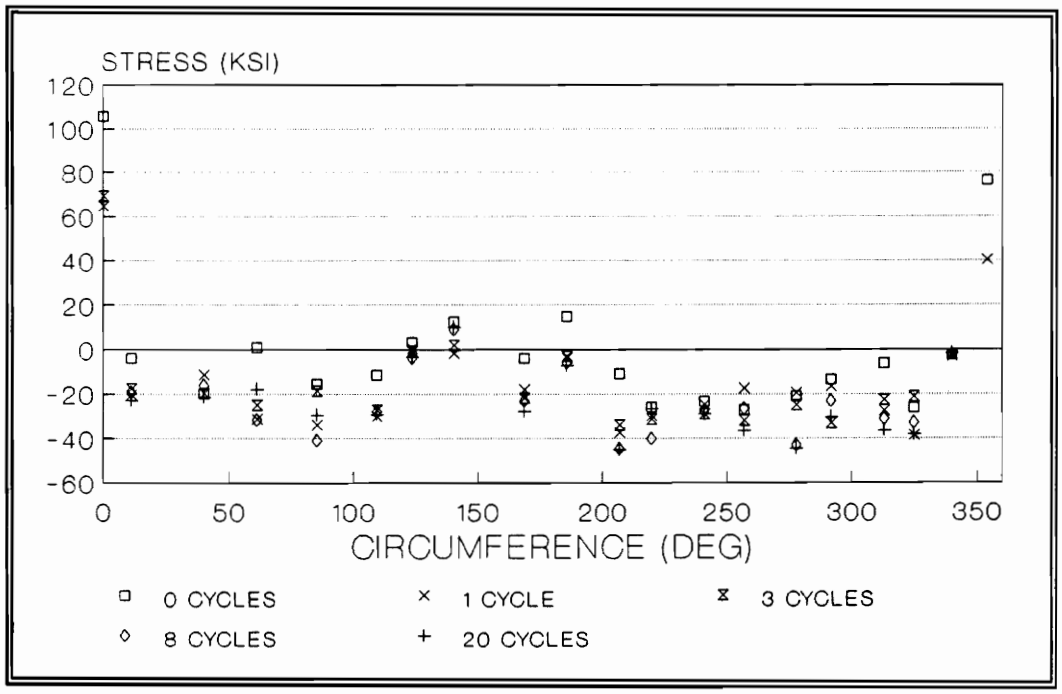

Figure 6-24 Stress Measurements Of Circle 1 Long. For 0, 1, 3, 8, And 20 Cycles

The last and first positions of Circle 1 were not included in the averaging. The mean stresses are drawn in Figure 6-25. The trend in decreasing stress mean (increasing compression) is clear. (Stress mean should not be confused with the term used in context with fatigue cycling.) There is approximately a 10 ksi decrease between the initial and first thermal cycle means and a more gradual change thereafter.

A statistical analysis of the stress means was performed by multiple analysis of variance (ANOVA) on SAS to determine if the differences are significant.(95) The difference between the initial means and first cycle means is significant at the 95% confidence level. In the other sets of cycle data significance could not be established even though there is a trend.

Figure 6-26 represents the data of Figure 6-25 plotted as a traditional x-y graph. This graph shows that the 316L residual stress values are changed the most at first but then settle down after a few cycles. From the previously reported information it can be said that under the experimental conditions the material behaves in the shakedown region of the Bree diagram of Figure 2-1. The shakedown region has plastic deformation which dampens to elastic stresses after a few cycles in a work hardening material. Tables of the raw data are given in Appendix A.

6.5.3 Stress in the Ground Area

The stresses in the ground area were monitored. Initially the stresses showed decreases similar to the locations outside the ground area. However, after three cycles there was an increase in these stress values. This is not understood. Two facts that may have relevance are pointed out. The grinding stresses are much deeper

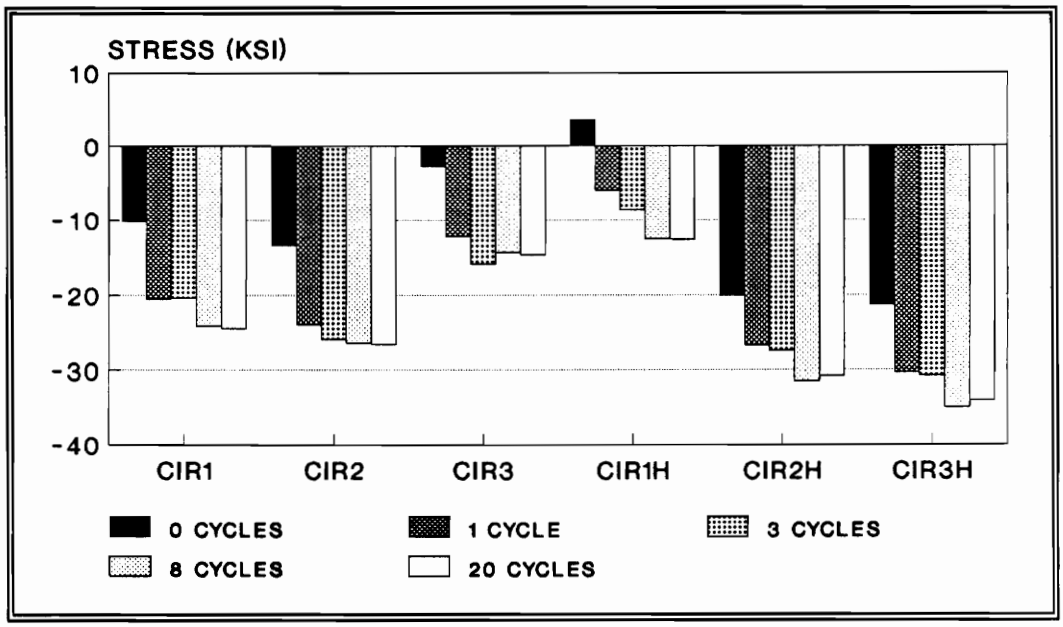

Figure 6-25 Stress Means Of All Circles Data

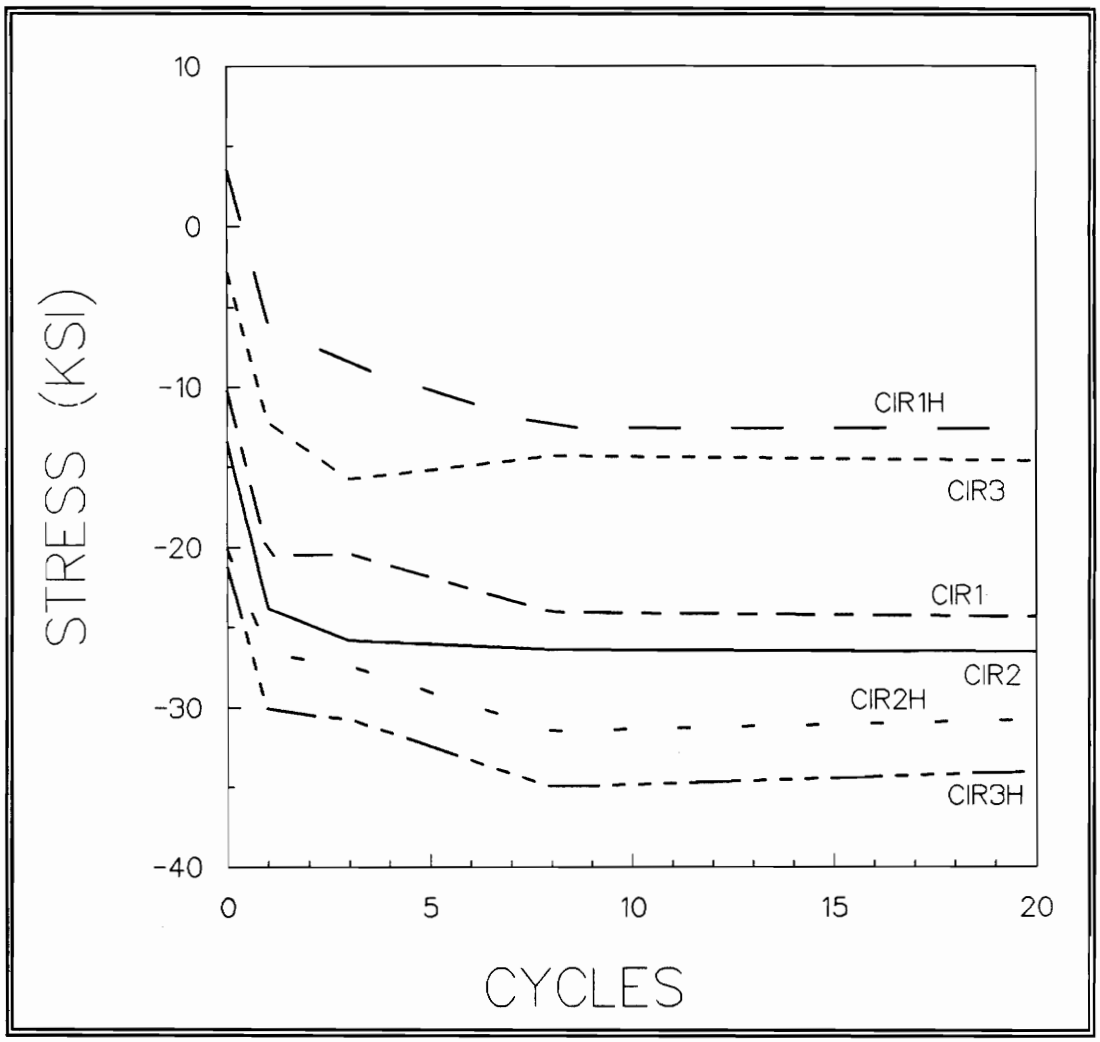

Figure 6-26 Stress Versus Cycle Of The Stress Means

than the penetration of the x-rays, and also, 280° F should not anneal these stresses. Somehow they are being changed. It was decided that this was outside the scope of this project. Ground stress values are given in Appendix A.

6.6 The Effect of Thermal Cycling on FWHM

Thus far all the references to residual stresses have been referring to macro residual stresses. There is another kind of stress in a material. They are micro residual stresses. Macro residual stresses can be thought of as stresses in an area which influence or cause residual stresses in another region. Macro residual stresses are extragranular and assumed uniform in each grain. Macro residual stresses affect the d-spacing in a material. However, on a much more localized level residual stresses exist and can be unevenly distributed. This type of residual stress is referred to as micro residual stresses. Micro residual stress is intergranular and is assumed not to be uniform in a grain. Micro residual stresses affect the FWHM, full width at half maximum (of a diffraction peak), of a material. Micro residual stresses would be especially prevalent in a multiphase material but are not exclusively present there. Micro residual stresses in a single phase, polycrystalline material often arise in uneven straining between or in the grains.

The change in macro residual stresses is not the only way to inspect the effects of thermal cycling on the pipe. Micro residual stresses can also be effected. A way of detecting change in micro residual stress is to monitor the FWHM. Increasing micro residual stresses cause flatter broader peaks, with larger FWHMs. The reverse is not inclusively true. A FWHM does not broaden due only to increasing micro residual stresses since other factors such as particle size can broaden a peak.

Assuming that the small ΔT thermal cycling of this experiment does not affect the particle size, the affects of thermal cycling on micro residual stresses can be studied by reviewing any change in the FWHM of the diffraction peaks. It should be noted that the TEC x-ray residual stress analyzer is not specifically designed to measure micro residual stresses, as it is designed for quantitative macro residual stress determination. Therefore, the FWHM analysis must be taken on a more qualitative level.

The affect of thermal cycling on FWHM is shown in Figure 6-27. Each bar on the graph is an average of all the diffraction peaks at all of the measured locations. The trend of increasing FWHM with number of cycles is easily visible. In terms of FWHMs even a small shift in degrees is a substantial change. Interestingly enough, all of the means are significantly different (by ANOVA tests) except for between the initial and the first cycles (which is probably due to the data of CIR1H and CIR2H). The FWHM means are shown in Table 6 on page 126. This contrasts the macro stress results, meaning that FWHM is not just a function of the stress value but is independent to some degree and is affected in a different manner by the thermal cycling, i.e. there is a statistically significant linear variation between thermal cycling and the FWHM. This is presented in Figure 6-28. The y-intercepts of the regression equations differ but the slopes are not dissimilar. Evidentially thermal cycling effects the FWHM linearly while most of the macro stress effects occurred during the initial quenching. This has serious implications for thermal fatigue (or mechanical if applicable) in this member. The macro residual stress state has stopped changing so one is inclined to think extended thermal cycling has no ill effects. However, the micro residual stresses are still changing with each cycle in a

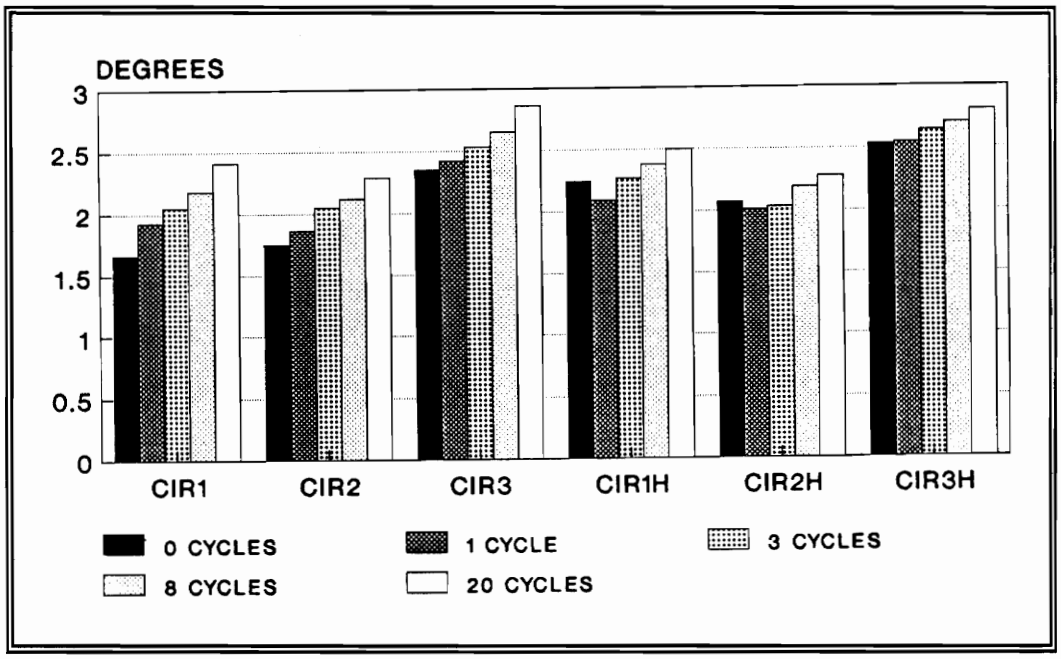

Figure 6-27 FWHM Means Of All Circles' Data

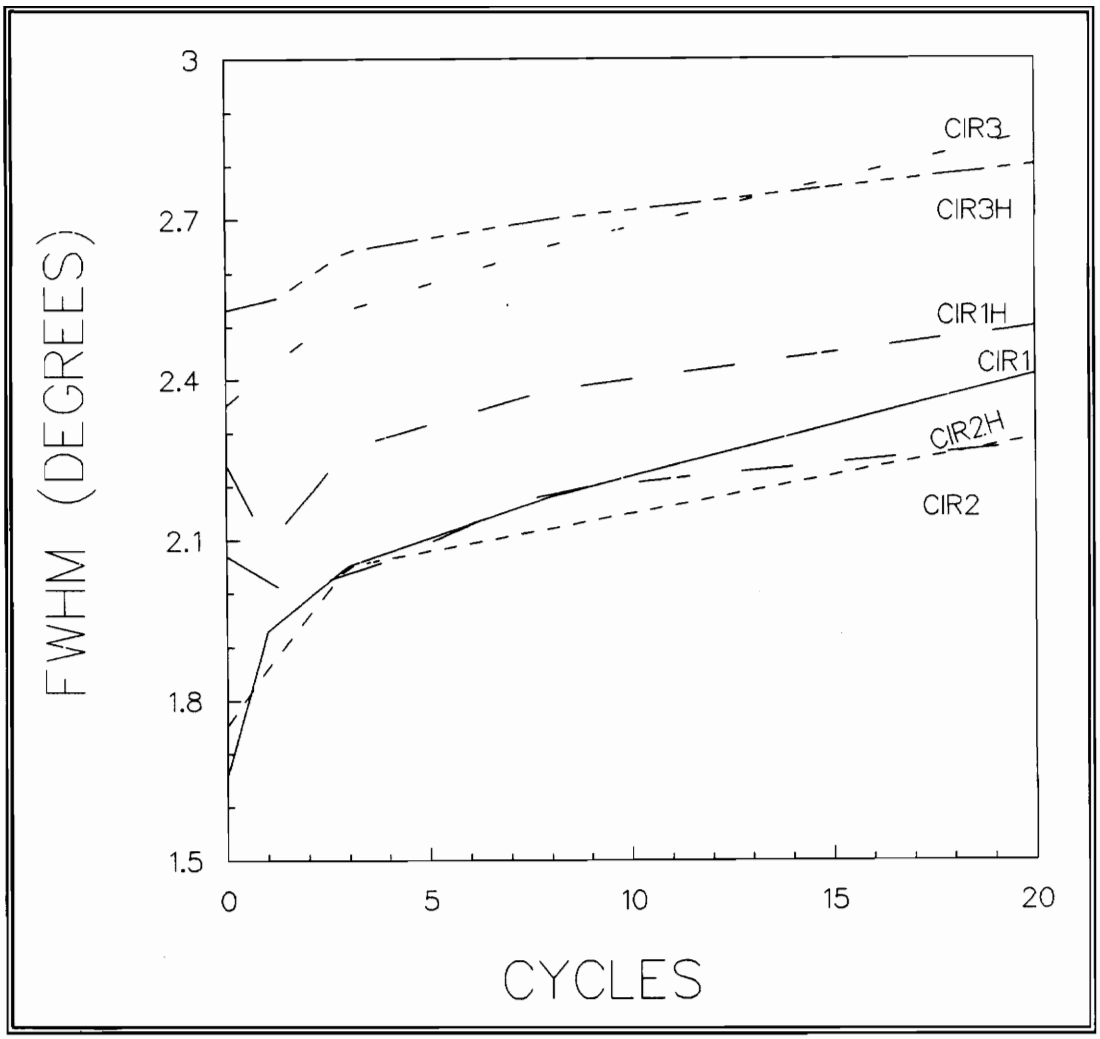

Figure 6-28 FWHM Versus Cycle Of The FWHM Means

linear fashion and could contribute to accelerating fatigue. A visual example of shift in FWHM is shown in Figure 6-29. Two diffraction peaks compare the differences in FWHM of the same location at 0 thermal cycle and after 20 thermal cycles.

Table 6 FWHM Means Of Circles' Data As A Function Of Cycle Measurements in Degrees

	0 Cycle	1 Cycle	3 Cycles	8 Cycles	20 Cycles
CIR1	1.66	1.93	2.05	2.18	2.41
CIR2	1.75	1.86	2.05	2.12	2.29
CIR3	2.37	2.42	2.53	2.65	2.86
CIR1H	2.24	2.09	2.27	2.38	2.50
CIR2H	2.07	2.01	2.03	2.19	2.28
CIR3H	2.53	2.54	2.64	2.70	2.80

An interesting aspect of the ground area is the large full width half maximums (FWHM). In the ground area the diffraction peaks are very broad, as would be expected by the large deformations from mechanical grinding. The comparison between ground areas' FWHM, both hoop and longitudinal, with those outside the ground area is given in Figure 6-30. The ten diffraction peaks of a single stress measurement were averaged to give the FWHM mean. GRD and GRDH stand for the longitudinal and hoop ground area stresses of positions 1 and 20 of Circle 1. Three of the data groups significantly fit regression lines drawn. The data points from the CIR1 were not significant (NS on the graph) but the closest line fit is shown for differentiation. From Figure 6-30 the conclusion would be that the higher the

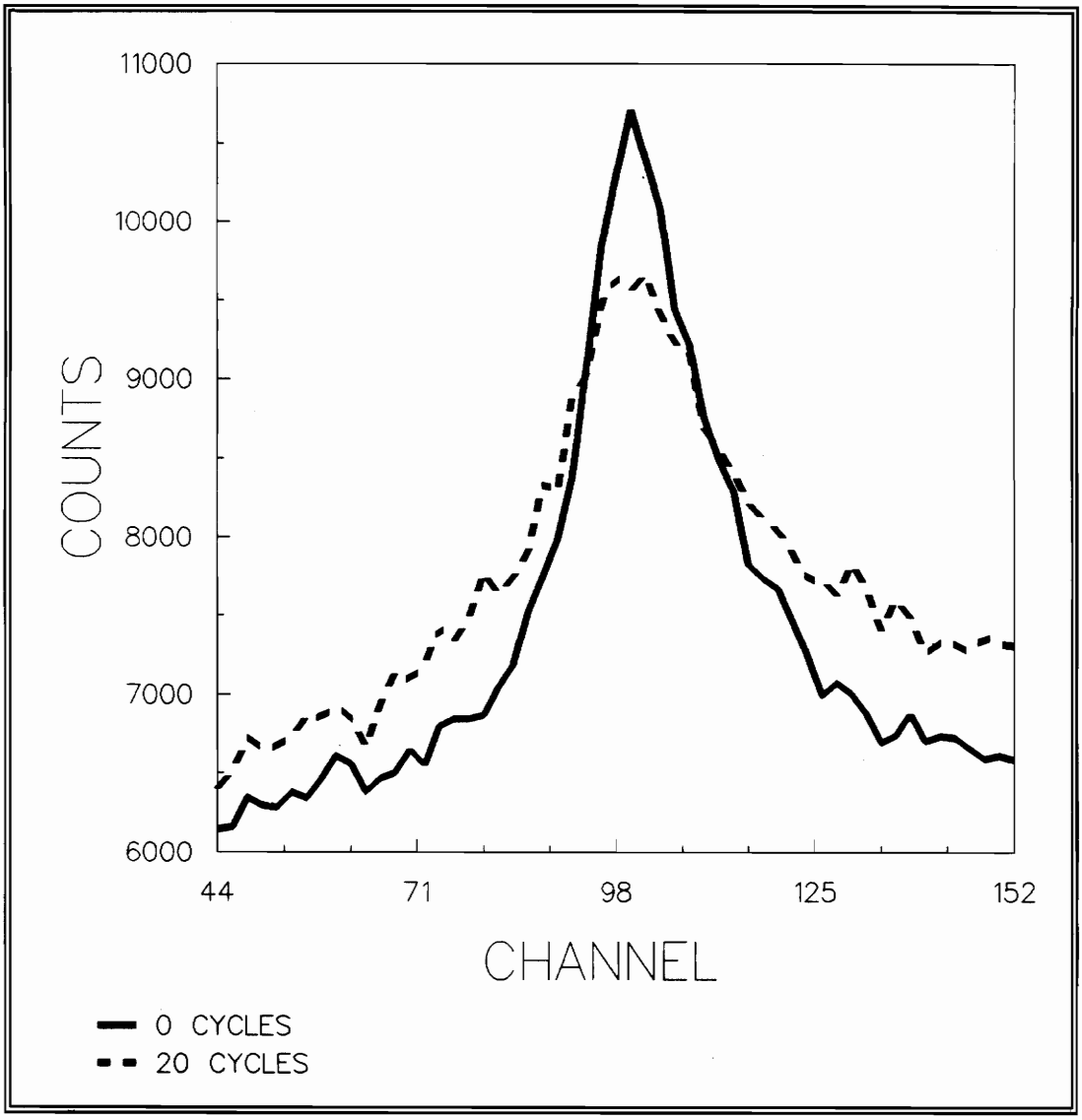

Figure 6-29 Example Of Broadening In The FWHM Between 0 And 20 Thermal Cycles

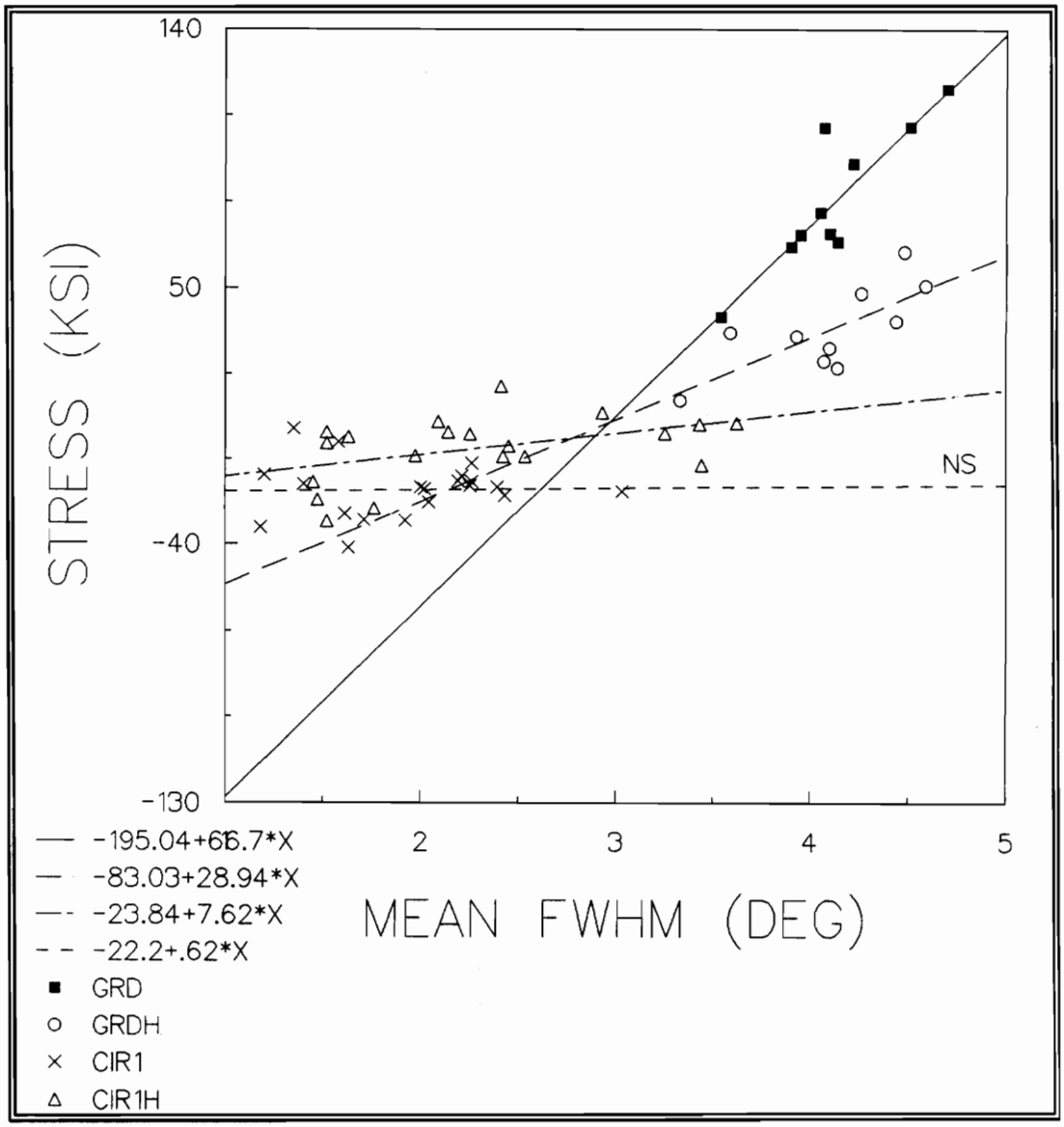

Figure 6-30 Fwhm In And Out Of The Ground Areas Versus Stress

stress the wider the diffraction peak. This is not strictly true as was discussed with FWHM versus cycling data where FWHM changed while the macro stress did not.

6.7 The Influence of Initial Stress State on Final Stress State

One issue we wanted to explore was the effect of the initial stress state on the final stress state in the same location. For example, does the stress state in the as-received pipe make any difference to the effects of thermal cycling? Does most of the change in stress happen only in an area with initially high tensile or compressive stresses? In order to study this, groups of stress values were formed based on initial residual stress sign and magnitude. The initial stress values of a group were then compared to the stress values after 20 cycles of that same set (group) of locations. The results are introduced now in Figure 6-31 and Figure 6-32. The bars denote the decrease (more compressive) in the mean stress value of the group after 20 cycles. The number of locations in the given range (group) of initial values is listed above that bar. The initial range of stress values is given on the horizontal axis. Because of space limitations the negative signs were excluded. The negative (compressive) range groups are on the left of each graph. If the as-received residual stresses have no effect on the final stress state, one would expect the regression lines shown to have zero slope. While the effect is not large, the beginning residual stress state does influence the effects of the thermal cycling. The tensile areas have more overall compressive change. This is not surprising because the pipe yields in tension and this would occur more readily in these areas.

In review of the data presented in this chapter one can find the initial hoop and longitudinal residual stress states documented along the length of the pipe and

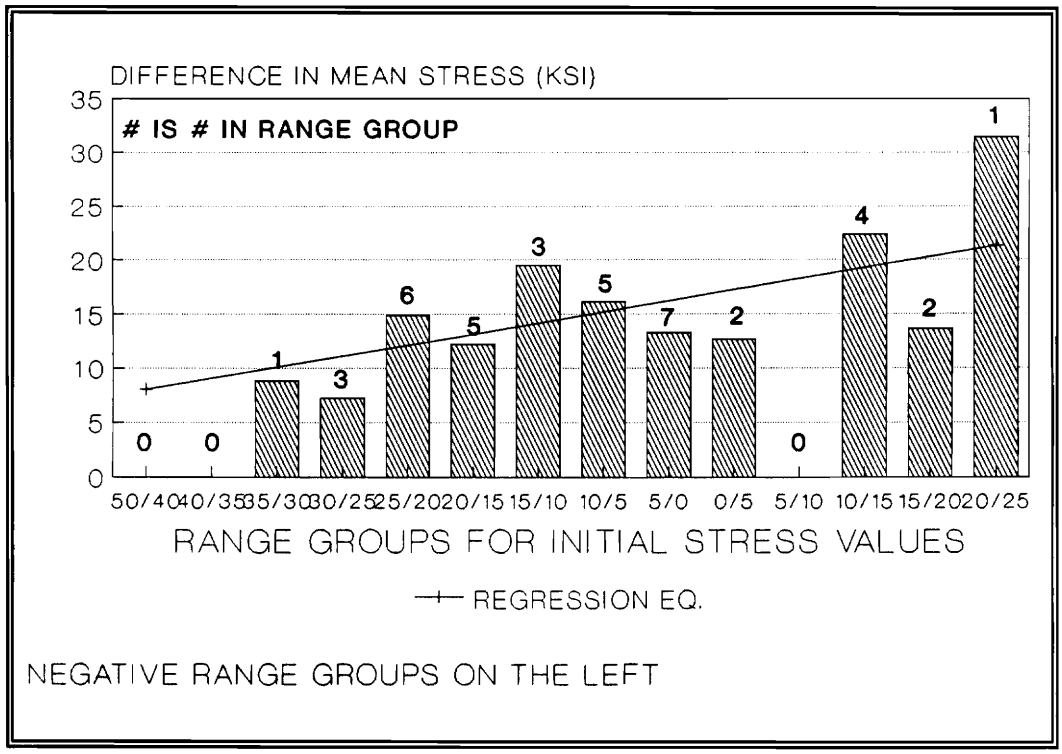

Figure 6-31 Decrease In Mean Long. Stress Between 0 and 20 Thermal Cycles Grouped In Ranges Bases On The Initial Stress Value (See Text)

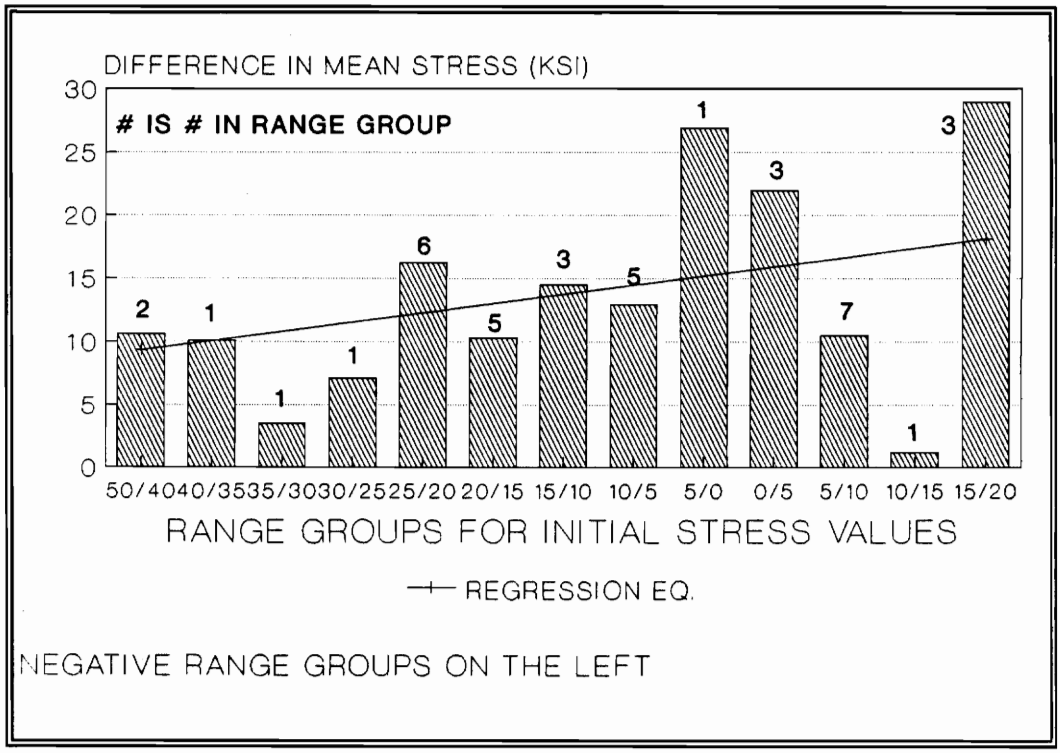

Figure 6-32 Decrease In Mean Hoop Stress Between 0 and 20 Thermal Cycles Grouped In Ranges Bases On The Initial Stress Value (See Text)

around the circumference of the pipe. It was shown by electropolishing and hole-drilling that residual stress does exist in the bulk of the pipe. The experimental temperature quenching profile was illustrated and compared to a FDM calculation. The effects of thermal cycling on both the micro and macro residual stresses were addressed. Lastly, the effects of residual stress state on final stress state was explored.

7.0 Conclusions and Suggested Work

Hindsight is usually 20/20 in life and research. Although the experiment could be better designed now that it has been completed, definite conclusions are drawn. The following conclusions are made from this research project:

- 316L is difficult to x-ray but with sufficiently large data sets statistically based analyses can be made,

- grinding of the weld bead induces large tensile residual stresses up to 105 ksi which may be excellent sites for the initiation of stress corrosion cracking,

- the azimuthal stresses, varying from -30 ksi to +20 ksi, are not symmetrical but show both periodic and random variation. These are believed to result from the multi-pass butt weld.

- the observed stresses are not merely skin effects but penetrate into the bulk to the specimen to approximately -25 ksi,

- thermal cycling even with the small ΔT of 280° F changes the residual stress state approximately 10 ksi compressive and causes plastic deformation. Thus, even small ΔT's have potential for damage.

- and the initial stress state influences the effects of the thermal cycling and, thus, the final stress state.

If time and money were available to perform the experiment again or to continue the work, several interesting aspects would be worth investigating. The following are suggested work for this research project:

- continue thermal cycling with macro and micro residual stress measurement to see if the current trend continue,

- add more Circles to be measured,

- alter the ΔT and determine the effects of a different temperature distribution,

- perhaps the most interesting route to follow would be to measure the residual stresses in the pipe before the welding procedure and be able to follow the effects of the welding and grinding on the stress state,

- and study the unexplainable behavior in the ground area.

References

(1) Mura, T., Micromechanics of Defects in Solids, Martinus Nijhoff Publishers, Hague, The Netherlands, 1982.

(2) Young, W.,ed., Residual Stresses in Design, Process and Materials Control, ASM International, USA, 1987.

(3) Tiara, S. and Inoue, T., "Thermal Fatigue Under Multiaxial Thermal Stresses," Thermal Stresses and Thermal Fatigue, Butterworts, London, 1969.

(4) Seshadri, R., "Design and Life Predictions of Furnace Tubes," Thermal Stress, Materials Deformation, and Thermo-Mechanical Fatigue, ASME, USA, 1987.

(5) Zudans, Z., ed., Thermal Stress Techniques in the Nuclear Industry, American Elsevier Pub. Co., New York, 1965.

(6) Jones, W., et al.,"Thermal Fatigue of Stainless Steel," Effects of Load and Thermal Histories On Mechanical Behavior of Materials, The Metallurigical Society, Inc., Warrendale, PA, 1987.

(7) ADINAT, 1981, "ADINA-A Finite Element Program For Automatic Dynamic Incremental Nonlinear Analysis of Temperatures," Report AE81-2, ADINA Engineering Inc., Cambridge, MA, 1981.

(8) Chiswick, H.,"The Plastic Deformation of Uranium on Thermal Cycling," Trans. Am. Soc. Metals, 1957, 622, 4.

(9) Beer, F. and Johnston, E.,Mechanics of Materials, McGraw-Hill Book Co., New York, 1981.

(10) Timoshenko,S. and Goodier, J.,Theory of Elasticity, McGraw-HIll Book Co., New York, 1970.

(11) Boley, B. and Weiner, J.,Theory of Thermal Stresses, Robert E. Krieger Pub. Co., Malabar, FL, 1985.

(12) Gatewood, B.,Thermal Stresses With Application To Airplanes, Missiles, Turbines, and Nuclear Reactors, McGraw-Hill Book Co., New York, 1957.

(13) Burgreen, D.,Elements of Thermal Stress Analysis, C. P. Press, Jamaica, NY, 1971.

(14) Carslaw, H.,Mathematical Theory of the Conduction of Heat in Solids, Dover Pub., New York, 1945.

(15) The Metals Handbook, American Society For Metals, Metals Park, Ohio, 8th ed.,1975, **10.**

(16) Guide to Materials Engineering Data and Information, ASM International, Metals Park, Ohio, 1986.

(17) Manson, S.,"Avoidance, Control, and Repair of Fatigue Damage,"Metal Fatigue Damage -- Mechanism Detection, Avoidance, and Repair With Special Reference to Gas Turbine Components, ASTM, 1971.

(18) Manson, S.,Thermal Stress and Low-Cycle Fatigue, McGraw-Hill Book Co., New York, 1966.

(19) White, D.,"Some Contributions of British Work on Thermal and High Strain Fatigue," Thermal Stresses and Thermal Fatigue, Butterworts, London, 1969.

(20) Tilly, G.,"Laboratory Simulation of Thermal Fatigue Experienced by Gas Turbine Blading," Thermal Stress and Thermal Fatigue, Butterworts, London, 1969.

(21) Krajczyk, A. and Zuchowsk, R.,"Specific Strain Work As a Measure of Material Damage Under Creep and Thermal Cycling," Mechanical Behavior of Materials, vol.2, Pergamon Press, New York, 1988.

(22) Chung, T.,"Experimental Study of Cyclic Creep of AISI Type 347 Stainless Steel in Temperature Range 100-250° C," Stainless Steels '84, The Institute of Metals, London, 1985.

(23) Grosskreutz, J.,"Fatigue Mechanisms in the Sub-Creep Range," Metal Fatigue Damage - Mechanism Detection, Avoidance, and Repair with Special Reference to Gas Turbine Components, ASTM, 1971.

(24) Bree, J.,"Elastic-plastic Behavior of Thin Tubes Subjected to Internal Pressure and Intermittent High-heat fluxes With Application to Fast-Nuclear Reactors," J. of Strain Analysis, 1967, 226, **2**

(25) Ponter, A. and Karadeni, S.,"An Extended Shakedown Theory for Structures That Suffer Cyclic Thermal Loading, Part 1:Theory, Part 2:Application," J. of Applied Mechanics, 1985, 877, **52.**

(26) Karadeniz, S. and Ponter,A.,"Bound Approach to the Shakedown Limit of Thin Shells Subjected to Variable Thermal Loading," J. of Strain Analysis, 1984, 221, **19.**

(27) Bree, J.,"Incremental Growth Due to Creep and Plastic Yielding of Thin Tubes Subjected to Internal Pressure and Cycling Thermal Stressess, J. of Strain Analysis, 1968, 122, **3.**

(28) Inoue, T., et al."Succeessive Deformation of a Viscoelastic-Plastic Tube Subjected to Internal Pressure Under Temperature Cycling," J. of Thermal Stresses, 1980, 185, **3.**

(29) Langer, B.,"Design Aspects of Eleated Temperature Technology," Creep and Fatigue in Elevated Temperature Technology, The Institute of Mechanical Engineers, London, 1975.

(30) Goodman, A.,"The Influence of Rapid Thermal Transitions Elastic-Plastic Ratchetting," Eng. Struct., 1981, **3.**

(31) Hyde, T., et al.,"Thermal Ratchetting of a Tube With Nonuniform Thickness," Int. J. Mech. Sci., 1986, 657, **28.**

(32) Seitoglu, H.,"Constraint Effects in Thermo-Mechanical Fatigue," J. of Eng. Mat. and Tech., 1985, 221, **107.**

(33) Zarka, J. and Casier, J.,"Practical Remarks About Cyclic Loadings on an Elastic-Plastic Structure," Nuc. Eng. and Des., 1978, 69, **51.**

(34) Furukawa, T. and Takeuti, Y.,"Coupled Thermal Stresses in a Circular Hollow Cylinder Due to the Thermal and Mechanicl Loads," Bulletin of JSME, 1986, 2392, **29.**

(35) Yuan, F. and Wu, S.,"Transient-temperature and Residual Stress Fields in Axisymmetric Metal Components After Hardening," Materials Science and Technology, 1985, 851, **1.**

(36) Burnett, J. and Padovan, J.,"Residual Stress Fields in Heat-Treated Case-Hardened Cylinders," J. of Thermal Stresses, 1979, 251, **2.**

(37) Jeanmart, P. and Bouvaist, J.,"Finite Element Calculation and Measurement of Thermal Stresses in Quenched Plates of High Strength 7075 Aluminium Alloy," Materials Science and Technology, 1985, 765, **1.**

(38) Schroder, R.,"Influences on Development of Thermal and Residual Stresses in Quenched Cylinders of Different Dimensions," Materials Science and Technology, 1985, 754, **1.**

(39) Wulpi, D.,Understanding How Components Fail, ASM, Metals Park, Ohio, 1985.

(40) Burnett, J.,"Prediction of Stress History in Carburized and Quenched Steel Cylinders," Materials Science and Technology, 1985, 863, **1.**

(41) Todaro, M., et al.,"Residual Stress in Quenched Steel Cylinders," Residual Stresses in Design, Process and Materials Control, ASM, Metals Park, Ohio, 1987.

(42) Ericsson, T. and Hildenwall, B.,"Thermal and Transformation Stresses," Residual Stress and Stress Relaxation, 1981.

(43) Delate, F. and Kolluri, S.,"Fracture of Thick Walled Cylinders Subjected to Transient Thermal Stresses," J. of Thermal Stresses, 1985, 235, **8.**

(44) Yu, H. and Macherauch, E.,"Calculation of Quenching Stresses With and Without Transformation Effects," Residual Stress and Stress Relaxation, 1981.

(45) Naborro, F.,"The Calculation of Thermal Stresses in Cylinders," Int. J. Eng. Sci., 1981, 651, **19.**

(46) Raniecki, B.,"Overlay Model For Determining Thermal-Hardening Stresses in Metallic Solids," Materials Science and Technology, 1985, 856, **1.**

(47) Ishikawa, H.,"A Thermoelastoplastic Solution For a Circular Solid Cylinder Subjected to Heating and Cooling," J. of Thermal Stresses, 1978, 211, **1.**

(48) Mishra, A. and Prasad, T.,"Residual Stresses Due to a Moving Heat Source," Int. J. of Mech. Sci., 1985, 571, **27.**

(49) Sjostrom, S.,"Interactions and Constitutive Models For Calculating Quench Stresses in Steel," Materials Science and Technology, 1985, 823, **1.**

(50) Fletcher, A. and Soomro, A.,"The Effect of Stress Relaxation Rate on the Generation of Thermal Stress During Quenching," Materials Science and Engineering, 1986, 101, **82.**

(51) Masubuchi, K.,Analysis of Welded Structures, Pergamon Press, New York, 1980.

(52) Weisman, C., ed.,"Fundamentals of Welding," Welding Handbook, vol.1, American Welding Society, Miami, 1976.

(53) Karlsson, L.,"Thermal Stresses in Welding," Mechanics and Mathematical Methods--Thermal Stresses I, 1986.

(54) Masubuchi, K.,"Residual Stresses and Distortions in Weldments: A Review of Present State-of-the-Art, Residual Stress and Stress Relaxation, 1981.,

(55) Wylde, J.,"The Influence of Residual Stresses on the Fatigue Design of Welded Steel Structures," Residual Stresses in Design, Process and Materials Control, ASM, Metals Park, Ohio, 1987.

(56) Mosley, W.,"Residual Stresses at Pinch Welds in Small Stainless Steel Tubes," Residual Stresses in Design, Process and Materials Control, ASM, Metals Park, Ohio, 1987.

(57) Karlsson, R.,"Transient Temperatures and Stress in Butt Welds-- A Finite Element Study," Thesis for the Degree of Licentiate of Engineering, Gö teborg, 1987.

(58) Karlsson, T.,"FE-Calculated Stresses in Single Pass and Multi-Pass Butt Welded Steel Pipes," Thesis for the Degree of Licentiate of Engineering, Gö teborg, 1988.

(59) Jonsson, M. and Josefson, B.,"Experimentally Determined Transient and Residual Stresses in Butt Welded Pipe," J. of Strain Analysis, 1988, 25, **3.**

(60) Josefson, B.,"Effects of Transformation Plasticity on Welding Residual Stress Fields in Thin-Walled Pipe and Thin Plates," Materials Science and Technology, 1985, 904, **1.**

(61) Ellingson, W. and Shack, W.,"Residual-Stresses Measurement on Multi-Pass Weldments of Stainless-Steel Piping," Experimental Mechanics, 1979, 317, **19.**

(62) Chrenko, R.,"Thermal Modifications of Welding Residual Stresses," Residual Stress and Stress Relaxation, 1981.

(63) Marsh, D.,"A Thermal Shock Fatigue Study of Type 304 and 316 Stainless Steel," Fatigue of Engineering Materials and Structures, 1981, 179, **4.**

(64) Ponter, A. et al.,"An Experimental Study of Simplified Methods For the Prediction of Deformation of Structures Subject to Severe Thermal Loading," J. of Strain Analysis, 1985, 225, **4.**

(65) Iorio, J. and Crespi, J.,"Some Aspects of Thermal Fatigue in Stainless Steel," Int. J. Pres. Ves. and Piping, 1986, 149, **23.**

(66) Jo, J., "Residual Stress Measurement In Railroad Car Wheels," Dissertation for the Degree Doctor of Philosophy, VPI & SU, September, 1989.

(67) Dehan, C.,"An Intelligent Workstation For Reliable Residual Stress Determination Using X-ray Diffraction," Thesis for the Degree Master of Science, Virginia Tech, Blacksburg, VA, July, 1989.

(68) Noyen, I. and Cohen, J.,Residual Stress Measurement by Diffraction and Interpretation, Springer-Verlag, New York, 1979.

(69) Dö lle, H., J. Applied Cryst., 1978, 489, **12.**

(70) Residual Stress Measurement By X-ray Diffraction, SAE J784a, SAE, Warrendale,PA, 1971.

(71) TEC Model 1600 X-ray Stress Analysis System Operation and Maintenance Manual, Technology for Energy Corporation, Knoxville, TN, 1985.

(72) ABSTAT, product of Anderson-Bell Corp. Parker, Colorado 80314

(73) Marshall, P., Austenitic Stainless Steels, Elsevier Applied Science Publishers, New York, 1984.

(74) Pickering, F., "Physical Metallurgical Development of Stainless Steels," Stainless Steels 84, The Institute of Metals, London, 1985.

(75) Harries, D., "Physical Metallurgy of Fe-Cr-Ni Austenitic Steels," Mechanical Behavior and Nuclear Applications of Stainless Steel At Elevated Temperatures, The Metals Society, London, 1982.

(76) Goodman, A. and Goodall, I., "Constitutive Relations For Stainless Steels," Mechanical Behavior and Nuclear Applications of Stainless Steel At Elevated Temperatures, The Metals Society, London, 1982.

(77) Uggowitzer, P., et al., "Fracture Toughness of Cold Worked Austenitic Steels," Mechanical Behavior of Materials, Pergamon Press, New York, 1988.

(78) Conway, J., et al., Fatigue, Tensile, and Relaxation Behavior of Stainless Steel, National Technical Information Center, Springfield, Virginia, 1975.

(79) Keller, D., "Progress on LMFBR Cladding, Structural, and Component Materials Studies During July,1971, Through June, 1972," Final Report, Task 32, Prepared For the U. S. Atomic Energy Commission, Battelle, Columbus, Ohio, 1972.

(80) Sritharan, T. and Jones, H., "Creep of Austenitic Stainless Steels At Low Stresses," Mechanical Behavior and Nuclear Applications of Stainless Steel At Elevated Temperatures., The Metal Society, London, 1982.

(81) Lankford, W., ed., The Making, Shaping, and Treating of Steel, United States Steel, Herbrick and Held, Pittsburgh, Pennsylvania, 1985.

(82) Farrar, R., "Influence of Microsegregation on Phase Transformation and Properties of Type 316 Weld Metals At Elevated Temperatures," Stainless Steels '84, The Institute of Metals, London, 1985.

(83) David, S., et al., "Solidification Behavior of Austenitic Stainless Steel Filler Materials," Welding Research Supplement 335-s, The Welding Journal, 1979.

(84) Lamb, M., et al., "Structure and Residual Stresses of Two Laser Surface Melted Stainless Steels," Stainless Steel '84, The Institute of Metals, London, 1985.

(85) Fletcher, A. and Lewis, C., "Effect of Free Edge on Thermal Stresses in Quenched Steel Plates," Materials Science and Technology, 1985, 781, **1**.

(86) "Measurement of Residual Stresses By the Hole-Drilling Strain-Gage Method: Measurement Group Tech Note TN503-3," Measurement Group Inc., Raleigh, NC, 1988.

(87) Boag, J., et. al, "Considerations of Using the Hole Drilling Method For Measuring Residual Stresses in Engineering Components," Residual Stresses in Design, Process and Materials Control, ASM, 1987.

(88) Determining Residual Stresses by the Hole-Drilling Strain Gage Method, ASTM Standard E837.

(89) Moore, M. and Evans, W., "Mathematical Correction For Stress in Removed Layers in X-ray Diffraction Residual Stress Analysis," SAE Transactions, 1959, 340, **66.**

(90) Nakagawa, Y., et al., Effects of Surface Finish on Residual Stress Distribution and SCC Susceptibility of Type 304 Austenitic Stainless Steel in a Boiling 42% MgCl2 Solution," ICM, 603, **3.**

(91) Brady, M., "Effect of Laser Surface Melting to Mitigate Chloride Stress Corrosion Cracking," Thesis for the Degree Master of Science, Blackburg, VA, 1990.

(92) CoStat, product of CoHort Software, Berkeley, CA, 1988.

(93) Moore, M. and Evans, W., "Mathematical Correction For Stress in Removed Layers in X-ray Diffraction Residual Stress Analysis," SAE Transactions, 1959, 340, **66.**

(94) Swift, G., "A Thermoelastic-plastic Analysis of Thermal Cycling in a Thick-walled Tube Using aVon Mises Yielding Criterian," Technical Report #VPI-E-8836, Department of Engineering Science and Mechanics, VPI&SU, Blacksburg, VA, December,1988.

(95) SAS, product of SAS Institute Inc., Cary, NC, 27511.

Appendix A

The following data are the macro residual stress measurementS obtained in the course of this project. The variable name convention is explained on Page 106 and continued on Page 108. See Figure 5-1, Page 72 for a view of the measurement locations. The position (POSTN) of the first measurement was arbitrarily chosen but in the Circles the first positions are aligned. Again, there are different numbers of measurement locations from Circle to Circle and Line to Line. The values are given in ksi.

The ground area data are intersperse in the Circles and Lines, but they are always in the same location. For the Lines ground areas would be POSTN 5, 6, and 7. In the Circles there are only two CIR1, POSTN 1 and 20.

FWHM data will not be given in an appendix as it is too voluminous.

POSTN	LN1	LN11	LN13	LN18	LN120
1.00000	-13.3800	-9.38000	-19.4200	-22.9900	--
2.00000	-15.7900	-17.1400	-25.2600	-19.7600	--
3.00000	-0.290000	10.7000	16.9600	9.92000	--
4.00000	1.29000	-0.880000	-0.110000	-1.20000	--
5.00000	113.390	86.4800	111.190	122.740	--
6.00000	114.560	75.6100	97.8000	130.990	--
7.00000	128.720	87.5000	108.520	145.110	--
8.00000	-25.9000	-30.9300	-35.8400	-35.3200	-39.5200
9.00000	-33.7800	-32.4400	-53.2300	-48.1500	--
10.0000	-33.3100	-21.3200	-24.8700	-42.7400	--
11.0000	-0.610000	1.28000	-2.27000	1.63000	1.69000

LINE 1 LONG.

POSTN	LN1H	LN1H1	LN1H3	LN1H8	LN1H20
1.00000	-28.2000	-33.2600	-36.0400	-36.1500	-37.5000
2.00000	-41.2000	-42.2200	-46.6200	-50.7300	-54.4200
3.00000	11.3000	14.2000	9.92000	11.6000	15.0100
4.00000	-4.10000	-7.57000	-3.72000	-7.56000	-14.6000
5.00000	65.1000	40.0900	40.1000	35.4400	--
6.00000	42.8000	48.1100	34.4000	34.0800	31.5000
7.00000	52.9000	36.9300	44.7200	41.1700	--
8.00000	-23.6000	-30.5200	-29.2300	-41.7200	-40.1300
9.00000	-36.1000	-49.5700	-60.7600	-49.9000	-57.2700
10.0000	-29.8000	-36.9800	-42.1600	-45.9400	-45.5500
11.0000	-15.3000	-15.8300	-8.89000	-14.0600	-27.7200

LINE 1 HOOP

POSTN	LN2	LN2H
1.00000	-8.15000	-27.2000
2.00000	-5.86000	-12.5000
3.00000	-3.54000	-20.8000
4.00000	-30.6700	8.90000
5.00000	--	59.1000
6.00000	127.320	62.9000
7.00000	56.4000	61.1000
8.00000	5.05000	7.10000
9.00000	-17.1500	-16.0000
10.0000	-7.95000	-27.9000
11.0000	--	--

LINE 2 LONG. AND HOOP

POSTN	LN3	LN31	LN33	LN38	LN320
1.00000	-21.0700	-37.2500	-32.4000	-43.1300	-35.0500
2.00000	-41.9800	-22.8900	-44.6000	-58.5800	-38.9800
3.00000	-17.2200	-24.3100	-15.1700	-17.0400	-17.8800
4.00000	-21.5700	-26.9600	-23.2000	-37.1800	-34.9900
5.00000	123.470	--	--	107.900	157.050
6.00000	140.550	104.110	141.750	--	--
7.00000	133.680	--	--	--	--
8.00000	-17.2200	-35.0400	-31.9200	-23.6200	-36.4300
9.00000	4.63000	-14.6600	-24.7800	-15.5500	-17.4000
10.0000	-16.0800	-42.2900	-33.6300	-41.5000	-41.5000
11.0000	5.95000	0.930000	12.4100	18.2000	7.56000

LINE 3 LONG.

POSTN	LN3H	LN3H1	LN3H3	LN3H8	LN3H20
1.00000	-29.5000	-22.9400	-26.4000	-25.3600	-34.5500
2.00000	-5.70000	-19.0600	-18.1500	-6.10000	-9.52000
3.00000	-18.9000	-17.1000	-25.5000	-25.4600	-24.7400
4.00000	-5.73000	-11.3500	-26.9500	-23.5200	-19.6700
5.00000	63.7000	46.3460	47.6100	43.3600	43.0700
6.00000	58.5000	--	--	--	--
7.00000	50.1000	--	--	--	--
8.00000	1.60000	-22.0400	-14.8000	-18.7800	-30.4800
9.00000	-21.7500	-28.1400	-34.0300	-30.8700	-37.0600
10.0000	-24.5000	-38.6300	-38.3200	-44.4400	-19.4800
11.0000	15.1000	-14.4900	-4.52000	-8.86000	-11.5500

LINE 3 HOOP

POSTN	CIR1	CIR11	CIR13	CIR18	CIR120
1.00000	105.670	64.3100	68.9000	92.9500	105.850
2.00000	-4.04000	-20.5100	-18.1300	-19.5500	-23.0300
3.00000	-20.0700	-11.6900	-19.9900	-16.1300	-21.5200
4.00000	0.780000	-31.6000	-25.3600	-31.8600	-17.8600
5.00000	-15.7400	-34.0600	-18.8500	-41.2100	-29.5000
6.00000	-11.5300	-30.2900	-27.4400	-28.2100	-29.1100
7.00000	3.12000	0.120000	-1.04000	-4.25000	-3.63000
8.00000	12.3500	-2.22000	1.51000	8.82000	9.90000
9.00000	-4.22000	-18.2300	-21.9500	-23.1300	-27.7500
10.0000	14.6200	-4.12000	-3.24000	-6.08000	-7.47000
11.0000	-11.1800	-37.7300	-34.2600	-44.7200	-45.1600
12.0000	-26.0400	-30.1400	-31.6100	-40.3200	-26.6900
13.0000	-23.5900	-24.8100	-29.3200	-27.7200	-29.0200
14.0000	-27.3000	-17.7600	-32.0700	-26.5600	-36.5300
15.0000	-21.1800	-19.7600	-25.1500	-43.0000	-44.6000
16.0000	-13.7700	-16.9100	-33.2400	-23.2900	-30.2800
17.0000	-6.37000	-27.9500	-22.8500	-31.1600	-36.5000
18.0000	-26.3600	-38.7500	-21.5500	-33.0500	-38.2000
19.0000	-2.67000	-3.53000	-2.78000	-2.46000	-1.80000
20.0000	76.0900	40.0300	66.1300	68.3200	119.120
21.0000	--	--	--	--	--
22.0000	--	--	--	--	--

CIRCLE 1 LONG.

POSTN	CIR1H	CIR1H1	CIR1H3	CIR1H8	CIR1H20
1.00000	10.6000	33.2500	38.5800	29.1500	50.8700
2.00000	3.00000	-1.20000	-5.53000	-9.12000	-9.30000
3.00000	6.35000	-1.05000	2.19000	-12.1800	2.70000
4.00000	15.6300	-4.50000	-2.38000	-9.07000	-0.640000
5.00000	-0.620000	-18.3000	-31.9000	-24.4300	-27.5200
6.00000	-10.8300	-29.4600	-35.4200	-43.0200	-45.0400
7.00000	19.1700	2.90000	-2.20000	-1.53000	-35.7000
8.00000	11.0700	7.30000	10.0200	14.2600	9.90000
9.00000	7.04000	1.90000	-7.92000	-6.38000	-3.07000
10.0000	19.8000	11.5000	7.52000	9.15000	4.11000
11.0000	-9.40000	-1.48000	-6.17000	-17.3200	-11.0700
12.0000	3.10000	-2.42000	-2.54000	-4.06000	-9.08000
13.0000	6.00000	-7.90000	-6.43000	-7.91000	-5.27000
14.0000	9.60000	-10.0300	-3.95000	-3.94000	-3.12000
15.0000	-11.8000	-18.2000	-9.67000	-11.8600	-19.1800
16.0000	4.44000	-25.0600	-23.1300	-40.4300	-37.0700
17.0000	7.30000	3.53000	0.270000	-18.2300	-4.51000
18.0000	-25.0000	-14.4000	-30.8000	-37.3700	-32.1100
19.0000	9.10000	-0.850000	-5.62000	-3.08000	-1.85000
20.0000	34.4400	22.2100	24.4700	48.1300	62.6300
21.0000	--	--	--	--	--
22.0000	--	--	--	--	--

CIRCLE 1 HOOP

POSTN	CIR2	CIR21	CIR23	CIR28	CIR220
1.00000	-0.730000	-8.17000	-9.33000	-10.3700	-14.2000
2.00000	-3.41000	-17.2400	--	--	--
3.00000	-30.0900	-32.8000	-32.5300	-15.8700	-21.2800
4.00000	-31.4700	-27.0500	--	--	--
5.00000	-15.0700	-30.0100	-31.5300	-33.6000	-25.0200
6.00000	4.96000	-6.62000	--	--	--
7.00000	-3.25000	-18.6500	-26.2100	-22.5400	-27.7800
8.00000	4.23000	-14.4700	--	--	--
9.00000	22.7100	4.49000	0.0600000	-2.41000	-8.74000
10.0000	-3.68000	-16.3900	--	--	--
11.0000	-19.6500	-24.4700	-38.4900	-29.1400	-29.0900
12.0000	-26.9400	-36.8800	--	--	--
13.0000	-17.6600	-23.9700	-33.2900	-40.6500	-39.3700
14.0000	-36.3300	-28.1600	--	--	--
15.0000	-6.20000	-26.3100	-29.9600	-39.9700	-24.6300
16.0000	-30.0800	-40.0800	--	--	--
17.0000	-21.4400	-34.7400	-33.0200	-46.1300	-56.4100
18.0000	-34.7300	-35.6900	--	--	--
19.0000	-8.99000	-14.5100	-20.9500	-22.5800	-31.6000
20.0000	-14.7800	-31.3800	--	--	--
21.0000	-3.13000	-35.3500	-29.1100	-26.9200	-13.9900
22.0000	-20.4800	-25.9500	--	--	--

CIRCLE 2 LONG.

POSTN	CIR2H	CIR2H1	CIR2H3	CIR2H8	CIR2H20
1.00000	-18.5000	-27.4000	-32.0900	-30.1900	-25.1500
2.00000	-20.0000	--	--	--	--
3.00000	-31.6000	-33.9900	-36.3300	-34.4500	-35.0900
4.00000	-26.7000	--	--	--	--
5.00000	-15.3000	-15.9900	-23.7600	-23.0100	-35.1100
6.00000	6.30000	--	--	--	--
7.00000	-11.2000	-22.4100	-16.1800	-19.4900	-13.0200
8.00000	-23.5000	--	--	--	--
9.00000	-5.82000	-17.0500	-12.3700	-21.5000	-11.1400
10.0000	-15.2000	--	--	--	--
11.0000	-8.40000	-11.1100	-13.9400	-21.5000	-19.4400
12.0000	-20.4000	--	--	--	--
13.0000	-15.5000	-22.4900	-29.5300	-33.5300	-27.6400
14.0000	-38.5000	-37.2600	--	--	--
15.0000	-8.20000	-21.8500	-22.8700	-39.4000	-44.3700
16.0000	-42.1000	--	--	--	--
17.0000	-24.6000	-37.9200	-44.0600	-42.5900	-52.7600
18.0000	-34.5000	--	--	--	--
19.0000	-23.9000	-45.3600	-46.4900	-47.0800	-45.1000
20.0000	-17.6900	--	--	--	--
21.0000	-23.0000	-27.5000	-23.4700	-33.4500	-29.4700
22.0000	-24.9000	--	--	--	--

CIRCLE 2 HOOP

POSTN	CIR3	CIR31	CIR33	CIR38	CIR320
1.00000	16.2800	5.07000	-2.68000	0.780000	3.96000
2.00000	30.9600	--	--	--	--
3.00000	15.7800	4.94000	1.60000	4.49000	0.830000
4.00000	26.2100	--	--	--	--
5.00000	-1.27000	-5.63000	-5.01000	8.11000	-3.86000
6.00000	-20.7300	--	--	--	--
7.00000	-10.4300	-28.5900	-33.6600	-30.9100	-34.7900
8.00000	-14.6100	--	--	--	--
9.00000	-5.22000	-10.2100	-13.6300	-11.6300	-13.7600
10.0000	11.3800	--	--	--	--
11.0000	11.9700	1.66000	-5.02000	-6.59000	3.19000
12.0000	-6.01000	--	--	--	--
13.0000	-8.50000	-5.95000	-14.7800	-9.08000	-9.57000
14.0000	-7.49000	--	--	--	--
15.0000	-23.5700	-38.6200	-27.8700	-31.7800	-26.5600
16.0000	-10.9400	--	--	--	--
17.0000	-15.3500	-15.9300	-18.0300	-22.3000	-21.7500
18.0000	-19.3900	--	--	--	--
19.0000	-22.7300	-28.7400	-38.8900	-44.1500	-43.9900
20.0000	--	--	--	--	--
21.0000	--	--	--	--	--
22.0000	--	--	--	--	--

CIRCLE 3 LONG.

POSTN	CIR3H	CIR3H1	CIR3H3	CIR3H8	CIR3H20
1.00000	-9.70000	-12.4100	-18.5100	-21.9600	-20.1000
2.00000	13.6000	--	--	--	--
3.00000	5.50000	-3.22000	1.72000	-3.10000	-7.45000
4.00000	17.2000	--	--	--	--
5.00000	-15.6000	-18.4800	-16.4000	-20.3500	-20.1300
6.00000	-37.5000	--	--	--	--
7.00000	-35.8000	-36.1100	-42.8300	-57.3500	-45.8800
8.00000	-40.6000	--	--	--	--
9.00000	-24.0000	-35.7500	-15.3200	-32.6400	-34.3600
10.0000	-23.6000	--	--	--	--
11.0000	-17.7000	-15.5300	-18.8900	-26.6600	-26.1300
12.0000	-37.6000	--	--	--	--
13.0000	-21.8000	-35.0900	-36.6000	-44.0900	-37.7600
14.0000	-20.9000	--	--	--	--
15.0000	-48.3500	-59.9700	-59.1600	-57.5500	-46.5200
16.0000	-23.0000	--	--	--	--
17.0000	-20.1000	-30.8000	-27.6900	-26.7300	-35.4900
18.0000	-21.7000	--	--	--	--
19.0000	-43.0000	-55.4300	-73.4600	-59.3300	-66.0400
20.0000	--	--	--	--	--
21.0000	--	--	--	--	--
22.0000	--	--	--	--	--

CIRCLE 3 HOOP

Vita

Nancy Abigail Morgan was born in Oak Ridge, Tennessee on February 2, 1964. While growing up in the beautiful foothills of the Appalachian Mountains, she discovered two loves-- the Lord and travel. She has tried to pursue both of these along with a B.S. and then M.S. in Material Engineering at Virginia Polytechnic Institute and State University. She now works for Exxon Research and Engineering in Florham Park, NJ.